A THESIS FOR THE DEGREE OF DOCTOR OF PHILOSOPHY

PHARMACEUTICAL POTENTIAL OF FISETIN

ILANDARAGE MENU NEELAKA MOLAGODA

Department of Marine Life Sciences
SCHOOL OF BIOMEDICAL SCIENCES
JEJU NATIONAL UNIVERSITY
REPUBLIC OF KOREA

February 2021

Pharmaceutical Potential of Fisetin

Ilandarage Menu Neelaka Molagoda

(Supervised by Professor Gi-Young Kim)

A thesis submitted in partial fulfillment of the degree of

DOCTOR OF PHYLOSOPHY

December 2020

The thesis has been examined and the approved by

The thesis director,

Seungheon Lee, Professor of Pharmacology, School of Biomedical Sciences, Jeju National University

.....

Sang-Rul Park, Professor of Ecology, School of Biomedical Sciences, Jeju National University

.....

Gi-Young Kim, Professor of Immunology, School of Biomedical Sciences, Jeju National University

.....

Chang-Hee Kang, Researcher Nakdonggang National Institute of Biological Resources

.....

Woong Han, Principal Researcher, Nakdonggang National Institute of Biological Resources

.....

03.12.2020

Date

Department of Marine Life Sciences

SCHOOL OF BIOMEDICAL SCIENCES

JEJU NATIONAL UNIVERSITY

REPUBLIC OF KOREA

Table of Contents

Acknowledgement

This is an output of the effort and support of several people to whom I am extremely grateful. First and foremost, I thank my supervisor, Professor Kim Gi-Young for hosting me at JNU as well as inspiring and guiding me throughout this research period. It has been a privilege to work with you and hope to be able to work with you again in the near future.

I am deeply grateful to the thesis committee, Prof. Seungheon Lee, Prof. Sang-Rul Park, Dr. Chang-Hee Kang and Dr. Woon Hang, for accepting my invitation to being part and for their insightful comments and suggestions.

I would like to take this opportunity to thank my former undergraduate supervisor Prof. Devika de Costa for guiding me to enter in to the JNU.

Every result described in this thesis was accomplished with the help and support of fellow lab mates and collaborators. Therefore, I am also profoundly grateful for the hard work of my co-authors and their substantial contribution to uplift the studies presented in this thesis. Thanks, Dr. Prasad Jayasooriya, Dr. Dilshara Matharage, Mr. Hasitha Karunarathne, Mr. Chanaka Jayasinghe, Mr. Gihan Kavinda. I am delighted to have worked with you and I look forward to working with you again.

Fortunately, I have also the privilege of having a lovely family and friends who had a fundamental role in getting me through the PhD process successfully. I would like to acknowledge my parents, my brother, my beloved wife, Gothami and daughter, Ära for their constant love and support.

Summary

Fisetin is a plant secondary metabolite which is ubiquitously expressed in some of the fruits and vegetables such as apple, strawberry, persimmon, onion, lotus root and cucumber. It is a low molecular weight bioactive polyphenolic flavonoid which could absorb broad range of UV spectrum due to the electron decentralizing ability that enables it to possess strong anti-oxidative properties. Pharmaceutical potentials of fisetin have been extensively studied focusing its anti-cancer activities. The compound itself shown to be effective against wide range of cancers such as prostate cancer, osteosarcoma, lung cancer and leukemia by triggering apoptosis. In spite of the apoptosis other cell signaling mechanisms such as autophagy, metastasis, angiogenesis, cell cycle arrest and transcription factor regulation are also associated with the mode of action of fisetin in cancers. However, melanogenic properties, anti-inflammatory effects, anti-inflammasome effect, osteogenic effect and anti-oxidative properties under the $PM_{2.5}$-induced conditions have not been extensively identified. Therefore, during the current study, we were able to identify the aforementioned properties specifically targeting wnt/β-catenin cell signaling pathway.

Firstly, we investigated that fisetin-mediated could promote the melanogenesis in B16F10 cells and zebrafish larvae through binding to GSK-3β at a non-ATP-competitive binding site, and the subsequent release of β-catenin, which promotes MITF-mediated tyrosinase activation. Although fisetin caused an unexpected increase in melanogenesis, fisetin may be useful for the treatment of many different diseases such as vitiligo and the inhibitory effect on GSK-3β is also paramount important. Secondly, fisetin attenuates LPS-induced inflammation and endotoxic shock by suppressing the β-catenin-mediated NF-κB signaling pathway indicating the possibility of using it as a potent anti-inflammatory drug for systemic inflammation.

Then, fisetin inhibited the inflammasome formation via two main cell signaling pathways. Firstly, Fisetin antagonizes the LPS recognition of TLR4 via competitively binding to the hydrophobic pockets of MD2 which consequently prevent the stimulation of canonical NF-κB cell signaling pathway to inhibit the transcription of IL-1β. Secondly, fisetin inhibits the formation of mtROS by promoting the elimination of damaged mitochondria in a p62 dependent manner. Inhibition of mtROS generation associate with the downregulation of NLRP3 inflammasome formation which will subsequently inhibits the cleavage of pro-IL-1β in to active IL-1β.

Next we demonstrated that fisetin promote osteoblast differentiation and vertebrae formation in MC3T3-E1 mouse osteoblast and zebrafish larvae respectively. During the study we noticed that fisetin stimulate the GSK-3β ser9 phosphorylation to liberate β-catenin from the destructive complex and thereby promote the nuclear translocation of β-catenin consequently upregulate the osteoblast differentiation and bone formation. Furthermore, fisetin could alleviate prednisolone mediated osteoporosis by inhibiting osteoclast differentiation in MC3T3-E1 cells and zebrafish larvae as well. Finally, we proved that fisetin potently inhibits $PM_{2.5}$-induced apoptosis in HaCaT human keratinocytes. Previous studies showed that $PM_{2.5}$ induced ROS levels via AhR dependent pathway while upregulated ROS levels are associated with initiation of ER stress via PERK-ATF4 axis. Initiation of ER stress responses resulted calcium accumulation in the cytosolic compartment that lead to the loss of mitochondrial membrane potential. Loss of mitochondrial membrane potential broke the balance between Bcl2 to Bax and thereby promoted the cleavage of caspase8, 9 and 3 and PARP which execute apoptosis. We investigated that fisetin effectively blocked the ROS formation, initiation of ER stress responses and consequently inhibited the $PM_{2.5}$-induced apoptosis in HaCaT human keratinocytes.

In conclusion, fisetin possess broad range of pharmaceutical potentials targeting various cells signaling pathways in different cells. Therefore, our results imply that fisetin could be a potent drug target for several diseases with minimum side effects. However, further studies are needed to warrant to show the fisetin-mediated pharmaceutical potentials in detailed *in-vivo* studies.

논문 요약

피세틴은 사과, 딸기, 감, 양파, 연근 및 오이와 같은 일부 과일 및 채소에서 다량 함유되어 있는 식물 2 차 대사산물이다. 강력한 항산화 특성을 보유하고 있으며, 전자분산 능력으로 인해 광범위한 UV 스펙트럼을 흡수 할 수 있는 저분자량 생리활성 플라보노이드이다. 피세틴의 약리학적인 잠재력은 항암활성을 중심으로 광범위하게 연구되고 있으며, 특히, 전립선암, 골육종, 폐암 및 백혈병과 같은 광범위한 암에 대해 효과적이다. 세포사멸유도 이외에도 포식능 증가, 암세포 전이 억제, 신생 혈관형성 저해, 세포주기 정지 및 전사 인자 조절과 같은 다른 세포 신호 전달 메커니즘은 암에서 피 세틴의 작용 방식과 관련있다.. 그러나 PM2.5 유발 조건에서 멜라닌 생성 특성, 항염증 효과, 골형성 효과 및 항산화 특성은 광범위하게 확인된 바가 없다. 따라서 현재 연구에서 우리는 wnt/β-catenin 세포신호 전달경로를 표적으로 하여 앞서 언급한 다양한 연구모델에서의 효과를 검증하과자 한다.

첫째, 피세틴은 비 ATP 경쟁 결합 부위에서 GSK-3β 에 결합하고 MITF 매개 티로시나아제의 활성화를 촉진하는 β-카테닌의 방출을 통해 B16F10 세포와 제브라피쉬 유충의 멜라닌 생성을 촉진 할 수 있음을 확인 할 수 있었다. 피세틴이 멜라닌 생성을 예상치 않게 증가 시켰지만, 피세틴은 백반증과 같은 다양한 질병의 치료에 유용 할 수 있으며, GSK-3β 에 대한 억제를 통한 다양한 질환의 치료제로도 사용이 가능 할 것으로 판단된다. 둘째, 피세틴은 β-카테닌 매개 NF-κB 신호 전달 경로를 억제하여 LPS 유발 염증 및 내독성 쇼크를 약화시켜 전신 염증에 대한 강력한 항염증제로 사용이 가능할 것으로 판단된다.

다음으로, 피세틴은 앞서 언급한 두 가지 주요 세포 신호 전달 경로를 통해 inflammasome 형성을 억제하였다. 첫째, 피세틴은 MD2 의 소수성 포켓에 경쟁적으로 결합하여 TLR4 의 LPS 인식을 길항하여, NF-κB 세포 신호 전달 경로의 억제를 통하여, IL-1β 의 전사를 억제함을 확인하였다. 둘째, 피세틴은 p62 의존적방식으로 손상된 미토콘드리아의 제거를 촉진함으로써 미토콘드리아내의 활성산소 형성을 억제한다. 미토콘드리아내의 활성산소 생성의 억제는 활성 IL-1β 로의 pro-IL-1β 의 절단을 연속적으로 억제하며, 이는 NLRP3 inflammasome 형성의 하향 조절과 연관되어 있다.

또한, 피세틴이 MC3T3-E1 마우스 조골세포 및 제브라피쉬 유충에서 각각 조골 세포 분화 및 척추 형성을 촉진한다는 것을 입증하였다. 연구에서 우리는 피세틴이 GSK-3β ser9 인산화를 자극하여, 파괴적인 복합체에서 β-catenin 을 방출시키게 되고, 더불어서 β-catenin 의 핵내 이동을 촉진하여 결과적으로 골아 세포 분화와 뼈 형성을 상향 조절한다는 것을 발견하였다. 또한 피 세틴은 MC3T3-E1 세포와 제브라피쉬 유충에서도 파골세포 분화를 억제함으로써 프레드니솔론 매개 골다공증을 완화 할 수 있음을 규명하였다. 마지막으로, 우리는 피 세틴이 HaCaT 인간 각질세포에서 $PM_{2.5}$ 로 유도된 세포사멸을 강력하게 억제한다는 것을 증명하였다. 이전 연구에 따르면 $PM_{2.5}$ 는 AhR 의존 경로를 통해 활성산소를 유도하는 반면 상향 조절 된 활성산소는 PERK-ATF4 축을 통한 소포체 스트레스의 시작과 관련이 있다. ER 스트레스 반응의 시작으로 세포질 구획에 칼슘이

축적되어 미토콘드리아 막 전위가 손실되었으며, 이는 Bcl-2 와 Bax 사이의 균형을 깨뜨려서 세포 사멸을 실행하는 caspase-8, caspase-9 및 caspase-3 과 PARP 의 절단을 촉진하였다. 결론적으로 피세틴이 활성산소의 형성, 소포체 스트레스 반응의 시작을 효과적으로 차단하고 결과적으로 HaCaT 인간 각질 세포에서 $PM_{2.5}$ 유도 세포 사멸을 억제한다는 것을 확인하였다.

List of figures

1 Chapter1

GSK-3β-Targeting Fisetin Promotes Melanogenesis in B16F10 Melanoma Cells and Zebrafish Larvae through β-Catenin Activation.

Abstract

Fisetin is found in many fruits and plants such as grapes and onions, and exerts anti-inflammatory, anti-proliferative, and anticancer activity. However, whether fisetin regulates melanogenesis has been rarely studied. Therefore, we evaluated the effects of fisetin on melanogenesis in B16F10 melanoma cell and zebrafish larvae. The current study revealed that fisetin slightly suppressed in vitro mushroom tyrosinase activity; however, molecular docking data showed that fisetin did not directly bind to mushroom tyrosinase. Unexpectedly, fisetin significantly increased intracellular and extracellular melanin production in B16F10 melanoma cells regardless of the presence or absence of α-melanocyte stimulating hormone (α-MSH). We also found that the expression of melanogenesis-related genes such as *tyrosinase* and *microphthalmia-associated transcription factor* (*MITF*), were highly increased 48 h after fisetin treatment. Pigmentation of zebrafish larvae by fisetin treatment also increased at the concentrations up to 200 μM and then slightly decreased at 400 μM, with no alteration in the heart rates. Molecular docking data also revealed that fisetin binds to glycogen synthase kinase-3β (GSK-3β). Therefore, we evaluated whether fisetin negatively regulated GSK-3β, which subsequently activates β-catenin, resulting in melanogenesis. As expected, fisetin increased the expression of β-catenin, which was subsequently translocated into the nucleus. In the functional assay, FH535, a Wnt/β-catenin inhibitor, significantly inhibited fisetin-mediated melanogenesis in zebrafish larvae. Our data suggested that fisetin inhibits GSK-3β, which activates β-catenin, resulting in melanogenesis through the revitalization of MITF and tyrosinase.

Keywords: fisetin; melanogenesis; α-MSH; GSK-3β; β-catenin

1.1 Introduction

Melanin is important for the prevention of damages that occurs as a result of exposure to ultraviolet (UV) light (D'Mello et al., 2016). The synthesis and storage of melanin occurs inside a specific organelle in the melanocytes, called the melanosome, which then transfers melanin into adjacent keratinocytes (Bonaventure et al., 2013). Two main types of melanin are synthesized inside the melanosomes, namely eumelanin (black to brown melanin) and pheomelanin (reddish or yellowish melanin) (Ogbechie-Godec and Elbuluk, 2017). The synthesis of these two types of melanin is regulated by three structurally related enzymatic proteins in the downstream melanogenic process: tyrosinase, tyrosinase-related protein 1 (TYRP1), and tyrosinase-related protein 2 (DCT) (Videira et al., 2013). When keratinocytes are exposed to the UV light, they secrete α-melanocyte stimulating hormone (α-MSH), a peptide hormone, which then binds to the melanocortin 1 receptor (MC1R) on the melanocytes and activates adenylyl cyclase (AC) leading to an increase in cyclic adenosine monophosphate (cAMP) (Graff et al., 2005). As a result of the increase in cAMP, protein kinase A (PKA) is increased and subsequently phosphorylates the transcription factor cAMP response element (CRE)-binding protein (CREB) at SER 133 (Rodriguez and Setaluri, 2014). The phosphorylation of CREB results in the initiation of a transcriptional cascade of melanogenic processes including the induction of MITF expression, which ultimately stimulates the expression of tyrosinase, TYRP-1, and DCT (Rzepka et al., 2016).

Glycogen synthase kinase-3 (GSK-3) is a multi-tasking serine/threonine kinase, which transfers a phosphate group to either the serine or threonine residues of its substrates (Beurel et al., 2015). It was initially described as a key molecule for the inhibition of glycogen synthase in glycogen metabolism. However, recent studies have confirmed that GSK-3 is also involved in regulating many critical biological processes, including inflammation (Ajmone-Cat et al., 2016),

tumorigenesis (Dembowy et al., 2015), Alzheimer's disease (AD) (Maqbool et al., 2016), and Parkinson's disease (PD) (Golpich et al., 2015), and its phosphorylation is required for the initiation, enhancement, or inhibition of the function of target substances. There are two structurally similar GSK-3 isoforms in mammals, GSK-3α and GSK-3β, but they are functionally different (Bartman et al., 2014). In particular, GSK-3β plays a vital role in targeting β-catenin for proteasomal degradation via ubiquitination. When Wnt receptor complexes are not bound to a ligand, tumor suppressors axin, adenomatous polyposis coli (APC), GSK-3β, casein kinase I (CK1), protein phosphatase 2A (PP2A), and the E3-ubiquitin ligase β-TrCP form the β-catenin-destruction complex to phosphorylate β-catenin at its N-terminal domain and thereby consign β-catenin to proteasomal degradation (Clevers and Nusse, 2012; Stamos and Weis, 2013a). In the presence of the Wnt ligand, a receptor complex is formed from the transmembrane protein frizzled (FZ), low-density lipoprotein receptor-related protein 6 (LRP6), and the scaffolding protein Dishevelled (Dvl) (Clevers and Nusse, 2012; Stamos and Weis, 2013a). The formation of the complex results the phosphorylation of LRP6 and the recruitment of axin to the complex and thereby leads to the inhibition of axin-mediated β-catenin phosphorylation, which ultimately results in the stabilization of β-catenin. The stabilization and accumulation of β-catenin trigger the translocation of β-catenin to the nucleus to form a complex with T-cell transcription factor/lymphoid enhancer factor (TCF/LEF) and thereby activates the expression of Wnt target genes (Clevers, 2006; MacDonald et al., 2009b). Interestingly, the phosphorylation at SER 9 inactivates GSK-3β and subsequently releases β-catenin from the destruction complex (Doble and Woodgett, 2003; Ma et al., 2013). Previously, Schepsky et al. found that β-catenin directly binds with MITF and positively stimulated MITF-specific target genes, such as tyrosinase, which resulted in melanogenesis (Schepsky et al., 2006).

Mouse B16F10 melanoma cells have been used as a sensitive and reliable model for melanin quantification assays (Siegrist and Eberle, 1986). However, mouse B16 melanoma cells and normal melanocytes is associated with different response to 12-tetraadecnoylphorbol 13-acetate (TPA). In B16 melanoma cells, TPA (at 160 nM) inhibited melanogenesis by inhibiting protein kinase C-mediated MITF (Bertolotto et al., 1998); on the other hand, in mouse normal melanocytes, TPA (at 48 nM) stimulated melanogenesis by activating MITF (Prince et al., 2003). In addition, exposure of TPA (at 85 nM, but not at 170 nM) stimulated melanin synthesis in human normal melanocytes by promoting tyrosinase activity (Chao-Hsing and Hsin-Su, 1991). Above studies showed that different cell types of normal melanocyte or melanoma inconsistently regulate melanogenesis or anti-melanogenesis because of different responsibility to TPA; thus, all reports used different concentrations of TPA, which indicates that according to the concentration of TPA, melanogenesis or anti-melanogenesis is regulated accompanied by TPA-responsive signaling. Especially, TPA at below 85 nM identically stimulated melanogenesis regardless of cell types such as mouse B16F10 melanoma cells and human normal melanocytes, which indicates that B16F10 cells are a sensitive melanogenesis model. Along with B16F10 melanoma cells, zebrafish larvae have been used as an attractive in vivo model for melanogenesis because the zebrafish model directly displays melanin strips, which can be visualized by the naked eye (Karunarathne et al., 2019a; Karunarathne et al., 2019b; Lajis, 2018). Zebrafish also shared genetic similarity with mouse and human during pigment expression from the neural crest-derived stem cells to melanocyte progenitor by activating MITF, TYRP-1, DCT, and tyrosinase (Choi et al., 2007; Singh and Nusslein-Volhard, 2015).

Fisetin (3,3′,4′,7-tetrahydroxyflavone) is a dietary flavonoid found in various fruits and vegetables, including strawberry, grape, apple, onion, and cucumber, at a concentration of 2–160 μg/g wet

food (Khan et al., 2018). Many studies have attempted to identify its biological effects, including neuroprotective, anti-arthritic, and anti-allergic activities (Ahmad et al., 2017; Jo and Park, 2017; Zheng et al., 2017). In particular, emerging data also indicate that fisetin possesses anti-cancer activity, in in vitro and in vivo studies, including lung (Khan and Mukhtar, 2015), bladder (Li et al., 2014), breast (Smith et al., 2016), prostate (Mukhtar et al., 2016), colon (Chen et al., 2015), and pancreatic cancers (Youns and Abdel Halim Hegazy, 2017). However, it is still contradictory whether fisetin is a positive or negative regulator of melanogenesis. Takekoshi et al. found that some flavonoids such as fisetin promotes melanin contents and tyrosinase activity in human melanoma cells (Takekoshi et al., 2014). On the other hands, Shon et al. reported that fisetin inhibits α-MSH-mediated intracellular and extracellular melanin content in murine B16F10 melanoma cells (Shon et al., 2016). Therefore, in the present study, using in vitro and in vivo approaches, we tried to pinpoint the precise effect of fisetin on molecular mechanism involved in melanogenesis.

In the present study, we found that fisetin positively regulated melanogenesis in both B16F10 cells and an in vivo zebrafish model through the activation of β-catenin signaling pathway. According to the molecular docking data, fisetin binds to the non-ATP–competitive site of GSK-3β; this suggests that fisetin promotes melanogenesis through the inhibition of GSK-3β and the subsequent release of β-catenin

1.2 Materials and Methods

1.2.1 Reagents and Antibodies

Fisetin, mushroom tyrosinase, phenylthiourea (PTU), and α-MSH were purchased from Sigma-Aldrich Chemical Co. (St. Louis, MO, USA). Fisetin was dissolved in dimethyl sulfoxide (DMSO) as a stock solution at 50 mM concentration and stored at −20 °C. DMEM medium, fetal bovine serum (FBS), and antibiotic mixture were purchased from WELGENE (Gyeongsan-si, Gyeongsangbuk-do, Korea). Antibodies against MITF, tyrosinase, β-catenin, β-actin, and nucleolin were purchased from Santa Cruz Biotechnology (Santa Cruz, CA, USA). Peroxidase-labeled anti-rabbit and anti-mouse immunoglobulins were obtained from KOMA Biotechnology (Seoul, Korea). All other chemicals were purchased from Sigma grades.

1.2.2 Cell Culture and Viability Assay

Mouse B16F10 melanoma cells were obtained from ATCC (Manassas, VA, USA). The cells were cultured at 37 °C in a 5% CO_2 humidified incubator in DMEM supplemented with 10% heat-inactivated FBS and antibiotic mixture. The cells were treated with various concentrations of fisetin for 96 h and MTT assay was performed at regular 24-h interval. Briefly, B16F10 melanoma cells were seeded at a density of 1×10^4 cells/mL in 24 well plate overnight. The cells were then treated with various concentrations of fisetin (0–200 μM) for 96 h. At every 24 h, final concentration of 0.5 mg/mL MTT solution was added to each well and incubated for 1 h at 37 °C to measure the mitochondrial related metabolism. Following the media removal, DMSO was added to each well and gently shaken for 10 min at room temperature. Dissolved formazan was transfer into 96 well plate and absorbance was determined at 540 nm by a microplate spectrophotometer (Thermo Fisher Scientific; Waltham, MA, USA).

1.2.3 In Vitro Mushroom Tyrosinase Activity

In vitro mushroom tryrosinase activity was performed according to the previous protocol with a little modifications (Curto et al., 1999). In a 96 well plate, 100 mM potassium phosphate buffer (pH 6.5), different concentrations of fisetin, 1.5 mM L-tyrosine, and 210 U/mL mushroom tyrosinase were mixed. Phenylthiourea (PTU) (100 nM) was used as a positive control. Then, the microplate was incubated at 37 °C for 40 min and the absorbance of the mixture was measured at 490 nm. The value of each measurement was represented as percentage changes from the untreated control (reaction mixture without fisetin). Fisetin-treated group diluted in buffer without tyrosinase was carried out to exclude color interference in the absorbance measurement. The inhibition percentage of tyrosinase activity was calculated using following equation; Inhibition rate (%) = $100 \times \{[(A - B) - (C - D)]\}/(A - B)$, where A is the absorbance at 490 nm (Abs490) without testing substance (L-tyrosine + tyrosinase), B is the Abs490 both without testing substance and tyrosinase (L-tyrosine), C is the Abs490 with testing substance (L-tyrosine + tyrosinase + sample) and D is Abs490 with testing substance but without tyrosinase (L-tyrosine + sample).

1.2.4 Flow Cytometry Analysis

B16F10 melanoma cells were seeded at a density of 1×10^4 cells/mL in 24 well plate overnight and then treated with fisetin (0–200 μM) for 96 h. The cells were collected and stained with Muse® cell viability assay kit (Luminex Co., Austin, TX, USA) for 10 min. The population of dead cell (%) was analyzed by Guava®Muse® Cell Analyzer (Luminex Co.).

1.2.5 Intracellular and Extracellular Melanin Content

The effect of fisetin on melanin content in B16F10 melanoma cells was investigated according to the previous protocol (Tsuboi et al., 1998). Briefly, B16F10 melanoma cells were cultured at a

density of 1×10^5 cells/mL in 6 well plate overnight. Then, the indicated concentrations of fisetin were treated for 96 h, and the culture media and the cell pellet were collected at every 24 h. The culture media was directly measured at 405 nm for extracellular melanin content. For intracellular melanin content, the cell pellets were washed with ice-cold PBS and dissolved in 400 μL of 1 M NaOH containing 10% DMSO at 90 °C for 60 min. Then, the absorbance was measured at 405 nm.

1.2.6 Reverse Transcription-Polymerase Chain Reaction (RT-PCR)

Total RNA was extracted using easy-BLUE™ total RNA extraction kit (iNtRON Biotechnology, Seongnam-si, Gyeonggi, Korea) according to the manufacturer's instruction. One microgram RNA was reverse-transcribed using MMLV reverse transcriptase (Bioneer, Daejeon-si, Korea). The cDNA was amplified using EzWay Taq PCR ReadyMix (KOMA Biotechnology) with specific primers of *MITF* (forward 5′-CCC GTC TCT GGA AAC TTG ATC G-3′ and reverse 5′-CTG TAC TCT GAG CAG CAG GTC-3′), *tyrosinase* (forward 5′-GTC GTC ACC CTG AAA ATC CTA ACT-3′ and reverse 5′-CAT CGC ATA AAA CCT GAT GGC′), and *GAPDH* (forward 5′- AGG TCG GTG TGA ACG GAT TTG-3′ and reverse 5′-TGT AGA CCA TGT AGT TGA GGT CA-3′). The following PCR conditions were applied for PCR amplification: *tyrosinase* and *MITF*: 25 cycles of denaturation at 95 ℃ for 45 s, annealing at 62 ℃ for 45 s and extended at 72 ℃ for 1 min; GAPDH 23 cycles of denaturation at 94 ℃ for 30 s, annealing at 60 ℃ for 30 s and extended at 72 °C for 30 s. *GAPDH* was used as an internal control to evaluate relative expression of *MITF* and *tyrosinase*.

1.2.7 Protein Extraction and Western Blotting Analysis

B16F10 melanoma cells were cultured at a density of 1×10^4 cells/mL in 6 well plate overnight. Then, the cells weretreated with the indicated concentrations of fisetin for 96 h and lysed with PRO-PREP lysis buffer (iNtRON Biotechnology). In a parallel experiment, the cells were washed with ice-cold PBS, and the cytosolic and nuclear protein was extracted using NE-PER^{TM} Nuclear and Cytoplasmic Extraction Reagents (Pierce, Rockford, IL, USA). After cleaning lysates by centrifugation, protein was quantified by the Bio-Rad protein assay reagents (Bio-Rad, Hercules, CA, USA). An equal amount of protein was separated by SDS-polyacrylamide gel, transferred onto nitrocellulose membrane (Schleicher & Schuell, Keene, NH, USA) and then immunoblotted with the indicated antibodies. The expressional value was normalized to the intensity of β-actin or nucleolin.

1.2.8 In Vivo Melanogenic Effect in Zebrafish Larvae

Zebrafish was raised and handled according to standard guidelines of the Animal Care and Use Committee of Jeju National University (approval No.: 2019-0052). All the zebrafish-related experiments are performed as previously described method (Agalou et al., 2018). In brief, inbreed AB strain of zebrafish was mated and the eggs were collected. The eggs were kept in E3 embryo media for 24 h and manually removed the chorion and treated the chemical for 72 h. Images were taken by Olympus SZ2-ILST stereomicroscope (Tokyo, Japan) and the heart rate of zebrafish was also measured to evaluate cardiotoxicity of fisetin. In order to evaluate the effect of fisetin in the presence of α-MSH, after dechorionation, zebrafish larvae were treated with 200 μM PTU for 24 h to remove all the pigments. Then, the larvae were washed with E3 embryo media and treated with 1 μg/mL α-MSH for 2 h prior to fisetin treatment for an additional 72 h.

1.2.9 Determination of Cardiotoxicity in Zebrafish

The cardiotoxicity of fisetin was determined by comparing the heart rate of zebrafish larvae, because monitoring the zebrafish heart rate is a great tool in drug development and cardiotoxicity study (Cornet et al., 2017; Zhang et al., 2003). Briefly, zebrafish larvae were placed under a stereomicroscope (Olympus SZ2-ILST) for 4 min at room temperature for allowing embryos to acclimate to the light. The heart rate was calculated by counting the number of heart beats in 1 min. The obtained results were expressed as average heart rate per min.

1.2.10 Molecular Docking Prediction

Recombinant mushroom tyrosinase (PDB ID: 5M6B) and GSK-3β (PDB ID: 1J1B) were obtained from RCSB protein database bank (PDB, http://www.rcsb.org), and canonical SMILES of fisetin and other chemicals such as tideglusib, enzastaurin, and LY2090314 were obtained from PubChem (https://pubchem.ncbi.nlm.nih.gov). Then, molecular docking score was calculated using mcule with Autodock vina. Four docking poses were provided and representative images were displayed using UCSF Chimera (https://www.cgl.ucsf.edu/chimera). The UCSF Chimera predicted active hydrogen binding to amino acids and distance.

1.2.11 Statistical Analysis

The images for RT-PCR and western blotting analysis were visualized by Chemi-Smart 2000 (Vilber Lourmat, Marne-la-Vallee, France). Each image was captured using Chemi-Capt (Vilber Lourmat) and transported into Adobe Photoshop. Images of zebrafish larvae were taken by Olympus SZ2-ILST stereomicroscope. All bands were quantified by Image J software (Wayne Rasband, National Institute of Health) and then statistically analyzed by Sigma plot 12.0. All data are presented as the mean ± the standard error of the median (SEM). Significant differences

between groups were determined using an unpaired one-way ANOVA with Bonferroni correction. Values of ***, $p < 0.001$, **, $p < 0.01$, and *, $p < 0.05$ were considered to indicate statistical significance. The results shown in each of the figures are representative of at least three independent experiments

1.3 Results

1.3.1 Fisetin is a Non-Specific Inhibitor of Mushroom Tyrosinase Activity in Vitro

Fisetin contains a typical flavonol backbone with three additional hydroxyl functional groups (Figure 1A), which enables its action as an anticancer agent against various types of cancers. As the melanogenic effect of fisetin has been poorly determined, we, therefore, performed the mushroom tyrosinase activity assay in vitro. Overall, fisetin very slightly increased the inhibition of tyrosinase activity and highest concentration of fisetin (200 μM) resulted in the highest inhibition of mushroom tyrosinase activity in vitro (39.9% ± 4.7%) (Figure 1B). From fisetin concentrations at over 25 μM, the inhibitory activity slightly increased (11.2% ± 1.3%, 17.7% ± 1.7%, 17.0% ± 2.4%, and 25.3% ± 1.8% at 25 μM, 50 μM, 75 μM, and 100 μM fisetin, respectively). Then, we performed molecular docking analysis to determine whether fisetin directly bound to recombinant mushroom tyrosinase (PDB ID: 5M6B). Accordingly, the docking analysis showed that fisetin did not directly bind to the tyrosinase (Figure 1C), which suggested that the slight inhibitory effect of fisetin on tyrosinase activity was non-specific and due to anti-oxidant activity. Therefore, we hypothesized that fisetin slightly blocks the oxidation of tyrosine induced by tyrosinase. Collectively, these results suggest that fisetin could slightly inhibit in vitro mushroom tyrosinase enzyme activity without direct binding to tyrosinase, and that tyrosinase was not a direct target molecule of fisetin in melanogenesis

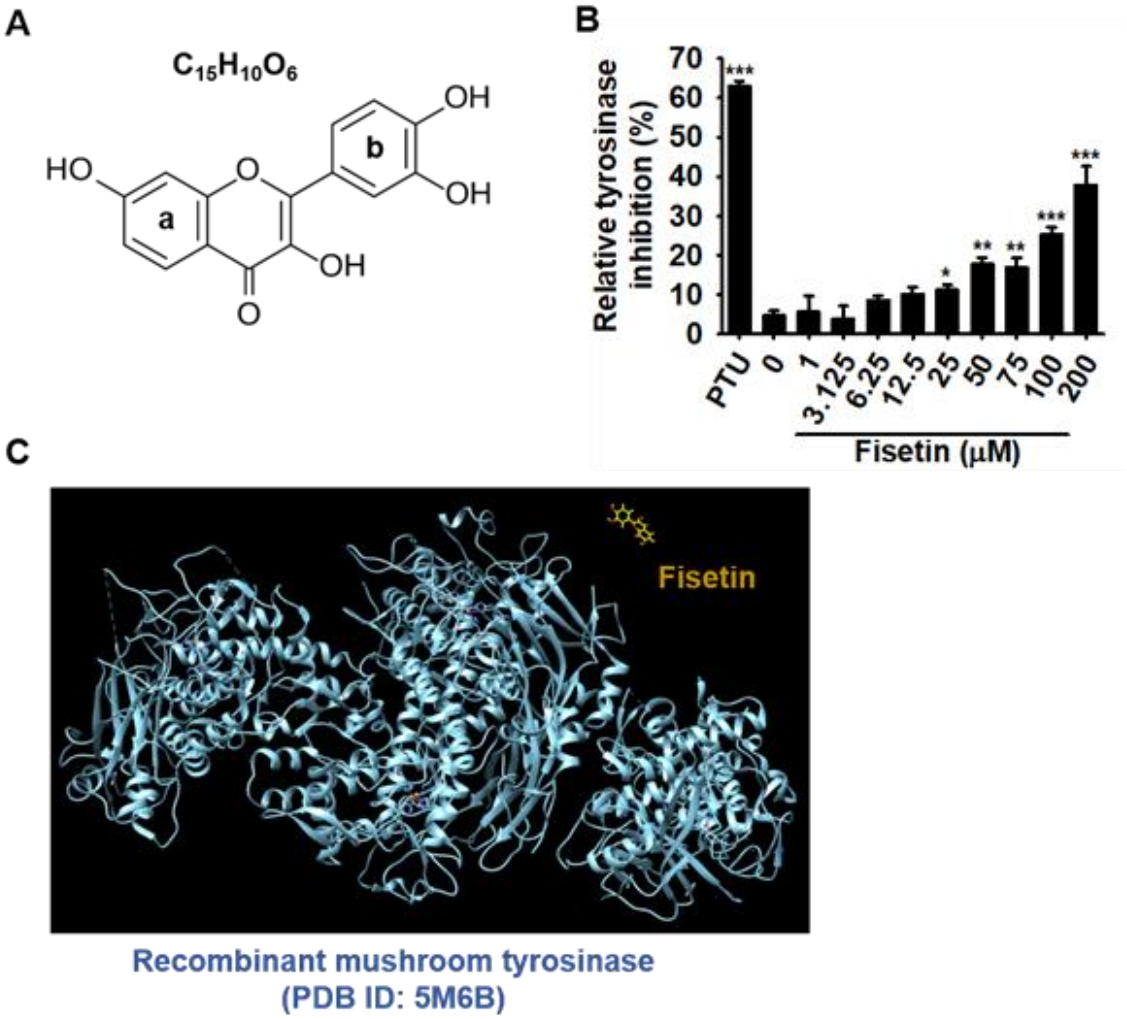

Figure 1. Fisetin non-specifically inhibits in vitro mushroom tyrosinase enzyme activity without directly binding of tyrosinase. (A) The chemical structure of fisetin. (B) The effect of fisetin on in vitro mushroom tyrosinase activity. Tyrosinase activity was determined by the oxidation of L-tyrosinase as a substrate. Phenylthiourea (PTU) (200 nM) was used as positive control. (C) The molecular docking of fisetin with recombinant mushroom tyrosinase (PDB ID: 5M6B). The results are the average of the three independent experiments; the data are expressed as the mean ± SEM (***, $p < 0.001$, **, $p < 0.01$, and *, $p < 0.05$).

1.3.2 High Concentrations of Fisetin Decrease Relative Viability of B16F10 Melanoma Cells

To optimize the concentrations of fisetin for cellular melanogenic activity, cell morphology and MTT activity were measured at every 24 h-interval for 96 h after the treatment of B16F10 melanoma cells with fisetin. The microscopic data showed that fisetin (≤25 μM) resulted in no changes in morphology; however, high concentrations of fisetin (≥50 μM) downregulated total cell numbers without shrunk and round shape of cells (Figure 2A). Consistent with cell morphological analysis, MTT data showed that high concentrations of fisetin (≥50 μM) gradually decreased relative cell viability of B16F10 melanoma cells (Figure 2B). Nevertheless, in flow cytometry data, no distinct dead cells were observed (Figure 2C), which indicates that fisetin-mediated decrease of cell viability is not due to cell death. The results indicate that high concentrations of fisetin results in a decreased number of cells, but is not cytotoxic. Therefore, fisetin at below 25 μM was used for the-subsequent experiments.

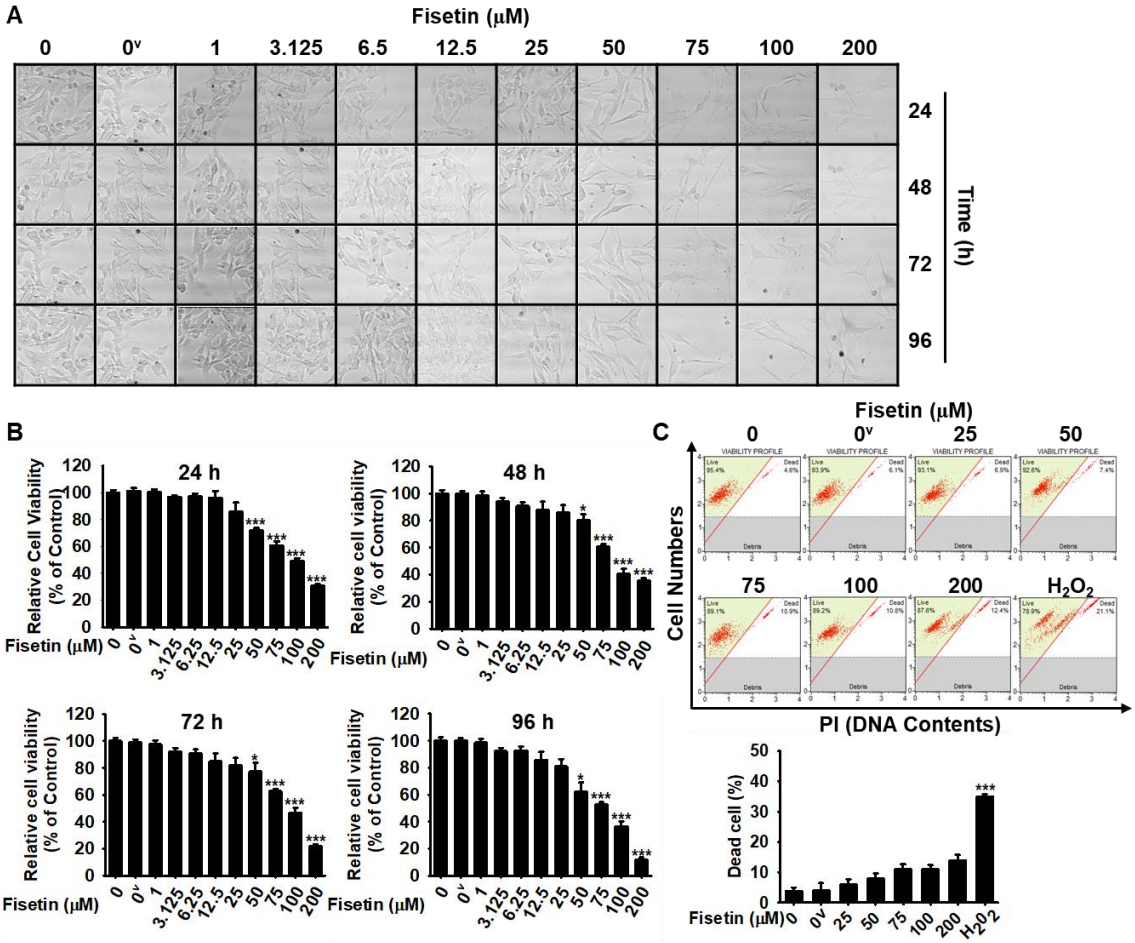

Figure 2. High concentrations of fisetin decrease the viability of B16F10 melanoma cells. (**A**) B16F10 melanoma cells were treated with the indicated concentrations (0–200 μM) of fisetin for 96 h and images were regularly captured at 24-h interval (10x). (**B**) After that, the same samples were used to determine the cell viability by MTT assay. (**C**) In a parallel experiment, the population of dead cells was analyzed by flow cytometry. The results are the average of three independent experiments; the data are expressed as the mean ± SEM (***, $p < 0.001$ and *, $p < 0.05$). 0^v represents 0.01% DMSO (vehicle control).

1.3.3 Fisetin Increases Intracellular and Extracellular Melanin Content of B16F10 Melanoma Cells

To quantify intracellular and extracellular melanin content, B16F10 melanoma cells were treated with fisetin (5 μM and 20 μM) in the presence or absence of α-MSH for 96 h. Intracellular melanin content was assessed using the cell pellet extract, and extracellular melanin content was measured by the absorbance of culture medium. Unexpectedly, as shown in Figure 3A,B, 5 μM fisetin resulted in a moderate increase in spontaneous intracellular (157.0% ± 24.8% at 72 h and 207.5% ± 8.9% at 96 h) and extracellular melanin content (316.9% ± 9.3% at 72 h and 353.4% ± 3.4% at 96 h), compared with the untreated control. Treatment with 20 μM fisetin significantly increased intracellular melanin content to 224.3% ± 19.0% at 72 h and 293.4% ± 6.3% at 96 h and extracellular melanin content to 450.7% ± 80.7% at 72 h and 426.5% ± 6.1% at 96 h. The fisetin-mediated increase of spontaneous melanin content was comparable to that induced by 500 ng/mL α-MSH, which indicates that fisetin promotes in vitro melanogenesis in B16F10 melanoma cells. We also examined the intracellular and extracellular melanin content in α-MSH-treated B16F10 melanoma cells after treatment with fisetin (5 μM and 20 μM) for 96 h. We observed that fisetin strongly increased the α-MSH-induced intracellular (Figure 3C) and extracellular (Figure 3D) melanin content in B16F10 melanoma cells in a time-dependent manner compared with those induced by α-MSH treatment alone. The maximum effect occurred at 96 h at both fisetin concentrations tested (344.5% ± 8.7% and 406.2% ± 6.8% for intracellular melanin content at 5 μM and 25 μM fisetin and 148.3% ± 4.4% and 172.3% ± 3.1% for extracellular melanin content at 5 μM and 25 μM fisetin, respectively), which was comparable with the α-MSH-induced values of 291.4% ± 5.2% for intracellular melanin content and 142.4% ± 5.9% for extracellular melanin

content. These results suggest that fisetin increases melanogenesis in B16F10 melanoma cells in both α-MSH-stimulated and unstimulated conditions.

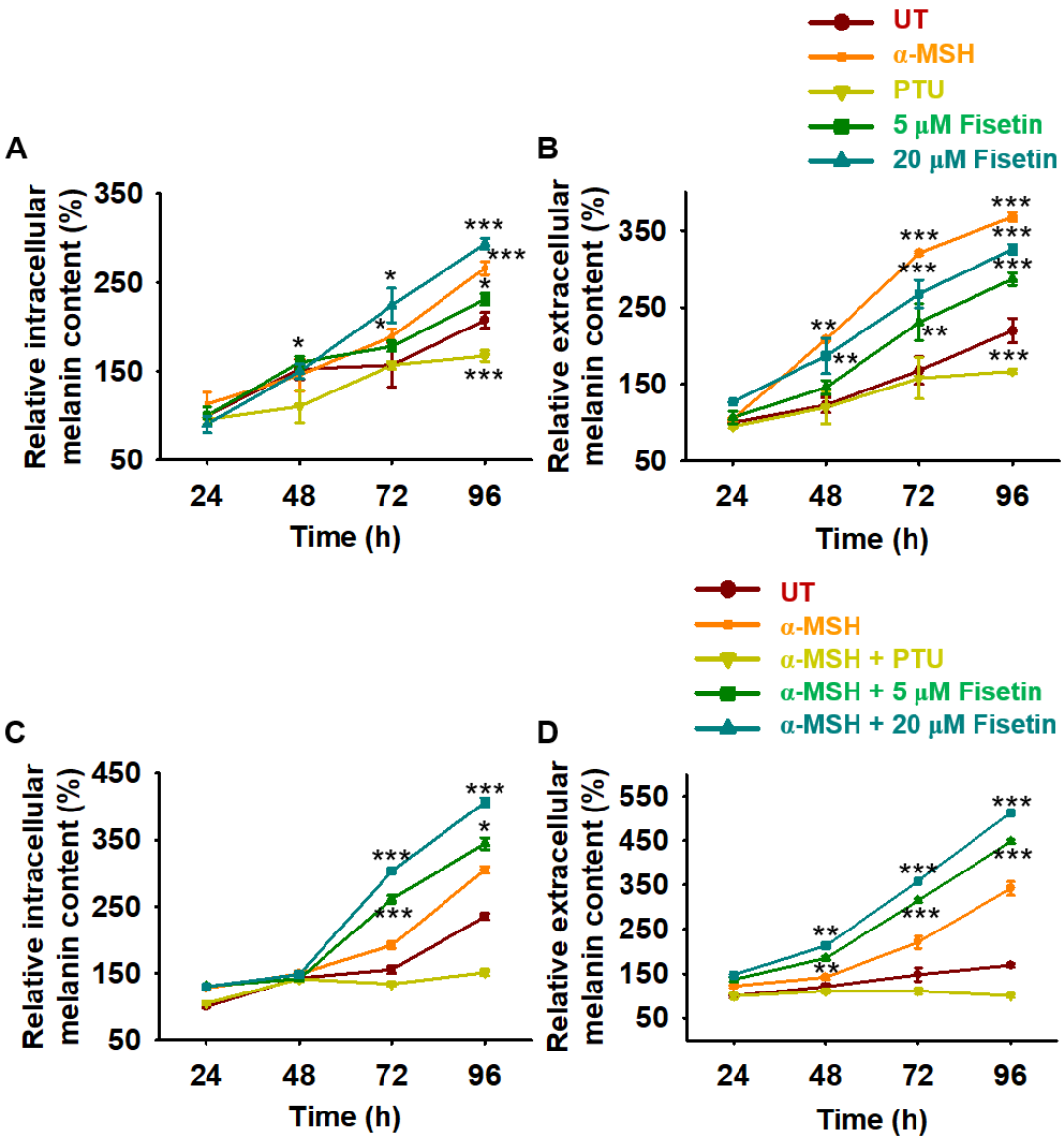

Figure 3. Fisetin increases intracellular and extracellular melanin production in B16F10 melanoma cells. (A, B) B16F10 melanoma cells were cultured at a density of 1×10^4 cells/mL in 6 well plate overnight. Then, fisetin (5 μM and 20 μM) was treated for 96 h, and the cell pellet and the culture media were collected at every 24 h. **(A)** The cell pellets were washed with ice-cold PBS and dissolved in 400 μL of 1 M NaOH containing 10% DMSO at 90 ℃ for 60 min. Then, the

absorbance was measured at 405 nm. **(B)** The culture media was directly measured at 405 nm for extracellular melanin contents. α-melanocyte stimulating hormone (α-MSH) (500 ng/mL) and PTU (200 nM) were used as the positive and the negative controls, respectively. **(C, D)** In a parallel experiment, B16F10 melanoma cells were treated with fisetin (5 μM and 20 μM) or PTU 2 h after treatment with 500 ng/mL α-MSH, and intracellular **(C)** and extracellular **(D)** melanin contents were measured at every 24 h for 96 h. The results are the averages of three independent experiments; the data are expressed as the mean ± SEM (***, $p < 0.001$, **, $p < 0.01$, and *, $p < 0.05$).

1.3.4 Fisetin Upregulates MITF and Tyrosinase Expression

As MITF is a key enzyme in the melanogenic pathway through the activation of tyrosinase activity, we examined the mRNA and protein expression of MITF and tyrosinase. B16F10 melanoma cells were treated with 20 μM fisetin and the mRNA was extracted. Fisetin significantly enhanced the expression of *MITF* and *tyrosinase* at 48 h, which completely disappeared from 72 h (Figure 4A). RT-PCR data also showed that fisetin concentration-dependently upregulated the expression of *MITF* and *tyrosinase* at 48 h and the highest concentration of fisetin (40 μM) was comparable with that of α-MSH treatment (Figure 4B). In addition, we purified the proteins after fisetin treatment for 72 h and measured the protein expression of MITF and tyrosinase. Consistent with RT-PCR data, we observed that fisetin increased the expression of both proteins in a dose-dependent manner and the highest concentration of fisetin induced the expression comparable with those of α-MSH treatment (Figure 4C). Altogether, these results indicate that fisetin increases both the mRNA and protein of MITF and tyrosinase, leading to melanogenesis.

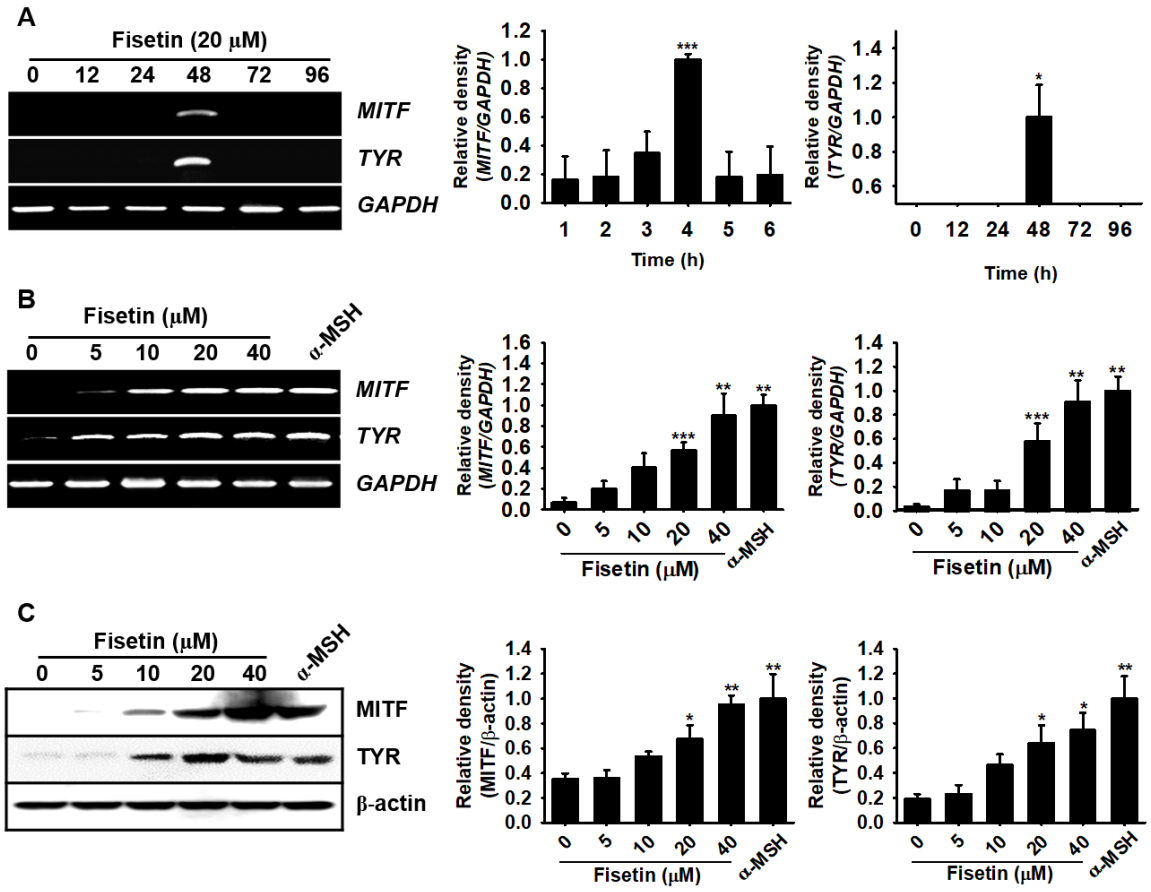

Figure 4. Fisetin increases the expression of microphthalmia-associated transcription factor (MITF) and tyrosinase (TYR) in B16F10 melanoma cells. B16F10 melanoma cells were cultured at a density of 1×10^4 cells/mL in 6 well plate overnight and then treated with the indicated concentrations of fisetin. **(A)** Time-dependent MITF and TYRexpression was detected by RT-PCR under stimulation with 20 μM fisetin for 96 h. **(B)** MITF and TYR expression was assessed 48 h after treatment with different concentrations of fisetin (0–40 μM) and 500 ng/mL α-MSH was used as a positive control. GAPDH was used as the house keeping gene for normalizing MITF and TYR expression. **(C)** B16F10 melanoma cells were treated with the indicated concentrations of fisetin for 72 h and western blotting was performed to analyze the expression of MITF and TYRprotein. β-Actin was used as a house keeping protein. The results are the average of three independent

experiments; the data are expressed as the mean ± SEM (***, $p < 0.001$, **, $p < 0.01$, and *, $p < 0.05$).

1.3.5 Fisetin Inhibits Melanogenesis in Zebrafish Larvae but Did not Affect Heart Rate

As fisetin upregulates melanogenesis in B16F10 melanoma cells, we wondered whether fisetin could also increase melanogenesis in zebrafish larvae. After 24 h postfertilization, the chorion of the larvae was manually removed and fisetin was treated for an additional 3 days. On day 4, the images and the heart rate of the larvae were measured to assess melanogenic effect and cardiotoxicity of fisetin. Consistent with data in B16F10 melanoma cells, we found that fisetin strongly increased melanogenesis in zebrafish larvae in a concentration-dependent manner, with a maximum effect (212.0% ± 41.9%) at 200 μM fisetin, compared with the untreated control (Figure 5A,B). In addition, the heart rate remained almost similar to the untreated condition (179.7 ± 3.7 beats/min) (Figure 5C). Then, we tested the melanogenic effect in the presence of α-MSH in zebrafish larvae. First, we treated PTU for 24 h to remove all pigments and then α-MSH was treated 2 h prior to the fisetin treatment (50–200 μM) for 72 h. We found that fisetin concentration-dependently upregulated α-MSH-induced melanogenesis (167.1% ± 9.7%, 189.3% ± 8.5%, and 235.1% ± 15.7% at 50, 100, and 200 μM fisetin, respectively), compared with that of α-MSH treatment alone (145.8% ± 3.2%) (Figure 5D,E), and no alteration was observed in the heart rate of the zebrafish larvae compared with the untreated conditions (Figure 5F). Therefore, these results suggest that fisetin itself upregulates melanogenesis in zebrafish larvae, without causing cardiotoxicity.

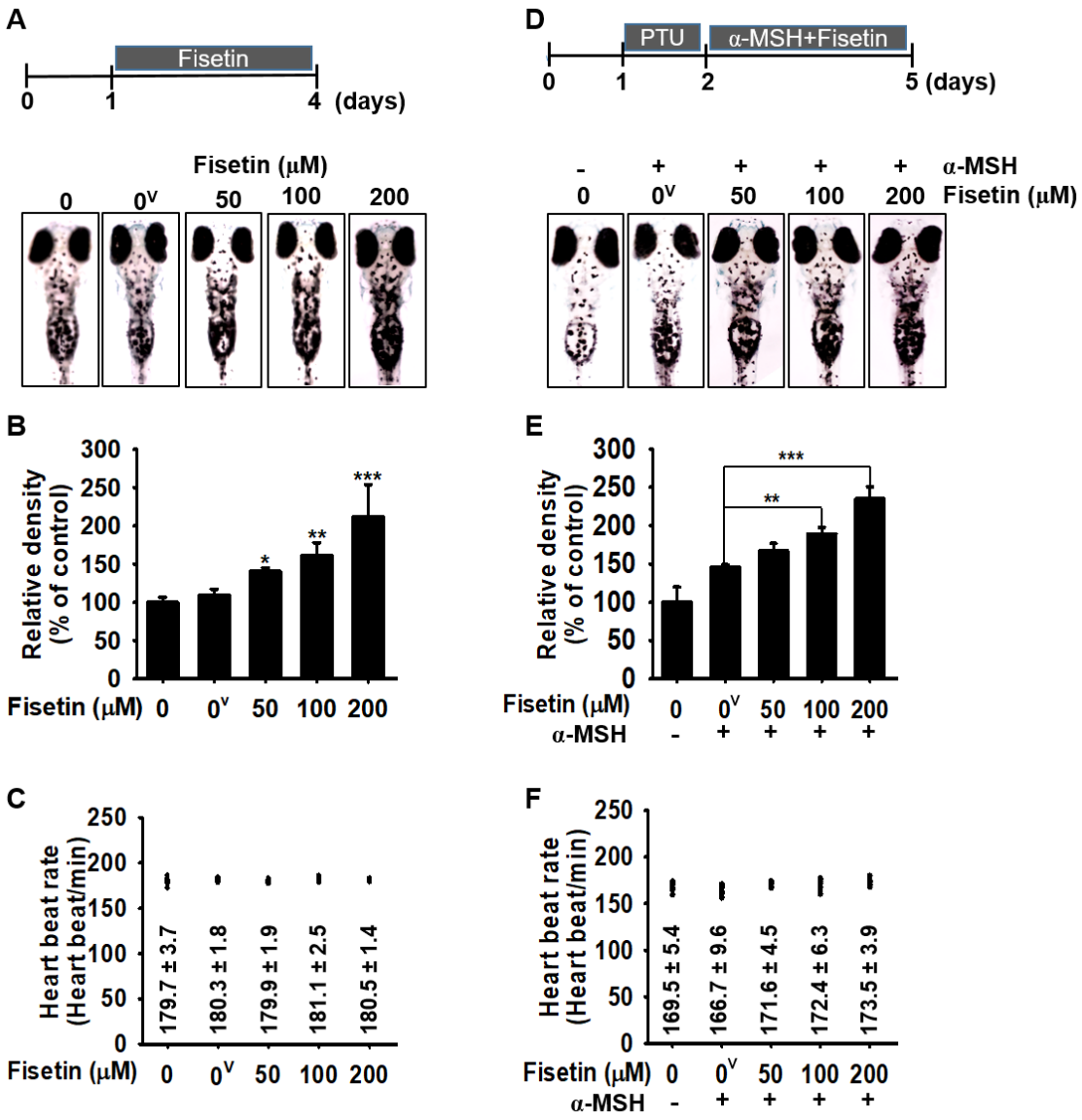

Figure 5. Fisetin increases melanogenesis in a zebrafish model. (**A**–**C**) Zebrafish larvae were manually dechorionated at 1 dpf and exposed to the indicated concentrations of fisetin for another 72 h. (**A**) Images of the zebrafish larvae were captured using Olympus microscopy (4×) and (**B**) the relative density was calculated using ImageJ software. (**C**) The heart rate of zebrafish larvae was measured to assess the cardiotoxicity of fisetin. (**D**–**F**) In a parallel experiment, 200 μM PTU was treated in zebrafish larvae for 24 h and then administrated with α-MSH 2 h before fisetin

treatment for 72 h. (**D**) The images were captured and (**E**) the relative density was calculated using ImageJ software. (**F**) The heart rate of zebrafish was used to measure the cardiotoxicity of the combined treatment. The results are the average of three independent experiments; the data are expressed as the mean ± SEM (***, $p < 0.001$, **, $p < 0.01$, and *, $p < 0.05$).

1.3.6 Fisetin Possibly Binds to GSK-3β

GSK-3β is a constitutively active serine/threonine protein kinase that is involved in the hormonal control of glucose homeostasis, Wnt/β-catenin signaling, transcription factor regulation, and microtubules (Beurel et al., 2015). To investigate the structural binding of fisetin to GSK-3β, we performed computational docking of GSK-3β-fisetin interactions. Based on the interacting docking score, binding of amino acids with hydrogen bonds, and hydrogen bond distances, four predicted molecular docking complex models are shown in Table 1. In docking pose 1, the major residue of GSK-3β that interacts with fisetin is GLY34, at a distance of 2.191 Å, with a −7.9 docking score. Docking pose 2 and 3 also proposed that fisetin docked to GSK-3β through VAL101, ARG107, and ASP166 at a distance of 2.373 Å, 2.346 Å, and 2.247 Å (docking score: −7.9) and ARG107 of a distance of 1.029 Å (docking score: −7.9) through hydrogen bonding. Significant hydrogen bonding was not found in docking pose 4, but the docking score was −7.7. As shown in Figure 6, fisetin docked into the pocket of GSK-3β in four major ways, which displayed close contact with hydrogen bonds in the most energetically favorable simulation. The ATP-binding site and the activation loop of GSK-3β lie between the two domains near the hinge. Our molecular docking models showed that fisetin binds to GSK-3β at a non-ATP-competitive binding site near to the hinge regions (Figure 6). To compare the GSK-3β binding sites of fisetin

with clinically available drugs, we performed the docking simulation with tideglusib (NP-12), enzastaurin (LY317615), and LY2090314. According to the molecular docking data, tideglusib, which is designed for the treatment of AD (del Ser et al., 2013) and progressive supranuclear palsy (PSP), bound irreversibly to the non-ATP-competitive GSK-3β site (Tolosa et al., 2014) (Figure 7). The GSK-3β binding site of fisetin was also much more similar to that of tideglusib, which indicated that fisetin also binds irreversibly to the non-ATP-competitive GSK-3β site. Enzastaurin, which was originally developed as a selective inhibitor for PKCβ (Graff et al., 2005), and indirectly reduced the phosphorylation of GSK-3β through binding to ATP-binding site (Figure 7). The GSK-3 inhibitor LY2090314, which is used for the treatment of cancer (Zamek-Gliszczynski et al., 2013), selectively targets the ATP-binding site as a competitive inhibitor (Figure 7). These data indicate that fisetin binds to a different binding site of GSK-3β than those previously identified.

Table 1. Classification of results gained from the docking of fisetin into glycogen synthase kinase-3β (GSK-3β).

Receptor	Docking Pose	Docking Score	Binding A.A. * (H-Bond) **	H-Bond Distance (Å)
GSK-3β (1J1B)	1	−7.9	GLY34	2.191
	2	−7.9	VAL101	2.373
			ARG107	2.346
			ASP166	2.247
	3	−7.9	ARG107	1.029
	4	−7.7	N.F.	N.F.

* A.A.: amino acid; ** H-bond: hydrogen bond.

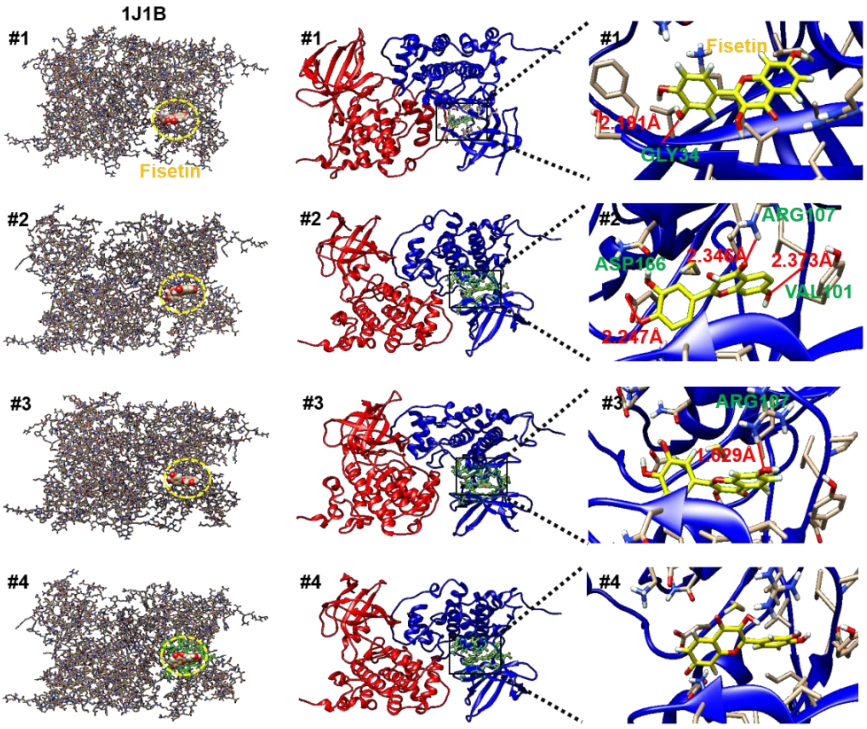

Figure 6. Four molecular docking models show the binding site of fisetin and GSK-3β (PDB ID: 1J1B).

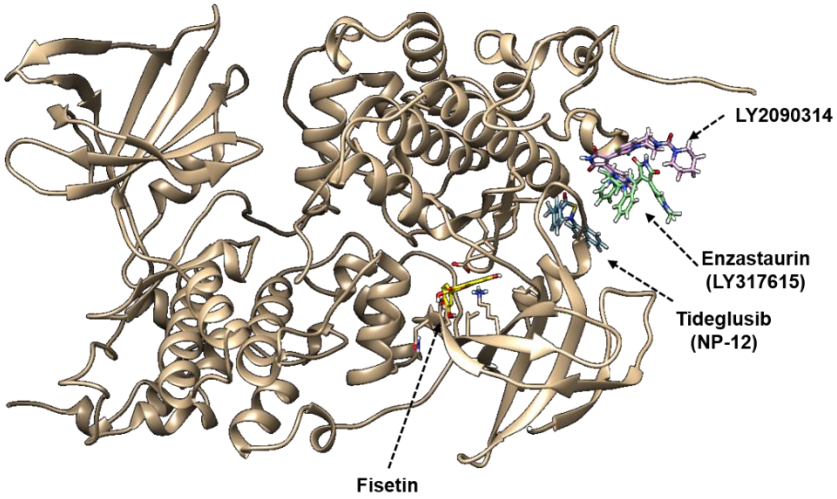

Figure 7. The molecular docking comparison of clinical GSK-3β inhibitors and fisetin with GSK-3β (PDB ID: 1J1B). The binding site of fisetin GSK-3β was compared with the clinically available drugs, tideglusib (NP-12), enzastaurin (LY317615), and LY2090314.

1.3.7 Activation of β-Catenin Positively Stimulates Fisetin-Mediated Melanogenesis

As the molecular docking prediction showed that fisetin binds to GSK-3β, we hypothesized that it promotes the release of β-catenin from the GSK-3β complex and thereby prevents the proteosomal degradation of β-catenin, leading to an increase in melanogenesis. Therefore, we investigated whether fisetin blocked the degradation of β-catenin and subsequently enhanced its nuclear translocation. Western blotting analysis confirmed that fisetin upregulated β-catenin expression in the cytosol and increased its nuclear translocation (Figure 8A). To evaluate the functional effect of β-catenin on fisetin-mediated melanogenesis, the intracellular and extracellular melanin content was detected in the presence of the Wnt/β-catenin inhibitor, FH535. Both fisetin-induced intracellular and extracellular melanin content significantly decreased in the presence of FH535 (Figure 8B,C), which suggested that fisetin-mediated melanogenesis was promoted by the

activation of β-catenin. Interestingly, FH535 not only decreased fisetin-induced melanogenesis, but also α-MSH-mediated melanogenesis, which suggested that β-catenin plays a pivotal role in both fisetin- and α-MSH-induced melanogenesis. To confirm these results, zebrafish larvae were treated with 10 μM FH535 for 2 h and then exposed to fisetin or α-MSH for a further 72 h (Figure 8D). Consistent with the anti-melanogenic effects of FH535 in B16F10 cells, FH535 significantly downregulated both fisetin- and α-MSH-induced melanogenesis in zebrafish larvae without any change of the heart rate (Figure 8E), which confirmed that Wnt/β-catenin is a key molecule in both fisetin- and α-MSH-induced melanogenesis without any toxicity. Collectively, these results showed that fisetin suppresses active GSK-3β, which blocks β-catenin degradation and leads to melanogenesis.

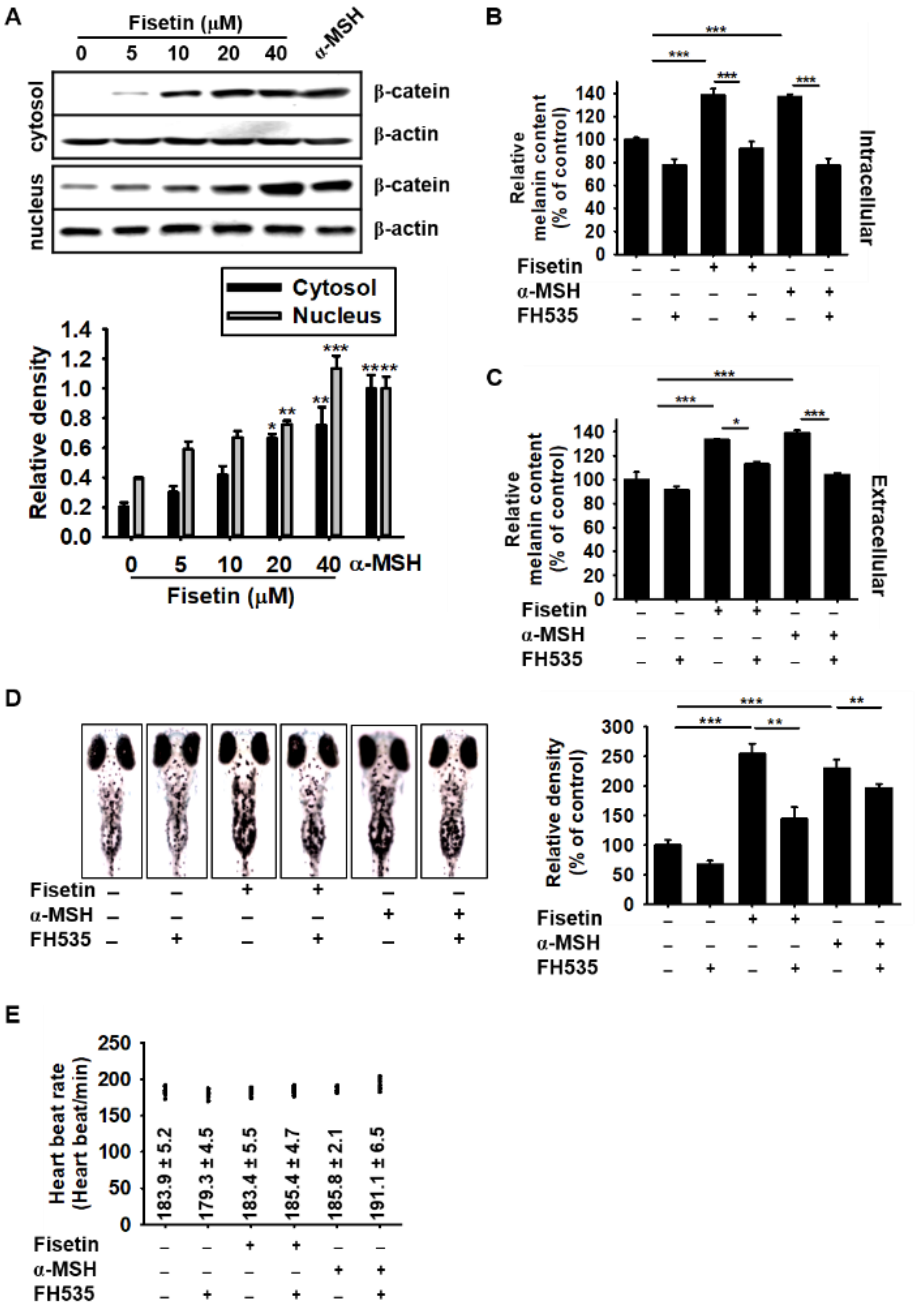

Figure 8. Fisetin-induced melanogenesis is associated with the Wnt/β-catenin signaling pathway. (A) B16F10 melanoma cells were treated with the indicated concentrations of fisetin for 48 h and the expression of β-catenin in the cytosol (top) and the nucleus (bottom) was measured by western blotting analysis. β-Actin and nucleolin were used as the house keeping proteins. **(B,C)**

The β-catenin inhibitor (10 μM), FH535, was pretreated for 2 h in B16F10 melanoma cells and then treated with 20 μM fisetin or 500 ng/mL α-MSH. After incubation of 72 h, the intracellular **(B)** and extracellular **(C)** melanin contents were examined. **(D,E)** Zebrafish larvae were manually dechorionated at 24 h and then 200 μM PTU was treated in zebrafish larvae for 24 h. Fisetin (200 μM) or α-MSH (1 mg/mL) were treated 72 h after treatment with FH535 for 2 h. **(D)** The images were collected at day 5 (right) and the relative density was calculated using ImageJ software (left). **(E)** The heart rate of the zebrafish was used to measure the toxicity of the combined treatment. The results are the average of three independent experiments; the data are expressed as the mean ± SEM (***, $p < 0.001$, **, $p < 0.01$, and *, $p < 0.05$).

1.4 Discussion

Fisetin is a bioactive diphenylpropane flavone structure that contains three aromatic rings with four additional hydroxyl groups and one oxo group (Khan et al., 2013a). It is abundant in various types of plants, but the natural biosynthesis of fisetin has not yet been described (Kashyap et al., 2018). Fisetin is a powerful chemopreventive and chemotherapeutic candidate in a variety of cancers and ischemia-induced brain damage through its anti-oxidant activity (Khan et al., 2013a). In addition, He et al. reported that orally administered fisetin could cross the blood-brain barrier and lead to the promotion of long-term synaptic potentiation in the hippocampus (He et al., 2018). Although fisetin has been evaluated for the beneficial pharmacological effects in animal models relevant to human diseases, whether fisetin positively or negatively regulates melanogenesis has still been contradictory (Shon et al., 2016; Takekoshi et al., 2014).

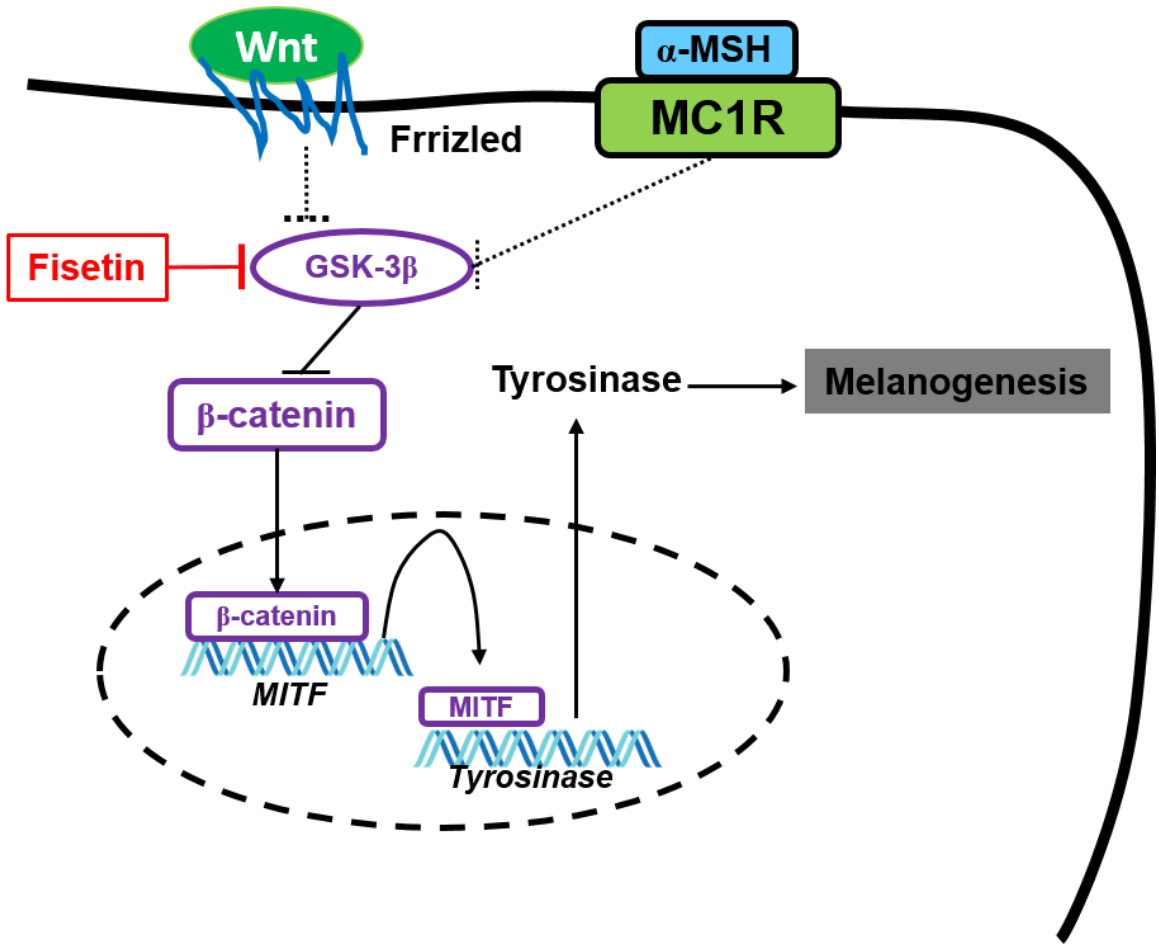

Figure 9. The possible mechanism of fisetin promoting melanogenesis. Fisetin possibly binds to GSK-3β and subsequently inhibits its activity, which releases β-catenin. Free β-catenin moves to the nucleus and binds in the specific promoter region of MITF, which transactivates MITF expression, resulting in stimulation of tyrosinase-mediated melanogenesis.

Previously, the regulation of melanin synthesis by oxidation state was evaluated, which subjected melanocytes to the release of melanin from melanosomes (Denat et al., 2014). Tyrosinase is a key component in melanogenesis since it catalyzes two major reactions in the Raper-Mason pathway. In one reaction, L-tyrosine is converted into its corresponding dopaquinone by the cresolase activity of tyrosinase and then subsequently dopaquinone is non-enzymatically converted to

DOPA accompanied by O^{2-} Generation (Tomita et al., 1984). In the other reaction, dopaquinone is also produced from L-DOPA by the catecholase activity of tyrosinase (Land et al., 2004). Therefore, we hypothesized that a powerful antioxidant, fisetin, as a negative regulator of melanogenesis in vitro and in vivo. As expected, high concentrations of fisetin (≥100 μM) inhibited in vitro mushroom tyrosinase activity, approximately 25%; however, the tyrosinase inhibition activity was low at below μM 25 fisetin, approximately below 10%. In addition, our molecular docking data confirmed that no direct binding was found between mushroom tyrosinase and fisetin, which indicates that fisetin could indirectly, inhibits melanin formation process. This discrepancy might be due to the initiation of cresolase and catecholase activity of tyrosinase enzyme at different time points. As Fenoll et al. (Fenoll et al., 2002) mentioned, addition of 3-methyl-2-benzothiazolinone hydrazine (MBTH), a potent nucleophile which traps enzyme-generated o-quinones in order to render MBTH-quinone adduct will provide a reliable measuring tool for determining the cresolase and catecholase activity of tyrosinase from fisetin. However, unexpectedly, fisetin (≤20 μM) significantly promoted intracellular melanin content and its release in B16F10 cells through the upregulation of MITF and tyrosinase expression, and also enhanced melanogenesis in zebrafish larvae. In addition, our molecular docking data present the first indication that fisetin targets GSK-3β, which consequently prevents the degradation of β-catenin and leads to the stimulation of melanogenesis (Figure 9). Nevertheless, whether fisetin directly regulates melanogenesis through human tyrosinase is disputable because mouse and human tyrosinase amino acid sequences are approximately 80% homologous.

Skin pigmentation provides the most important photoprotective effect against UV radiation (D'Mello et al., 2016) and it is a crucial factor in the removal of pigment formation from the skin by the cosmetic industry. Therefore, numerous attempts investigated to understand the underlying

molecular mechanism that governs pigment production and their transfer into the adjacent keratinocytes (Rzepka et al., 2016; Videira et al., 2013). In particular, a rate-limiting enzyme of melanogenesis, tyrosinase, promotes the generation of O_2^- in its catalytic response, which produces DOPA and dopaquinone (Tomita et al., 1984), and suggested that the balance between the pro-oxidant and antioxidant state determines melanogenesis by the regulation of tyrosinase activity. At present, many antioxidants exerted anti-melanogenic activity through the suppression of tyrosinase and its regulatory genes, such as *MITF* (Liu-Smith and Meyskens, 2016). As expected, fisetin, a powerful antioxidant slightly inhibited in vitro mushroom tyrosinase activity in the current study; in contrast, fisetin significantly increased intracellular and extracellular melanin contents in B16F10 cells and melanogenesis in a zebrafish larva model. This showed that fisetin directly regulated the intracellular signaling pathways and resulted in the positive regulation of melanogenesis. Consistent with the present data, Takekoshi et al. previously found that some flavonoids with hydroxyl group of the phenol ring (at 4′ in b, Figure 1A) such as fisetin (20 μM) increased melanin content and tyrosinase activity in human melanoma cells (Takekoshi et al., 2014). On the other hand, Son et al. reported that high concentrations of fisetin at over 50 μM decreased intracellular and extracellular melanin content in murine B16F10 melanoma cells (Shon et al., 2016). We believe that the discrepancy on the dual effect of fisetin is dependent on its concentration because our unpublished data showed that high concentration of fisetin decreased melanogenesis in B16F10 melanoma cells (at 40 μM) and zebrafish larvae (at 400 μM). In addition, Kumagai et al. revealed that fisetin at 10 μM had no influence on melanogenesis and fisetin with methyl group significantly increased melanogenesis, which they indicate that methyl group is a key regulator for melanogenesis (Kumagai et al., 2011); however, the data are confident that methylfisetin at 10 μM more strongly upregulates melanogenesis than fisetin at 10 μM but fisetin

at 20 μM significantly increases melanogenesis. Collectively, fisetin bilaterally regulates melanogenesis in a concentration-dependent manner. We need further studies to confirm concentration-dependent bilateral effect of fisetin on melanogenesis.

MC1R is a G protein-coupled receptor, which activates AC and then leads to an increase in cAMP in response to α-MSH, which results in the activation of PKA (Graff et al., 2005). Finally, PKA increased tyrosinase expression through the activation of CREB-mediated MITF (Rzepka et al., 2016). This signaling pathway is the most common and crucial signaling pathway in melanogenesis. In the current study, we postulated that fisetin stimulated melanogenesis in vitro and in vivo through the activation of the cAMP-dependent signaling pathway, because our data showed that fisetin markedly increased tyrosinase, resulting from MITF expression at transcriptional and translational levels, which suggests that fisetin does not pass through the cAMP-dependent pathway of melanogenesis. The other negative regulatory pathway is the ERK signaling pathway, which induces the phosphorylation of ERK1/2 through the activation of the c-kit-Ras-Raf axis and consequently enhances proteasome-mediated MITF degradation, which resulted in the anti-melanogenic effect. We also found that ERK1/2 was not a direct target of fisetin in accordance with the molecular docking prediction (data not shown). In addition, MITF transcription is upregulated by activating the Wnt/β-catenin signaling pathway, through the inhibition of GSK-3β, which results in melanogenesis. The accumulation of β-catenin stimulates TCF/LEF, which consequently transactivates the MITF promoter, dependent on TCF/LEF DNA consensus elements (Widlund et al., 2002). Interestingly, the molecular docking analysis revealed that fisetin strongly binding to GSK-3β at the non-ATP-competitive binding site and thereby enabled the release of β-catenin from the destructive complex. We also found that fisetin significantly increased intracellular β-catenin expression in B16F10 cells and that the inhibition of

β-catenin, suppressed fisetin-mediated melanogenesis in B16F10 melanoma cells and zebrafish larva, which showed that fisetin influences melanogenesis through the activation of β-catenin via the inhibition of GSK-3β.

GSK-3β is an ubiquitously expressed serine/threonine protein kinase that is involved in glycogen synthesis in response to insulin (Eldar-Finkelman et al., 1996) and energy metabolism, neuronal cell development, and body pattern formation (Kockeritz et al., 2006). Consistent with our data, a previous study determined that GSK-3β negatively regulated melanogenesis through the induction of the proteasome-mediated degradation of β-catenin, which caused the suppression of tyrosinase expression (Widlund et al., 2002). However, a more recent study showed that GSK-3β is crucially implicated in AD and PD through the direct interaction with tau, β-amyloid, and α-synuclein (Lei et al., 2011), which suggested that GSK-3β inhibition has become an attractive target for therapeutic intervention against AD and PD. In addition, owing to the conserved nature of the ATP-binding sites of GSK-3β, the drugs that effectively target GSK-3β act at nanomolar concentrations and non-ATP-competitive GSK-3β inhibitors act at relatively high (micromolar) concentrations (Pandey and DeGrado, 2016). Recently, Nabavi et al. broadly examined the chemistry, sources, bioavailability, and clinical impact of fisetin, and reported that fisetin was the potent neuroprotective flavonoid against AD and PD (Nabavi et al., 2016). Therefore, fisetin is important, not only for the induction of melanogenesis, but may also provide a good platform to cure neurodegenerative diseases, including AD and PD. Other than AD and PD, GSK-3β has emerged as an interesting therapeutic target in pathological mechanisms, including inflammatory diseases, cancers, cardiovascular diseases, diabetes, and bone disorders (Beurel et al., 2015). Previous studies of John et al. revealed that GSK-3β inhibition prevent melanoma cell migration by downregulating the expression of N-cadherin and FAK phosphorylation (John et al., 2012)

indicating the possibility of using fisetin as therapeutic agent for metastatic melanoma. On the other hand, fisetin can be used as a remedy for hypo-pigmentary disorders such as vitiligo with the minimum side effects. Therefore, further study is needed to evaluate the various functions of fisetin in a broad spectrum of diseases.

1.5 Conclusions

We investigated the fisetin-mediated promotion of melanogenesis in B16F10 cells and zebrafish larvae through binding to GSK-3β at a non-ATP-competitive binding site, and the subsequent release of β-catenin, which promotes MITF-mediated tyrosinase activation. Although fisetin caused an unexpected increase in melanogenesis, fisetin may be useful for the treatment of many different diseases such as vitiligo and the inhibitory effect on GSK-3β is also paramount important

2 Chapter2

Fisetin-mediated β-catenin Activation Inhibits Lipopolysaccharide-induced Inflammatory Response by Suppressing NF-κB Activation, Leading to a Decrease in Endotoxic Shock

Abstract

Fisetin is a naturally occurring flavonoid that possesses several pharmacological benefits including anti-inflammatory activity. However, its precise anti-inflammatory mechanism is not clear. In the present study, we found that fisetin significantly inhibited the expression of proinflammatory mediators, such as nitric oxide (NO) and prostaglandin E_2 (PGE_2), and cytokines, such as interleukin-6 (IL-6) and tumor necrosis factor-alpha (TNF-α), in lipopolysaccharide (LPS)-stimulated RAW 264.7 macrophages. Additionally, fisetin attenuated LPS-induced mortality and abnormalities in zebrafish larvae and normalized the heart rate. Fisetin decreased the recruitment of macrophages and neutrophils to the LPS-microinjected inflammatory site in zebrafish larvae, concomitant with a significant downregulation of proinflammatory genes, such as *inducible NO synthase* (*iNOS*), *cyclooxygenase-2a* (*COX-2a*), *IL-6*, and *TNF-α*. Fisetin inhibited the nuclear localization of nuclear factor-kappa B (NF-κB), which reduced the expression of proinflammatory genes. Further, fisetin inactivated glycogen synthase kinase 3β (GSK-3β) via phosphorylation at Ser9, and inhibited the degradation of β-catenin, which consequently promoted the localization of β-catenin into the nucleus. The pharmacological inhibition of β-catenin with FH535 reversed the fisetin-induced anti-inflammatory activity and restored NF-κB activity, which indicated that fisetin-mediated activation of β-catenin results in the inhibition of LPS-induced NF-κB activity. In LPS-microinjected zebrafish larvae, FH535 promoted the migration of macrophages to the yolk sac and decreased resident neutrophil counts in the posterior blood island and induced high expression of *iNOS* and *COX-2a*, which was accompanied by the inhibition of fisetin-induced anti-inflammatory activity. Altogether, the current study confirmed that the dietary flavonoid, fisetin, inhibited LPS-induced inflammation and endotoxic shock through a crosstalk between GSK-3β/β-catenin and the NF-κB signaling pathways.

Keywords: Fisetin; Inflammation; Endotoxic shock; β-Catenin; Nuclear factor-kappa B

2.1 Introduction

Phagocytes, including macrophages and neutrophils, are the front-line immune defense cells that initiate inflammatory responses against invading pathogens (Prame Kumar et al., 2018). However, bacterial endotoxins, including lipopolysaccharide (LPS) lead to dysregulated immune responses and promotion of tissue-damaging responses (Prame Kumar et al., 2018; Tursi and Elisei, 2019). The chronic status of dysregulated immune responses is a significant cause of many inflammatory disorders, including cancer, cardiovascular diseases, and autoimmune diseases (Tursi and Elisei, 2019).

LPS is an integral component of the outer membrane of gram-negative bacteria (Rathinam et al., 2019). During infection, LPS is released, particularly, as a result of antibiotic treatment (Munford, 2008). Previous studies have demonstrated that the toll-like receptor 4 (TLR4) signaling pathway is involved in LPS-induced inflammation (Jackie et al., 2019; Rathinam et al., 2019). In the intracellular domain of TLR4, myeloid differentiation primary response gene 88 (MyD88) activates the mitogen-activated protein kinase (MAPK) by recruiting interleukin-1 receptor-associated kinase 4 (IRAK-4) and tumor necrosis factor receptor-associated factor 6 (TRAF6), which subsequently activates the canonical inhibitor κB (IκB) kinase (IKK) to degrade IκBα. Ultimately, IκBα degradation promotes the nuclear translocation of free nuclear factor-kappa B (NF-κB) heterodimers, p50 and p65, thereby enhancing the transcriptional activities of NF-κB (Fang et al., 2018; Walsh et al., 2015). NF-κB is a well-characterized ubiquitous transcription factor that positively regulates the expression of inflammatory genes, such as *inducible nitric oxide synthase* (*iNOS*), *cyclooxygenase-2* (*COX-2*), *interleukin-6* (*IL-6*), and *tumor necrosis factor-α* (*TNF-α*) (Lawrence, 2009; Tornatore et al., 2012). Therefore, targeting the NF-κB signaling pathway has been considered as a promising therapeutic strategy against LPS-induced

inflammatory disorders (Gupta et al., 2010).

β-Catenin acts as a central mediator in intracellular signal transduction via the binding of extracellular Wnt to its receptors, such as frizzled (FZD) and low-density lipoprotein receptor-related protein (LRP) (MacDonald and He). In the absence of Wnt, β-catenin is constitutively targeted for proteasomal degradation via the formation of a destructive complex with adenoma polyposis coli (APC), axin, glycogen synthase kinase-3β (GSK-3β), and casein kinase I (CKI) (Stamos and Weis, 2013b). In the presence of Wnt, GSK-3β is inactivated due to phosphorylation at Ser9, and thereby promoting β-catenin stabilization and nuclear translocation (Kisoh et al., 2017). Although both the Wnt/β-catenin and NF-κB signaling pathways are conserved throughout mammalian development, the pathways independently regulate cell proliferation, cell survival, and cell differentiation. Nevertheless, a previous study on bacteria-colonized intestinal epithelial cells revealed that the overexpression of active β-catenin via GSK-3β inhibition reduced NF-κB activity and resulted in the downregulation of target inflammatory genes, thereby indicating that β-catenin downregulates the NF-κB-mediated inflammatory response (Deng et al., 2002). Recently, Ma et al. confirmed that the crosstalk between Wnt/β-catenin and NF-κB positively or negatively modulates inflammation in a cell type- and/or gene-specific manner (Ma and Hottiger, 2016), which suggests that NF-κB activation is noncanonically regulated through the Wnt/β-catenin signaling pathway. Agonists of the Wnt/β-catenin signaling pathway could thus serve as promising anti-inflammatory candidates in NF-κB-induced inflammatory disorders, such as septic shock.

Flavonoids exhibit many biological activities, including anti-inflammatory, anti-oxidant, anti-bacterial, and anti-allergic effects (Kumar and Pandey, 2013). Among the bioactive flavonoids, fisetin (3,7,3′,4′-tetrahydroxyflavone) isolated from fruits and vegetables, including strawberry, apple, persimmon, grape, onion, and cucumber, possesses potent anti-oxidant and anti-cancer

activities (Khan et al., 2013b). In addition, many previous studies have demonstrated that fisetin exerts its anti-inflammatory activity via inhibiting canonical NF-κB activation (Huang et al., 2018b; Sahu et al., 2016). Recently, we found that fisetin directly binds to GSK-3β at non-ATP-binding sites, thereby promoting the nuclear localization of β-catenin via the inhibition of GSK-3β during melanogenesis (Molagoda et al., 2020b). Such findings indicated that fisetin could regulate noncanonical NF-κB activity via β-catenin activation. Nevertheless, the anti-inflammatory effect of fisetin against LPS-induced inflammation has not been studied. In the current study, we sought to determine whether fisetin inhibited LPS-induced inflammation in RAW 264.7 macrophages and endotoxic shock in zebrafish larvae via a crosstalk between GSK-3β/β-catenin and NF-κB pathways.

2.2 Material and Methods

2.2.1 Reagents and Antibodies

Fisetin, 3-(4,5-Dimethylthiazol-2-yl)-2,5-diphenyl-tetrazolium bromide (MTT), 1-phenyl-2-thiourea (PTU), and methylene blue were obtained from Sigma Chemical Co. (St. Louise, MO, USA). Mouse anti-human antibodies against iNOS (sc-7271), COX-2 (sc-19999), p50 (sc-8414), p65 (sc-8008), GSK-3β (sc-81462), phospho (p)-GSK-3β at Ser9 (sc-37800), β-catenin (sc-59737), β-actin (sc-69879), nucleolin (sc-13057), and peroxidase-labeled anti-mouse immunoglobulins were purchased from Santa Cruz Biotechnology (Santa Cruz, CA, USA). Peroxidase-labeled anti-rabbit antibody was purchased from KOMA Biotechnology (Seoul, Republic of Korea). 2,5-Dichloro-N-(2-methyl-4-nitrophenyl) benzenesulfonamide (FH535) was obtained from Tocris (Bristol, UK). Dulbecco's Modified Eagle Medium (DMEM), fetal bovine serum (FBS), antibiotic mixture, and trypsin-ethylenediaminetetraacetic acid (EDTA) solution were purchased from WELGENE (Gyeongsan, Gyeongsangbukdo, Republic of Korea). Alexa Fluor® 488, Alexa Fluor® 647, and goat anti-rabbit secondary antibody were purchased from Abcam (Cambridge, MA, UK). Dako faramount aqueous mounting solution was purchased from Dako (Carpinteria, CA, USA). All other chemicals were purchased from Sigma Chemical Co.

2.2.2 Cell Culture and Viability

RAW 264.7 macrophages were obtained from American Type Culture Collection (ATCC, Manassas, VA, USA) and cultured in DMEM supplemented with 5% FBS at 37℃ in 5% CO_2. For the analysis of cell viability, the cells were seeded at a density 1×10^5 cells/mL in 24 well plate and incubated with the indicated concentrations of fisetin. After 24-h incubation, MTT solution was added to each well and incubated for 0.5 h at 37℃. Following the media removal, dimethyl sulfoxide was added and then gently shaken for 10 min at room temperature. Dissolved formazan

was transfer into 96 well plate and absorbance was measured at 540 nm with a microplate spectrophotometer (BioTek Instruments Inc., Winooski, VT, USA).

2.2.3 Flow Cytometry Analysis

RAW 264.7 macrophages were seeded at a density of 1×10^5 cells/mL overnight and then treated with the indicated concentrations of fisetin for 24 h. After harvesting, the cells were washed with ice-cold phosphate-buffered saline (PBS) and incubated with Muse® cell count and viability kit (Luminex Co., Austin, TX, USA) for 10 min. Cell count and viability was measured by Muse® Cell Cycler (Luminex Co.).

2.2.4 Isolation of Total Cellular RNA from RAW 264.7 Macrophages and RT-PCR

Total RNA was isolated from RAW 264.7 macrophages using easy-BLUE™ total RNA extraction kit (iNtRON Biotechnology, Seongnam, Gyeonggido, Republic of Korea) according to the manufacturer's instruction. The RNA was reverse-transcribed by Moloney murine leukemia virus (MMLV) reverse transcriptase kit (BIONEER, Daejeon, Republic of Korea). In brief, synthetic cDNA was amplified using specific primers of *iNOS* (199 bp) sense 5′-CCT CCT CCA CCC TAC CAA GT-3′ and anti-sense 5´-CAC CCA AAG TGC TTC AGT CA-3′; *COX-2* (141 bp) sense 5′-TGC TGT ACC AGC AGT GGC AA-3′ and anti-sense 5′-GCA GCC ATT TCC TTC TCT CC-3′; *TNF-α* (276 bp) sense 5′-ATG AGC ACA GAA AGC ATG AT-3′ and anti-sense 5′-TAC AGG CTT GTC ACT CGA AT-3′; *IL-6* (141 bp) sense 5′-AAG TGC ATC ATC GTT GTT TTC A-3′ and anti-sense 5′-GAG GAT ACC ACT CCC AAC AG-3′; and *GAPDH* (123 bp) sense 5′- AGG TCG GTG TGA ACG GAT TTG-3′ and anti-sense 5′-TGT AGA CCA TGT AGT TGA GGT CA-3′ (Molagoda et al., 2019a). The following PCR conditions were applied for PCR amplification: *iNOS*, *COX-2*, and *IL-6*: 25 cycles of denaturation at 95℃ for 45 s, annealing at 55℃ for 45 s, and

extended at 72℃ for 1 min, *TNF-α* 25 cycles of denaturation at 95℃ for 45 s, annealing at 53℃ for 45 s, and extended at 72℃ for 1 min. *GAPDH* was used as an internal control to evaluate relative expression of *iNOS, COX-2*, *IL-6*, and *TNF-α*.

2.2.5 Western Blot Analysis

Total cellular protein extracts were prepared by RIPA lysis buffer (iNtRON Biotechnology). The total protein lysates were centrifuged at 16,000 g at 4℃ for 20 min. In a parallel experiment, cytoplasmic and nuclear proteins were prepared using NE-PER^{TM} nuclear and cytosolic extraction reagents (Pierce, Rockford, IL, USA). Protein concentrations were measured by a Bio-Rad protein assay kit (Bio-Rad, Hercules, CA, USA) and immediately used for western blotting. Briefly, equal amount of protein was separated on SDS-polyacrylamide gels, transferred to polyvinylidene fluoride membrane (PVDF, Thermo Fisher Scientific, Waltham, MA, USA), and immunoblotted with the indicated antibodies. Each protein was detected using an enhanced chemiluminescence plus kit (Thermo Fisher Scientific). β-Actin and nucleolin was used as the internal control for total and nuclear protein, respectively

2.2.6 NO Assay

RAW 264.7 macrophage (1×10^5 cells/mL) were seeded into 24-well plates and treated with the indicated concentrations of fisetin for 2 h prior to the stimulation with 500 ng/mL LPS for 24 h. Supernatants were collected and assayed for NO production by Griess reagent. In brief, the samples were mixed with Griess reagent (1% sulfanilamide in 5% phosphoric acid and 0.1% naphthyl ethylenediamine dihydrochloride) and then incubated at room temperature for 30 min. The absorbance was measured at 540 nm by a microplate spectrophotometer (BioTek Instruments Inc.). Amount of NO was calculated according to the sodium nitrite standard concentrations.

2.2.7 Measurement of IL-6, TNF-α and PGE_2

Enzyme linked immunosorbent assay (ELISA) kits were used to detect the expression levels of IL-6 (Thermo Fisher Scientific), TNF-α (BD Pharmingen, San Diego, CA, USA), and PGE_2 (Cayman Chemicals, Ann Arbor, MI, USA) according to the manufacturer's instructions. Briefly, RAW 264.7 macrophages (1×10^5 cells/mL) were plated in 24-well plates and pretreated with the indicated concentrations of fisetin for 2 h prior to stimulation with 500 ng/mL LPS for 24 h. Supernatant was collected and used for each ELISA.

2.2.8 Immunostaining

RAW 264.7 macrophages (1×10^4 cells/mL) were seeded on 3% gelatin-coated coverslips overnight and treated with the indicated concentrations of fisetin for 2 h prior to the exposure with LPS for 1 h. The cells were fixed with 4% paraformaldehyde (PFA) for 10 min at 37℃, washed three times with ice-cold PBS, and permeabilized with 0.1% Triton X-100 for 10 min at room temperature, followed by washing with ice-cold PBS containing 0.1% tween 20 (PBST) for 5 min. The cells were blocked with 10% donkey serum and incubated with p65 and β-catenin antibody (1:100 in 10% donkey serum) overnight at 4℃. After washing with ice-cold PBST, Alexa Fluor® 488 and Alexa Fluor® 647 secondary antibodies were added for p65 and β-catenin, respectively and incubated for 2 h at room temperature. For the counterstaining, the cells were incubated with DAPI (300 nM) for 10 min, washed three times with ice-cold PBST, and mounted with Dako faramount aqueous mounting media. Fluorescence images were captured by a CELENA® S digital imaging system (Logos Biosystems, Anyang, Gyeonggido, Republic of Korea).

2.2.9 Maintenance of Zebrafish Embryo and Larvae

Zebrafish were maintained and raised according to standard guidelines of the Animal Care and Use Committee of Jeju National University (Jeju Special Self-governing Province, Republic of Korea; approval No.: 2020-0013). Zebrafish were raised at 28.5℃ with a 14:10-h light:dark cycle in a water-recirculating tank system (pH 7.4 and 0.03% salinity). Fertilized embryos were collected after natural spawning and cultured at 28.5℃ in E3 embryo media containing 2 mg/L methylene blue. To inhibit melanin formation, 0.003% PTU was added to the egg water throughout the experimental period.

2.2.10 LPS Microinjection and Cardiac Toxicity Evaluation

Three days post fertilized (dpf) zebrafish larvae were anesthetized using 0.04% tricaine and LPS (0.5 mg/mL, 2 nL in each larva) was microinjected into the yolk sac using Drummond NANOJECT III injector (Drummond Scientific, Broomall, PA, USA). The negative control group was microinjected with PBS. After microinjection of LPS, the larvae were immediately placed in E3 media containing the indicated concentrations of fisetin. Dead larvae were removed within 0.5-hour post injection (hpi). Each group of larvae (n=20) was cultured at 28.5℃ and observed for signs of phenotypic abnormality and mortality. The heart rate of the larvae was manually counted for one minute and used as an indicator for the cardiac toxicity evaluations. All mentioned parameters were observed using an Olympus SZ2-ILST stereomicroscope (Tokyo, Japan).

2.2.11 Neutral Red Staining

Neutral red is a vital dye that accumulates in the lysosomes through endocytosis. As macrophage cells undergo efficient endocytosis, neutral red more robustly labels macrophages than any other cell types. Optimal staining of macrophages in live embryos was achieved by incubating embryos

in 2.5 μg/mL neutral read solution containing 0.003% PTU at 28.5℃ in the dark for 6-8 h. After staining, macrophage migration was observed using an Olympus SZ2-ILST stereomicroscope.

2.2.12 Sudan Black Staining

Sudan black is an azo stain that detects the presence of lipids with dark stains representing neutrophils. A stock solution of sudan black was prepared from sudan black powder (0.6 g) dissolved in pure ethanol (200 mL). A buffer solution was made from phenol (16 g) dissolved in pure ethanol (30 mL) plus $Na_2HPO_4 \cdot 12H_2O$ (0.3 g) dissolved in distilled water (100 mL). A working staining solution was made by mixing stock solution (30 mL) with buffer (20 mL). Whole larvae were fixed with 4% methanol-free PFA in PBS for 2 h at room temperature and rinsed in PBS. The larvae were incubated in sudan black solution for 40 min, washed extensively in 70% ethanol, and then progressively rehydrated with PBS plus 0.1% Tween-20. The stained neutrophils were observed using an Olympus SZ2-ILST stereomicroscope.

2.2.13 Isolation of Total Zebrafish mRNA and RT-PCR

Total RNA was extracted from zebrafish larvae at 3-dpf which were injected with PBS or LPS (0.5 mg/mL) at the indicated time points (0-24 hpi). In a parallel experiment, LPS-microinjected zebrafish larvae were raised in the presence of fisetin and FH535 for 18 hpi. Total RNA was extract from the larvae using easy-BLUE^{TM} total RNA extraction kit (iNtRON Biotechnology). The RNA was reverse-transcribed by MMLV reverse transcriptase kit (BIONEER) and synthetic cDNA was amplified using specific primers: *iNOS* (137 bp) sense 5′-GGA GAT GCA AGG TCA GCT TC-3′ and anti-sense 5′-GGC AAA GCT CAG TGA CTT CC-3′; *COX-2a* (201 bp) sense 5′-CCT GTT GTC AAG GTC CCA TT-3′ and anti-sense 5′-TCA GGG ATG AAC TGC TTC CT-3′; *TNF-α* (149 bp) sense 5′-TAG AAC AAC CCA GCA AAC-3′ and anti-sense 5′-ACC AGC GGT AAA

GGC AAC-3′; *IL-6* (200 bp) sense 5′-AGA CCG CTG CCT GTC TAA AA-3′ and anti-sense 5′-CCA TCT CTC CGT CTC TCA CC-3′; and *β-actin* (155 bp) sense 5′-CGA GCG TGG CTA CAG CTT CA-3′ and anti-sense 5′-GAC CGT CAG GCA GCT CAT AG-3′. The following PCR conditions were applied for PCR amplification: *iNOS, IL-6,* and 27 cycles of denaturation at 95℃ for 45 s, annealing at 58℃ for 45 s, and extended at 72℃ for 1 min; *TNF-α* and *COX-2*, 32 cycles of denaturation at 95℃ for 45 s, annealing at 57℃ for 45 s, and extended at 72℃ for 1 min; *β-actin*, 27 cycles of denaturation at 95℃ for 45 s, annealing at 61℃ for 45 s, and extended at 72℃ for 1 min. *β-Actin* was used as an internal control to evaluate relative expression of *iNOS, COX-2, TNF-α, IL-6,* and. Primer sequences of *iNOS, TNF-α* and *β-actin* were obtained from previous study (Liu et al., 2014), and *COX-2a* and *IL-6* were designed in this study.

2.2.14 Statistical Analysis

RT-PCR and western blotting images were captured by ImageQuant LAS 500 (GE Healthcare Bio-Sciences AB, Uppsala, Sweden). All bands were shown a representative of three independent experiments and quantified by Image J software (Wayne Rasband, National Institute of Health, Bethesda, MD, USA). The results shown in each of figure are a representative from three independent experiments. Statistical analysis was conducted using SigmaPlot software (version 12.0). Significant differences between groups were determined using Student's *t*-test or one-way ANOVA with Bonferroni correction. Values were presented as standard error of the mean (SEM). *** and $^{\#\#\#}$, $p < 0.001$, **, $p < 0.01$, and *, $p < 0.05$ were considered to indicate statistical significance.

2.3 Results

2.3.1 High Concentrations of Fisetin Decrease the Viability of RAW 264.7 Macrophages

To investigate the effect of fisetin on the viability of RAW 264.7 macrophages, the macrophages were treated with the indicated concentrations of fisetin for 24 h in the presence or absence of LPS. No significant change in cell viability was observed at concentrations of up to 8 μM fisetin compared to that of the untreated cells (97.8 ± 1.6%, 97.3 ± 1.7%, 97.5 ± 1.5%, 96.2 ± 1.9% at 1, 2, 4, and 8 μM fisetin); however, higher concentrations of fisetin significantly decreased the viability of RAW 264.7 macrophages (89.5 ± 1.3% and 78.8 ± 5.7% at 10 and 20 μM, respectively) (Figure 10A). Additionally, LPS caused a decrease in cell viability (75.7 ± 2.4%) by potently inducing the differentiation of RAW 264.7 macrophages. Additionally, 10 μM and 20 μM fisetin further reduced cell viability in the presence of LPS (66.0 ± 0.4% and 55.2 ± 0.5%, respectively). However, cytotoxicity hall marks such as apoptotic bodies, floating cells and cells debris were not visible until 20 μM under both LPS presence and absence conditions (Figure 10B). To further confirm the fisetin-induced decrease in cell viability, the total percentages of viable cells and dead cells were measured using flow cytometry in the presence and absence of LPS (Figure 10C-D). These results aligned with those of the MTT assay, the percentage of total viable cells was 78.2 ± 1.5%, while that of dead cells was 21.4 ± 1.2%, at 20 μM fisetin (Figure 10C), which are comparable to those of the H_2O_2-treated cells (positive control; H_2O_2 induces cell death). Furthermore, LPS-related cytotoxicity was elevated by both 10 μM and 20 μM fisetin (74.96 ± 0.39% of viability up to 62.28 ± 0.77% and 55.05 ± 0.98% respectively from 10 μM and 20 μM fisetin while 25.03 ± 0.39% of dead cells up to 37.71 ± 0.77% and 44.95 ± 0.97% respectively from 10 μM and 20 μM fisetin). (Figure 10D). Collectively, these results indicate that high

concentrations of fisetin exhibit cytotoxicity in RAW 264.7 macrophages; however, cytotoxicity was not observed below a concentration of 8 μM.

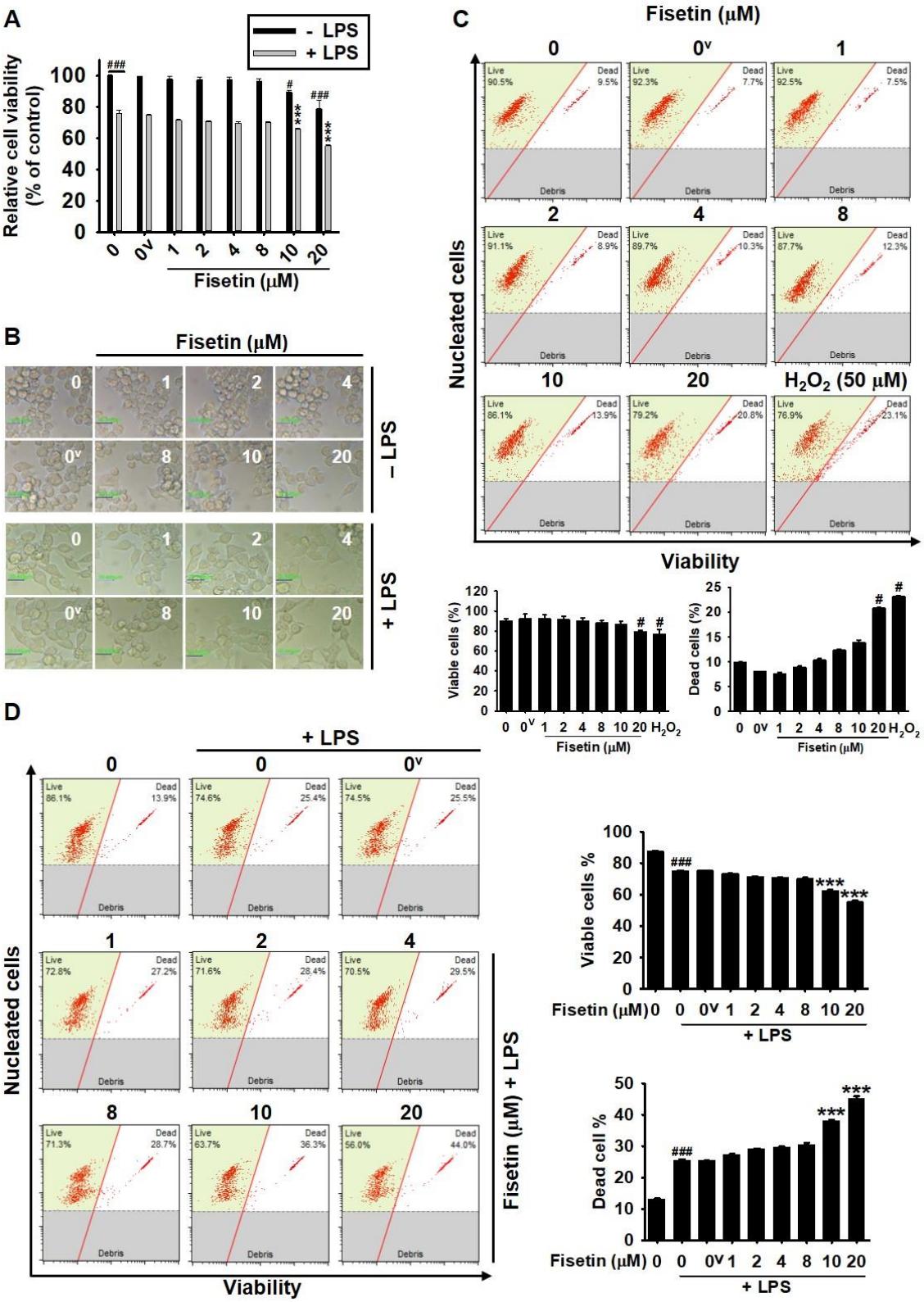

Figure 10. High concentrations of fisetin decreases the cell viability of RAW 264.7 macrophages. RAW 264.7 macrophages were seeded at a density of 1×10^5 cells/mL and incubated with the indicated concentrations of fisetin for 24 h in the presence or absence of 500 ng/mL LPS. **(A)** To measure cell viability, an MTT assay was performed. **(B)** Microscopic images of the fisetin treated RAW 264.7 macrophages in the presence and absence of LPS were taken using Ezscope i900PH phase contrast microscope (× 10). Scale bars = 40 µm. **(C-D)** In a parallel experiment, total viable cells and dead cells in the **(C)** absence and **(D)** presence of LPS were determined by flow cytometry using a Muse® Cell Viability Kit. The total percentage of viable cells and dead cells are represented. Each value indicates the mean ± standard error median (SEM) and is representative of the results obtained from three independent experiments. Significant differences among the groups were determined using an unpaired one-way ANOVA with Bonferroni correction. $^{###}p < 0.001$ and $^{\#}$, $p < 0.05$ *vs.* the untreated group; ***, $p < 0.001$ and *vs.* the LPS-treated cells.0^{v}; Vehicle control (0.2% DMSO).

2.3.2 Fisetin Inhibits LPS-induced Proinflammatory Mediators and Cytokines in RAW 264.7 Macrophages

To confirm the anti-inflammatory effect of fisetin, RAW 264.7 macrophages were pretreated with fisetin for 2 h and stimulated with 500 ng/mL LPS for 6 h. RT-PCR revealed that LPS significantly increased *iNOS* and *COX*-2 expression; however, fisetin downregulated the LPS-induced expression of *iNOS* and *COX*-2 in a concentration-dependent manner (Figure 11A). In agreement with this result, fisetin markedly downregulated LPS-induced iNOS and COX-2 protein expression by approximately 2-fold at a concentration of 8 µM (Figure 11B). Additionally, NO

production in LPS-stimulated macrophages was approximately 4-fold (15.8 ± 0.4 μM) higher than that in the untreated cells (4.2 ± 0.4 μM). In contrast, pretreatment with fisetin reduced LPS-induced NO production in a concentration-dependent manner (11.7 ± 0.3 μM, 5.2 ± 0.5 μM, 5.1 ± 0.1 μM at 2, 4, and 8 μM fisetin, respectively) (Figure 11C). Thereafter, fisetin was observed to decrease the release of PGE_2 in the culture media in response to LPS treatment. ELISA revealed that LPS resulted in an approximately 10-fold increase in PGE_2 production (1888.7 ± 35.2 pg/mL) relative to that in the untreated cells (190. 7 ± 48.3 pg/mL) (Figure 11D). Further, treatment with fisetin gradually weakened LPS-induced PGE_2 production in a concentration-dependent manner (1796.1 ± 67.1 pg/mL, 1604.4 ± 6.5 pg/mL, 1445.8 ± 21.2 μM at 2, 4 and 8 μM fisetin, respectively) (Figure 11D). In addition, fisetin was observed to drastically attenuate LPS-induced expression of *IL-6* and *TNF-α* at 6 h in a concentration-dependent manner (Figure 11E). Accordingly, fisetin at a concentration of 8 μM significantly reduced LPS-induced IL-6 and TNF-α release up to 235.4 ± 4.9 pg/mL and 492.4 ± 11.7 pg/mL from 555.4 ± 7.4% pg/mL and 1310.7 ± 182.7% pg/mL, respectively (Figure 11F and Figure 11G). Furthermore, the treatment effect of fisetin under the LPS pretreated conditions was also evaluated. Interestingly, we noticed that fisetin could inhibit the LPS induced *iNOS, COX, IL-6* and *TNF-α* (S.1A) accompanied with the inhibitory levels of NO production (S.1B). Above all, we couldn't observe any significant changes in the expression patterns of fisetin pretreated and fisetin post treated conditions. Altogether, these results indicate that fisetin negatively modulates LPS-induced proinflammatory mediator and cytokine expression in RAW 264.7 macrophages.

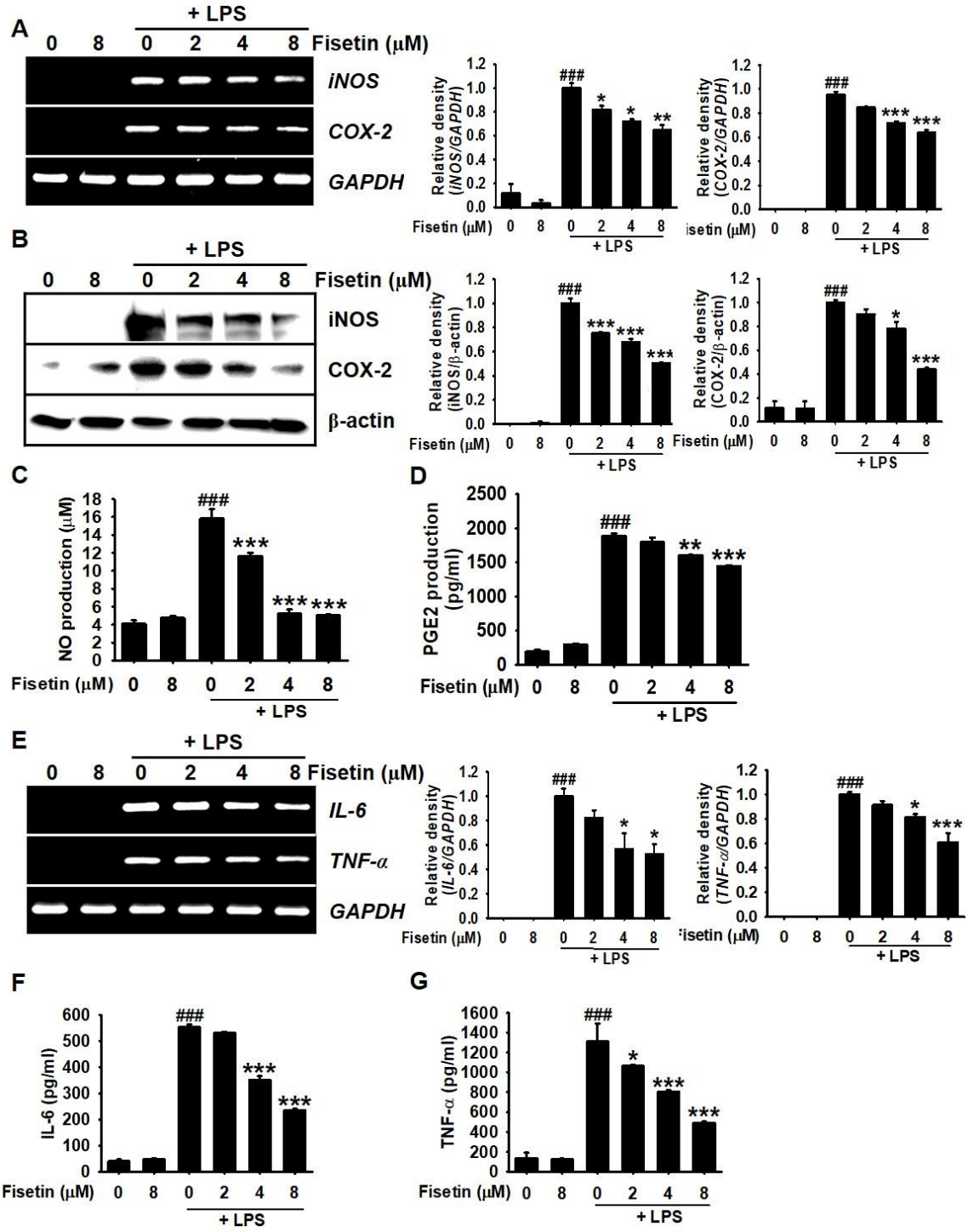

Figure 11. Fisetin decreases LPS-induced inflammatory mediator and cytokine levels in RAW 264.7 macrophages. RAW 264.7 macrophages (1×10^5 cells/mL) were incubated with the indicated concentrations of fisetin 2 h before treatment with 500 ng/mL LPS. **(A)** Total mRNA

was isolated at 6 h after 500 ng/mL LPS treatment, and RT-PCR was performed to analyze the expression of *iNOS* and *COX-2*. *GAPDH* was used as an internal control. **(B)** Total proteins were isolated at 24 h and equal amounts of cell lysates were resolved on SDS-polyacrylamide gels and probed with antibodies against iNOS and COX-2. β-Actin was used as an internal control. **(C)** The amount of NO production in the culture medium was determined using the Griess assay. **(D)** The amount of PGE_2 was determined at 24 h using an ELISA according to the manufacturer's instructions. **(E)** Total mRNA was isolated at 6 h and subjected to RT-PCR for *IL-6* and *TNF-α*. *GAPDH* was used as an internal control. The amount of **(F)** IL-6 and **(G)** TNF-α was measured at 24 h by an ELISA. Each value indicates the mean ± standard error median (SEM), and is representative of the results obtained from three independent experiments. Significant differences among the groups were determined using the Student's *t*-test ($^{###}$, $p < 0.001$ vs. the untreated cells) and one-way ANOVA with Bonferroni correction (***, $p < 0.001$, **, $p < 0.05$, and *, $p < 0.01$ vs. the LPS-treated cells).

2.3.3 Fisetin Attenuates Mortality, Abnormality, and Lowered Heart Rate in LPS-microinjected Zebrafish Larvae

To confirm that fisetin exhibits anti-inflammatory activity in an LPS-induced endotoxic shock model, 3 dpf zebrafish larvae were microinjected with LPS in the presence or absence of fisetin. Thereafter, mortality, abnormality (congenital malformations), and heart rate were measured. LPS-microinjection induced 30% death and 60% abnormality in zebrafish larvae at 36 dpf, and 10% normal survival (Figure 12A). However, fisetin gradually decreased LPS microinjection-induced mortality to 10% at a concentration of 100 μM and caused complete blockage at concentrations ≥

200 μM. Abnormality rates were 70%, 40%, and 10% at 100, 200, and 400 μM fisetin, respectively. In particular, fisetin-immersed larvae did not exhibit LPS-induced phenotypes, such as necrotic yolk, cyrtosis, and yolk crenulation—however, one (5%) did show a swollen pericardial sac—thereby indicating that fisetin attenuates LPS-induced severe endotoxic shock and phenotypes such as necrotic yolk. The morphological shapes of the LPS-microinjected larvae are shown in Figure 12B: normal (i), death (ii), necrotic yolk (iii), swollen pericardial sac (iv), cyrtosis (v), and yolk crenulation (vi). We found that the swollen pericardial sac represents the dominant phenotype in all LPS-microinjected larvae. In brief, all LPS-microinjected abnormal larvae (60%) exhibited swollen pericardial sac, either alone, or together with necrotic yolk (8.5%), cyrtosis (8.5%), or yolk crenulation (8.5%) (Figure 12C). Additionally, we examined the heart rate of the larvae as an indicator of the toxicity evaluations. As shown in Figure 12D, LPS microinjection resulted in a significant lowering of the heart rate (107 ± 6 heart beats/min) comparted to that in the PBS-microinjected larvae (185 ± 8 heart beats/min). Upon increasing the concentration of fisetin, the impaired heart rate gradually recovered almost up to the normal level at 400 μM (177.5 ± 6.9 heart beats/min). Altogether, these data indicate that fisetin attenuates LPS-induced septic shock in zebrafish larvae accompanied by decreased mortality, morphological abnormalities, and lowered heart rate.

A

Group	Phenotype (%) (*n*=20)/(36 h)		
	Normal	Death	Abnormality
Untreated	100	/	/
400 μM Fisetin	100	/	/
2 nL, LPS (0.5 mg/mL)	10	30	60
100 μM Fisetin + LPS	20	10	70
200 μM Fisetin + LPS	60	/	40
400 μM Fisetin + LPS	90	/	10

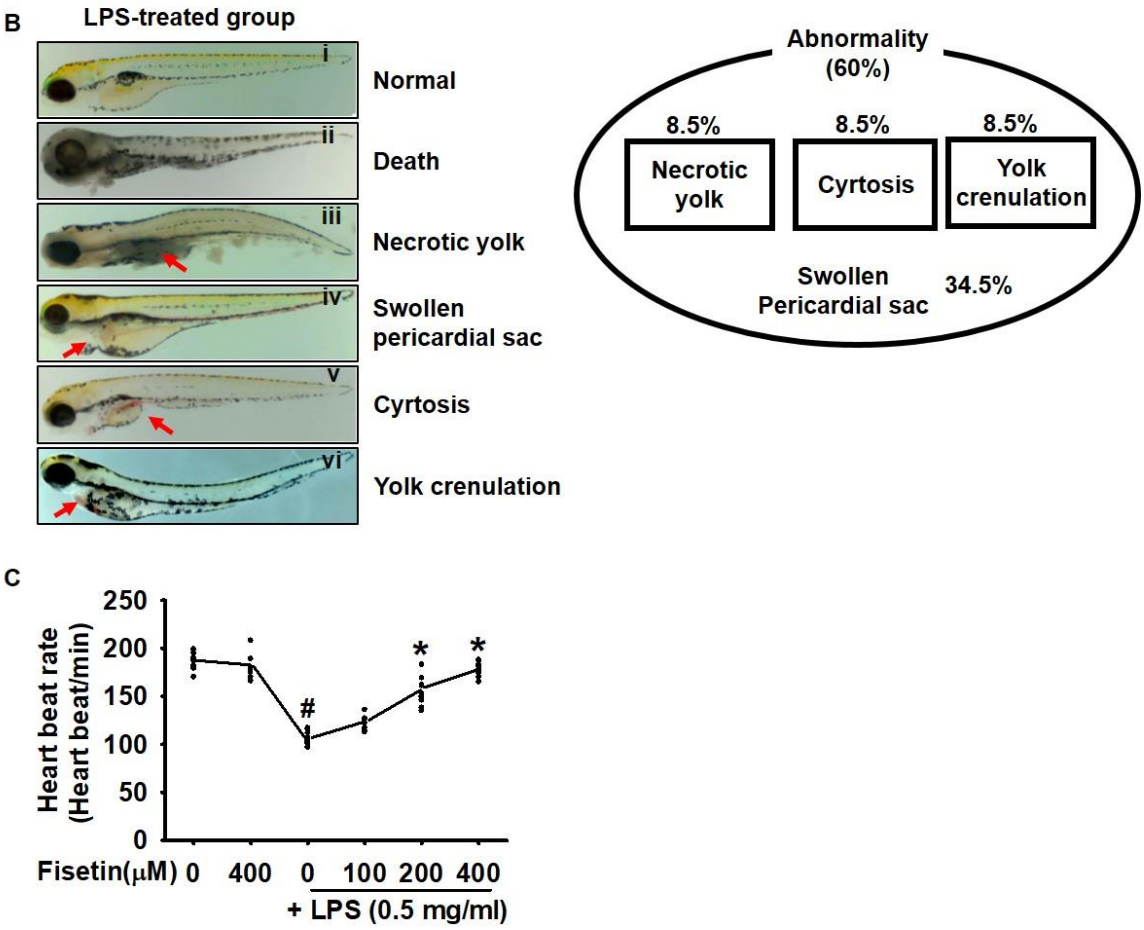

Figure 12 Fisetin attenuates LPS-induced mortality, abnormalities, and lowered heart rate in zebrafish larvae. Zebrafish larvae at 3 dpf (*n*=20) were microinjected with 2 nL of 0.5 mg/mL LPS and immediately immersed in the indicated concentrations of fisetin. **(A)** Phenotype-based

evaluations were performed at 36 hpi. **(B)** LPS-microinjection increases abnormalities in zebrafish at 36 hpi; this was observed using stereomicroscopy; (i) normal, (ii) death, (iii) necrotic yolk, (iv) swollen pericardial sac, (v) cyrtosis, and (vi) yolk crenulation. **(C)** Heart rates were measured to assess toxicity. Each value indicates the mean ± standard error median (SEM), and is representative of the results obtained from 20 fish for each group. Significant differences among the groups were determined using Student's *t*-test ($^{\#}$, $p < 0.01$ vs. the untreated group) and one-way ANOVA with Bonferroni correction (*, $p < 0.01$ vs. the LPS-treated larvae).

2.3.4 Fisetin Inhibits LPS-induced Proinflammatory Gene Expression and Concomitantly Decreases Macrophage and Neutrophil Recruitment to the Inflammatory Sites in Zebrafish Larvae

To confirm whether fisetin inhibits the LPS-induced inflammatory response, 3 dpf zebrafish larvae were microinjected with LPS for 24 h. Thereafter, the time-dependent expression of proinflammatory mediators such as *iNOS* and *COX-2a* and cytokines such as *IL-6* and *TNF-α* was evaluated. In the LPS-microinjected condition, all genes tested in this study were expressed and reached maximal levels at 18 h, with a slightly different expression patterns (Figure 13A). *iNOS* and *TNF-α* were significantly expressed at 6 h and their expression lasted for 24 h, whereas *COX-2a* and *IL-6* were highly expressed at 18 h. To evaluate the anti-inflammatory effect of fisetin *in vivo*, LPS-microinjected zebrafish larvae were grown in the presence of the indicated concentrations of fisetin for 18 h, and the expression level of the proinflammatory genes was detected. RT-PCR showed that fisetin concentration-dependently decreased the expression of *iNOS*, *COX-2a*, *IL-6*, and *TNF-α* in LPS-microinjected zebrafish larvae (Figure 13B). In particular,

a concentration of 400 μM fisetin was the potent at downregulating the expression of all proinflammatory genes tested in this study (i.e., the levels reached those in the untreated larvae). Furthermore, we sought to determine whether fisetin prevents the recruitment of macrophages and neutrophils to the inflammatory site in LPS-microinjected zebrafish larvae. Neutral red staining revealed that LPS injection significantly increased the macrophage counts at the site where LPS was injected (inflammatory site) in the yolk sac (red dot in the red box) at 24 h; however, immersion in fisetin resulted in a gradual decrease in the accumulation of macrophages in the yolk sac (Figure 13C), indicating that fisetin inhibits the recruitment of macrophages from the circulating blood to the yolk sac, leading to the generation of anti-inflammatory responses. In alignment with the inhibition of macrophage recruitment, LPS-microinjection significantly decreased the large and clear cytolymph lipid droplets (accumulation of neutrophils, yellow dot box) in the posterior blood island (PBI) as neutrophils infiltrated the inflammatory site, i.e., the yolk sac (Figure 13D). We also found that fisetin impaired the migration of neutrophils to the inflammatory site in a concentration-dependent manner, which indicates that fisetin attenuates the recruitment of neutrophils to the LPS-microinjected site. These results indicate that fisetin inhibits the LPS-induced inflammatory response by suppressing the expression of proinflammatory genes and reducing macrophage and neutrophil recruitment to the inflammatory sites.

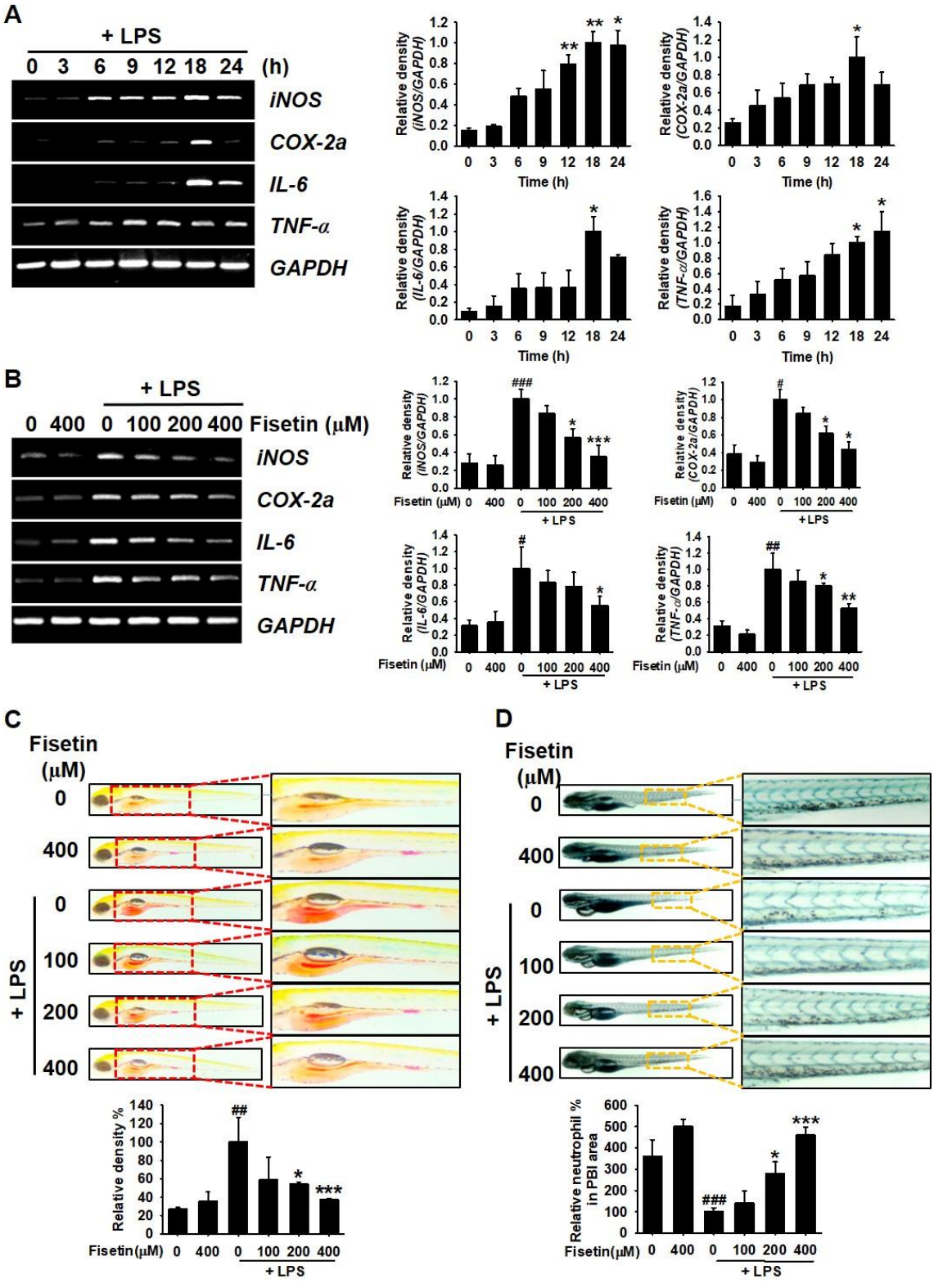

Figure 13. Fisetin inhibits LPS-induced inflammatory response in zebrafish larvae. Zebrafish larvae at 1 dpf were cultured in 0.003% PTU containing E3 embryo media. Briefly, 2 nL of 0.5 mg/mL LPS was microinjected into the yolk at 3 dpf. Zebrafish larvae were immediately immersed in E3 embryo media containing different concentrations of fisetin. **(A)** In LPS-microinjected conditions, 10 zebrafish were euthanized at the indicated time points and subjected to RT-PCR for evaluating the expression of *iNOS*, *COX-2a*, *IL-6*, and *TNF-α*. **(B)** At 18 hpi, 20 zebrafish larvae from each treatment were euthanized and the expression of *iNOS*, *COX-2a*, *IL-6*, and *TNF-α* was measured by RT-PCR. **(C)** Neutral red staining of macrophages and **(D)** Sudan black staining of the neutrophils were performed at 24 hpi. Each value indicates the mean ± standard error median (SEM) and is representative of the results obtained from three independent experiments. Significant differences among the groups were determined using the Student's *t*-test ($^{###}$, $p < 0.001$, $^{##}$, $p < 0.01$, and $^{#}$, $p < 0.05$ vs. the untreated larvae) and one-way ANOVA with Bonferroni correction (***, $p < 0.001$, **, $p < 0.01$, and *, $p < 0.05$ vs. the LPS-treated larvae).

2.3.5 Fisetin Inhibits LPS-induced NF-κB Activity in RAW 264.7 Macrophages

As NF-κB is considered as a major transcription factor in LPS-induced inflammatory response, we investigated whether fisetin negatively regulates the activation of the NF-κB pathway. Western blotting using nuclear extracts from RAW 264.7 macrophages confirmed that fisetin decreased LPS-induced nuclear localization of NF-κB p50 and p65 in a concentration-dependent manner (Figure 14A). Additionally, immunohistochemistry confirmed that LPS rapidly stimulated the translocation of NF-κB p65 into the nucleus; however, fisetin inhibited the nuclear translocation of NF-κB p65 in the presence of LPS (Figure 14B), indicating that fisetin inhibits

LPS-induced NF-κB activation, resulting in the inhibition of inflammatory responses.

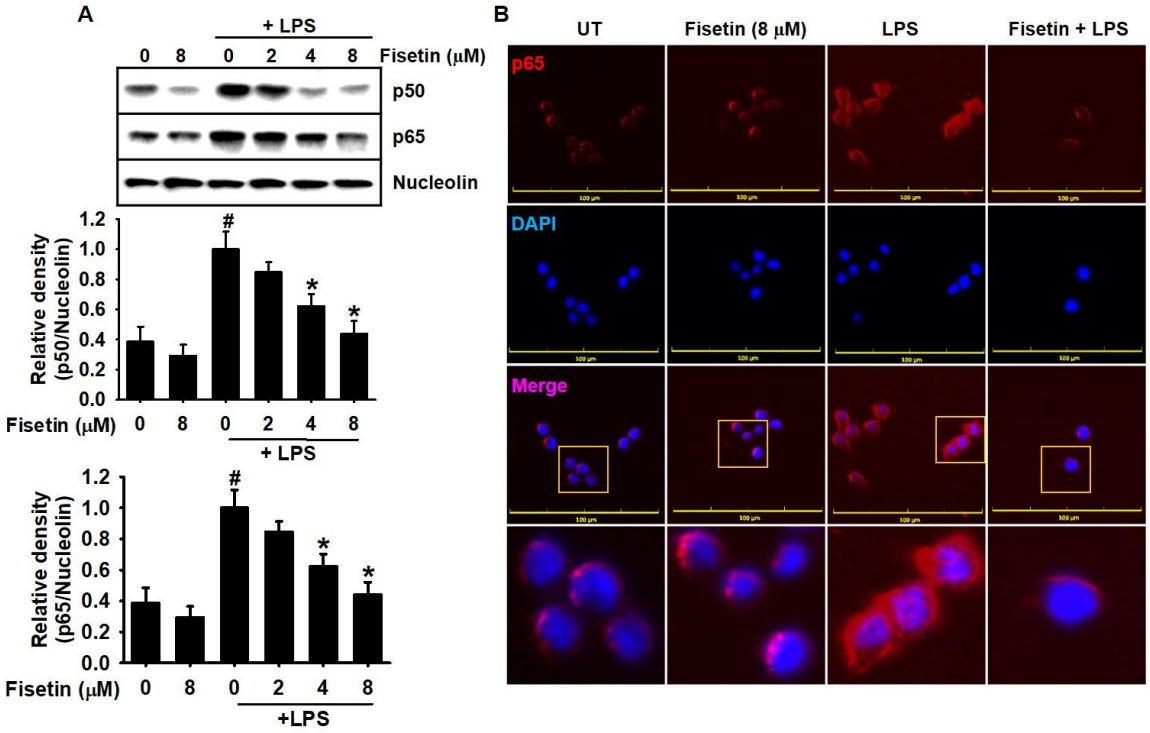

Figure 14. Fisetin inhibits LPS-induced nuclear translocation of NF-κB in RAW 264.7 macrophages. RAW 26.4.7 cells (1×10^5 cells/mL) were pretreated with fisetin 2 h before LPS treatment (500 ng/mL; 0.5 h). **(A)** Nuclear proteins were isolated and equal amounts of proteins were resolved on SDS-polyacrylamide gels, transferred to PVDF membranes, and probed with antibodies against p50 and p65. Nucleolin was used as an internal control. **(B)** The nuclear translocation of p65 was detected by fluorescence microscopy. Each value indicates the mean ± standard error median (SEM), and is representative of the results obtained from three independent experiments. Significant differences among the groups were determined using Student's *t*-test ($^{\#}$, $p < 0.05$ vs. the untreated group) and one-way ANOVA with Bonferroni correction (*, $p < 0.05$ vs. the LPS-treated cells).

2.3.6 Fisetin Enhances Phosphorylation of GSK-3β at Ser9 and Subsequent Activation of β-catenin in RAW 264.7 Macrophages

Recently, our research team revealed that fisetin binds to GSK-3β at non-ATP-binding site—through molecular docking prediction—and consequently activates β-catenin in B16F10 melanoma cells (Molagoda et al., 2020b). Deng et al. reported that β-catenin negatively regulates the inflammatory responses by inhibiting the expression of proinflammatory mediators and cytokines (Deng et al., 2002). These data indicate that fisetin inhibits GSK-3β and subsequently stabilizes β-catenin, which attenuates LPS-induced inflammation. Therefore, we determined whether fisetin affects the expression of GSK-3β and β-catenin as well as the nuclear translocation of β-catenin. Fisetin concentration-dependently increased the phosphorylation of GSK-3β at Ser9—an inactive form—and enhanced the level of total β-catenin (Figure 15A) and its nuclear translocation (Figure 15B). Immunohistochemistry also revealed that fisetin enhanced the nuclear translocation of β-catenin regardless of the presence of LPS; however, an abundance of β-catenin was found in the cytosol after LPS treatment (Figure 15C). Altogether, these results indicate that fisetin blocks the degradation of β-catenin by inhibiting GSK-3β, and consequently enhances the nuclear translocation of β-catenin.

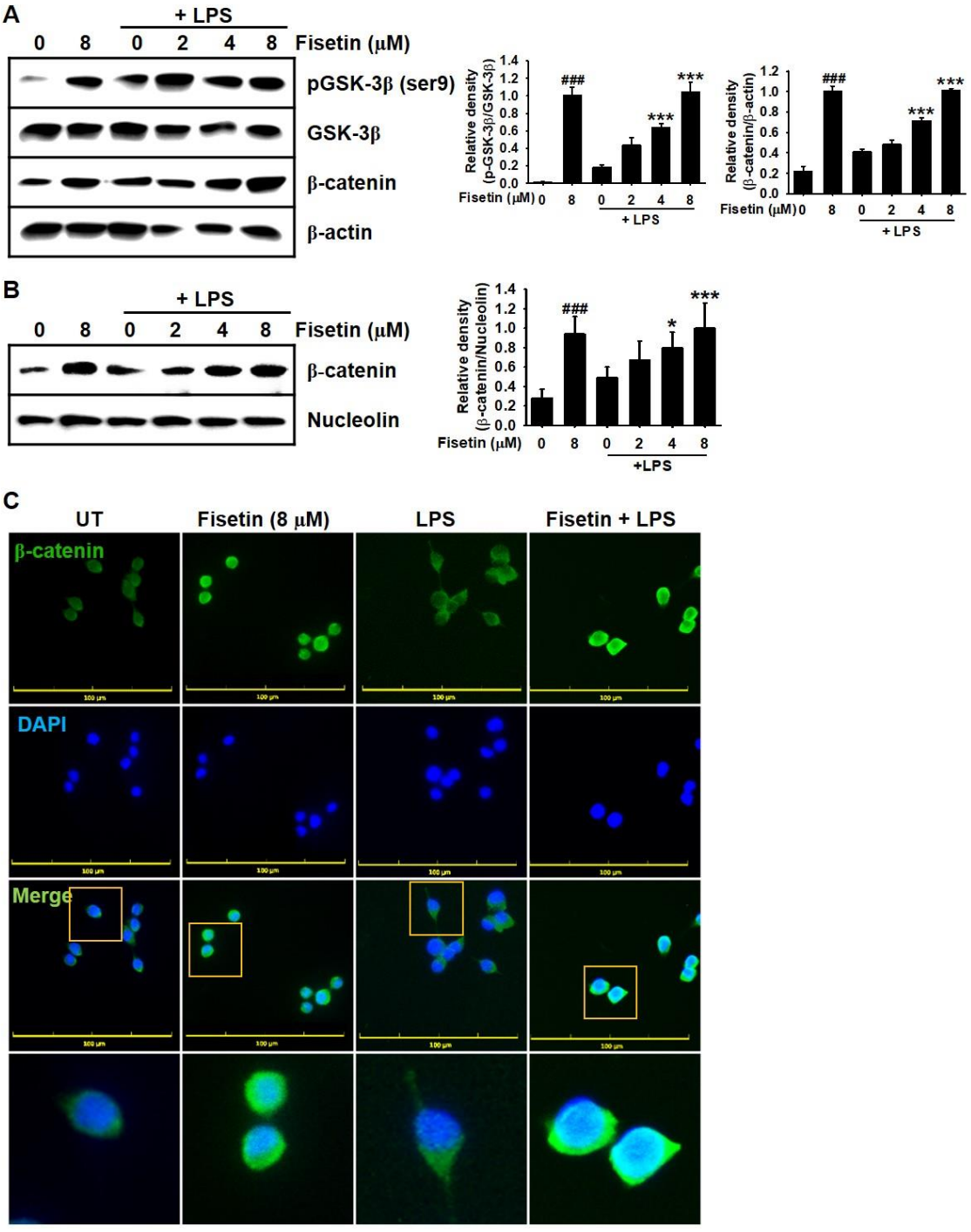

Figure 15 Fisetin promotes the expression of β-catenin and its nuclear translocation in LPS-stimulated RAW 264.7 macrophages. RAW 264.7 macrophages (1×10^5 cells/mL) were pretreated with fisetin 2 h prior to LPS treatment (500 ng/mL; 0.5 h). **(A)** Total proteins were

isolated and equal amounts of proteins were resolved on SDS-polyacrylamide gels, transferred to PVDF membranes, and probed with antibodies against total GSK-3β, phosphor-GSK-3β (Ser9), and β-catenin. β-Actin was used as an internal control. **(B)** In a parallel experiment, nuclear proteins were isolated and western blotting was performed to verify the nuclear translocation of β-catenin. Nucleolin was used as an internal control. **(C)** Nuclear translocation of β-catenin was detected by immunofluorescence. Each value indicates the mean ± standard error median (SEM), and is representative of the results obtained from three independent experiments. Significant differences among the groups were determined using Student's *t*-test ($^{###}$, $p < 0.001$ vs. the untreated cells) and one-way ANOVA with Bonferroni correction (***, $p < 0.001$ and *, $p < 0.01$ vs. the LPS-treated cells).

2.3.7 Fisetin Inhibits β-Catenin-mediated NF-κB Activity, Causing a Significant Decrease in LPS-induced IL-6 and TNF-α Release

To confirm the crosstalk between β-catenin and NF-κB, RAW 264.7 macrophages were treated with FH535, an inhibitor of Wnt/β-catenin (Handeli and Simon, 2008), for 2 h prior to treatment with fisetin and LPS. FH535 itself considerably increased nuclear NF-κB p50 and p65 levels compared to those in the untreated cells, and moderately upregulated LPS-induced NF-κB p50 and p65 levels (Figure 16A). In contrast, fisetin significantly inhibited the nuclear translocation of NF-κB p50 and p65 in the presence of FH535 or LPS; however, combined treatment with FH535 and LPS reversed the inhibitory effect of fisetin on LPS-induced NF-κB p50 and p65 translocation to the nucleus (Figure 16A). We also evaluated the effect of fisetin on LPS-induced IL-6 and TNF-α release in the presence of FH535. As shown in Figure 16B and16C, FH535 itself increased IL-6 (647.1 ± 53.6 pg/mL) and TNF-α (695.9 ± 243.3 pg/mL) release compared to that in the untreated cells (53.4 ± 10.4 pg/mL for IL-6 and 115.5 ± 29.6 pg/mL for

TNF-α). Furthermore, simultaneous treatment with FH535 and LPS further elevated IL-6 (1577.9 ± 24.4 pg/mL) and TNF-α (1834.6 ± 91.8 pg/mL) levels compared to the LPS-treated condition (1170.1 ± 14.3 pg/mL and 1447.4 ± 36.8 pg/mL for IL-6 and TNF-α, respectively); however, fisetin significantly inhibited FH535-induced IL-6 (46.4 ± 2.5 pg/mL) and TNF-α (120.9 ± 36.8190 pg/mL) release. Furthermore fisetin significantly inhibited the IL-6 (1250.6 ± 11.8 pg/mL) and TNF-α (1437.7 ± 69.9 pg/mL) levels that were induced in response to combined treatment with LPS and FH535. Nevertheless, fisetin-mediated inhibitory levels were not significant to the LPS only treated group in the presence of FH535. Altogether, these results indicate that fisetin inhibits LPS-induced NF-κB activation in RAW 264.7 macrophages by activating β-catenin, which attenuates the expression of the proinflammatory cytokines, such as IL-6 and TNF-α.

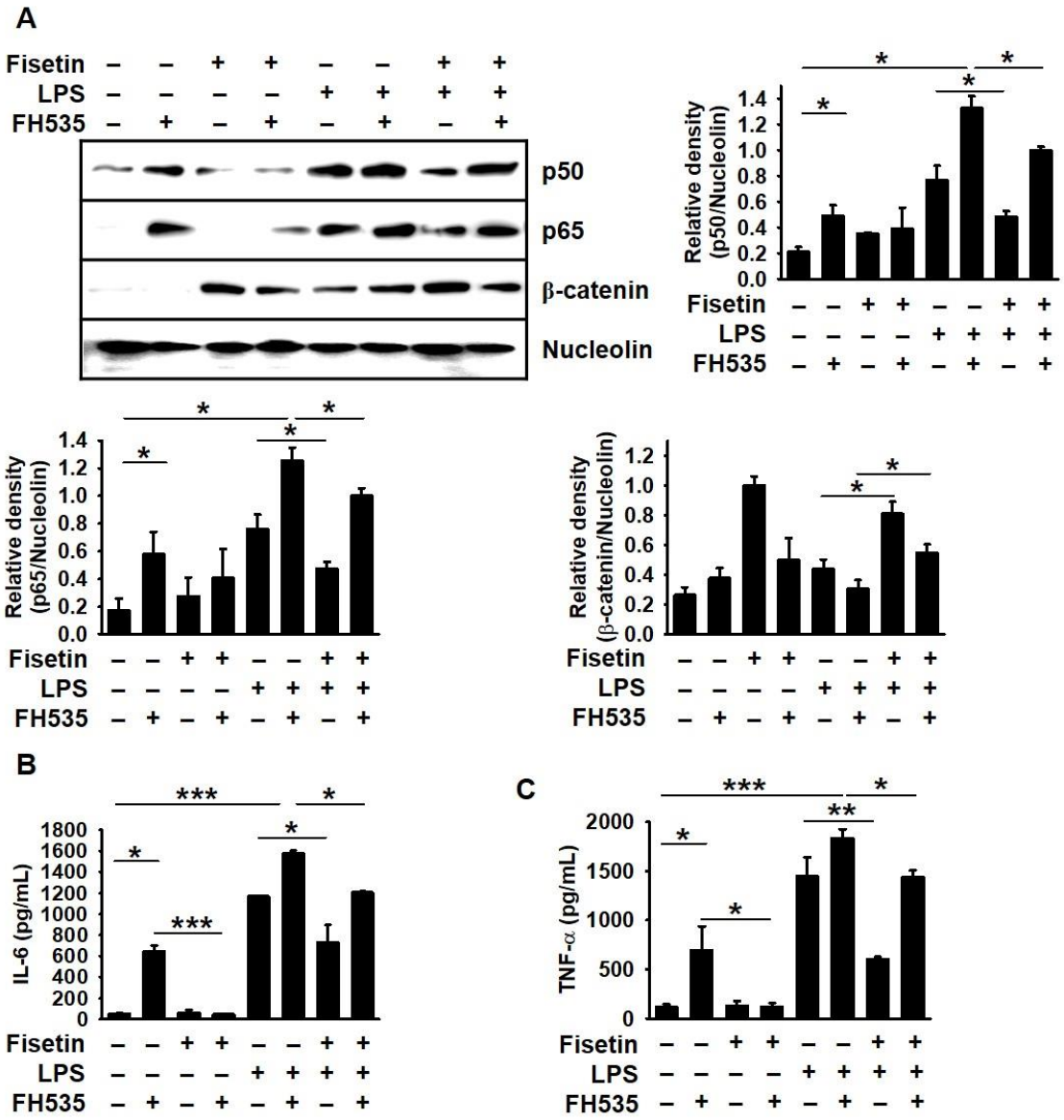

Figure 16 Fisetin inhibits LPS- or FH535-mediated IL-6 and TNF-α release by stimulating β-catenin-mediated NF-κB inactivation. RAW 264.7 macrophages (1×10^5 cells/mL) were incubated with 10 μM FH535 for 2 h prior to treatment with 8 μM fisetin and 500 ng/mL LPS. **(A)** Nuclear proteins were extracted and western blotting was performed with specific antibodies against p65, p50, and β-catenin. Nucleolin was used as an internal control. **(B and C)** In a parallel

experiment, the culture supernatants were collected and extracellular levels of **(B)** IL-6 and **(C)** TNF-α were measured by ELISA. Each value indicates the mean ± standard error median (SEM), and is representative of the results obtained from three independent experiments. Significant differences among the groups were determined using one-way ANOVA with Bonferroni correction (***, $p < 0.001$, **, $p < 0.005$, and *, $p < 0.01$).

2.3.8 Fisetin-induced Anti-inflammatory Response Is Related to Activation of β-Catenin in an Endotoxic Shock Model of Zebrafish Larvae

To confirm the significance of the β-catenin signaling pathway in fisetin-induced anti-inflammatory responses, we pharmacologically blocked the canonical β-catenin signaling pathway with FH535 in zebrafish larvae. We found that FH535 at 10 μM and 20 μM induced 20% and 100% mortality after 24-h of treatment. Further, 10 μM of FH535 increased the mortality up to 40% in LPS-microinjected larvae (data not shown). Interestingly, FH535-induced mortality was completely blocked in the presence of fisetin (data not shown), indicating that fisetin could reduce the mortality by activating the β-catenin signaling pathway. Thus, we investigated whether, in the presence of FH535, fisetin influences the recruitment of macrophages and neutrophils in LPS-microinjected zebrafish larvae. Interestingly, we found that FH535 by itself significantly increased the neutral red intensity (macrophages) in the yolk sac (Figure 17A) and increased sudan black-stained spots (neutrophils) in the whole body, with neutrophils being retained at the PBI (Figure 17B). As expected, in FH535-treated conditions, fisetin inhibited the recruitment of macrophages and neutrophils to the inflammatory site in LPS-microinjected zebrafish larvae, which indicated that fisetin-induced β-catenin activation hindered macrophage and neutrophil recruitment to the

inflammatory sites. Subsequently, we investigated the expression of *iNOS* and *COX-2a* under the same experimental conditions. We found that both inflammatory genes were highly expressed in the presence of FH535 or LPS. Additionally, fisetin inhibited FH535- or LPS-induced *iNOS* and *COX-2a* expression (Figure 17B). Nevertheless the inhibitory effect of fisetin on the combinatorial treatment of LPS and FH535 was significant, the levels were not statistically significant to the LPS only treated conditions. These data imply that fisetin negatively regulates LPS-induced inflammation and endotoxic shock via activating the β-catenin signaling pathway.

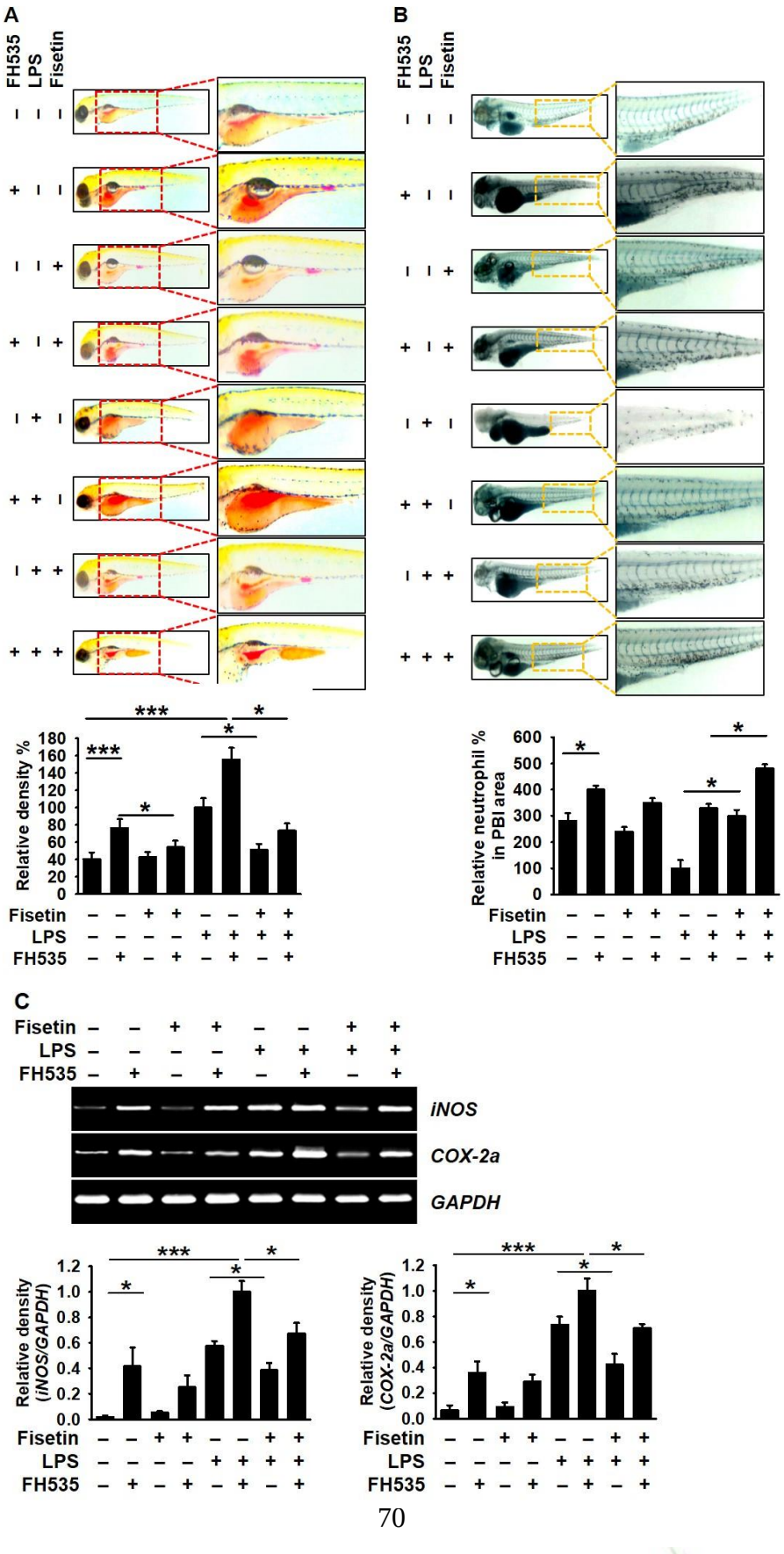

Figure 17. Fisetin inhibits LPS-induced inflammation and endotoxic shock by stimulating the β-catenin signaling pathway in zebrafish larvae. Zebrafish larvae at 3 dpf were pretreated with 10 μM FH535 for 2 h prior to LPS (2 nL of 0.5 mg/mL) microinjection. Then, the larvae were grown in E3 media containing 400 μM fisetin. **(A)** Neutral red-stained macrophages are shown at 18 hpi. **(B)** Sudan black-stained neutrophils were observed at 18 hpi. **(C)** At 18 hpi, 10 zebrafish from each condition were collected and the expression of *iNOS* and *COX-2a* was detected by RT-PCR. GAPDH was used as an internal control. Each value indicates the mean ± standard error median (SEM) and is representative of the results obtained from three independent experiments. Significant differences among the groups were determined using one-way ANOVA with Bonferroni correction (***, $p < 0.001$, **, $p < 0.005$, and *, $p < 0.01$).

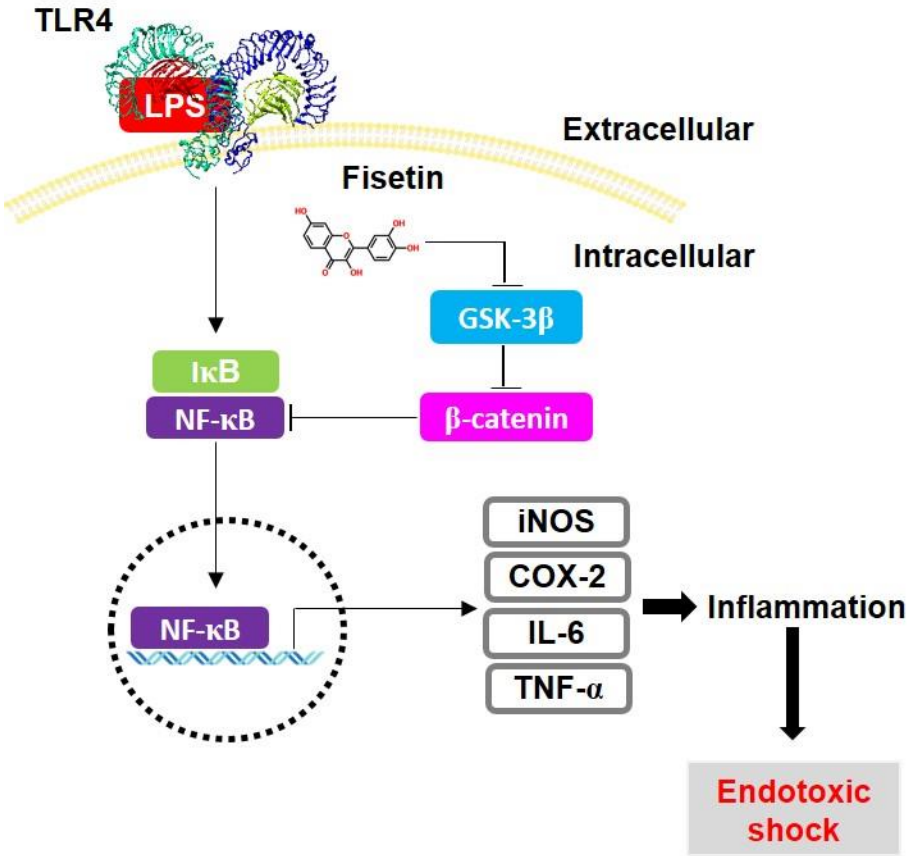

Figure 18. Graphical representation of the molecular mechanism of the anti-inflammatory effect of fisetin. Fisetin inhibits GSK-3β-mediated NF-κB activation in the presence of β-catenin, leading to the inhibition of inflammation-induced septic shock. Once macrophages are exposed to high concentrations of the bacterial endotoxin, LPS, they initiate an inflammatory response and endotoxic shock by upregulating the expression of NF-κB-induced inflammatory genes, such as *iNOS*, *COX-2*, *IL-12*, *IL-6*, and *TNF-α*. Fisetin binds to the noncompetitive ATP-binding sites of GSK-3β and phosphorylates GSK-3β at Ser9, resulting in the inactivation GSK-3β and release of β-catenin from the destruction complex (Molagoda et al., 2020b). The released β-catenin inhibits the transcriptional activity of NF-κB, thereby alleviating LPS-induced inflammation and endotoxic shock.

2.4 Discussion

Endotoxic shock is a systemic inflammation accompanied by the excessive release of inflammatory mediators and cytokines, resulting in high cardiac output and mortality (Werdan et al., 2009). Non-steroidal anti-inflammatory drugs (NSAIDs), including aspirin, celecoxib, and diclofenac, are commonly used to combat systemic inflammation; however, they are associated with digestive problems such as upset stomach, heartburn, ulcers, and kidney injuries (Goldstein and Cryer, 2015). Therefore, small compounds, such as flavonoids, may provide a good alternative to prevent and reduce the risk of inflammation and endotoxic shock with relatively low side effects. Fisetin is a bioactive diphenyl propane flavone that is abundant in various plants. Its pharmacological properties including anti-cancer, antioxidant, and anti-inflammatory activity have been reported (Huang et al., 2018b; Kumar and Pandey, 2013; Molagoda et al., 2020b; Sahu et al., 2016). Nevertheless, the molecular mechanisms underlying the anti-inflammatory properties of fisetin are unclear. In the current study, we evaluated the anti-inflammatory effect of fisetin on LPS-

induced inflammation and endotoxic shock in RAW 264.7 macrophages and zebrafish larvae. Our findings suggest that fisetin inhibits LPS-induced inflammation and endotoxic shock by suppressing β-catenin-mediated NF-κB activity, which subsequently attenuates the expression of proinflammatory mediators, such as NO and PGE_2, and cytokines, such as IL-6 and TNF-α (Figure 18).

Systemic inflammation is characterized by increase in proinflammatory cytokine levels, including IL-6, IL-12, and TNF-α, and other proinflammatory mediators, including NO and PGE_2, via the activation of NF-κB (Ali et al., 2010; Hop et al., 2017; Kishimoto and Tanaka, 2015; Vila-del Sol and Fresno, 2005; Zheng et al., 2016). Accumulating evidence on LPS-induced inflammatory disorders has revealed that LPS triggers the expression of inflammatory genes via the TLR4-dependent signaling pathway (Jackie et al., 2019; Rathinam et al., 2019). Binding of LPS to TLR4 leads to the phosphorylation of the IκB kinase (IKK) complex through the recruitment and activation of MyD88 and IRAK4, and in turn, phosphorylates IκB, which is degraded by the proteasome and allows the nuclear translocation of free NF-κB (Fang et al., 2018; Walsh et al., 2015). Therefore, targeting the NF-κB signaling pathway is thought to be a pivotal therapeutic strategy in the pathology of LPS-induced inflammatory disorders. Two research groups have previously reported that fisetin reduces ovalbumin-induced airway inflammation by inhibiting MyD88-mediated NF-κB activation (Goh et al., 2012; Huang et al., 2018b). In the present study, we reconfirmed that fisetin alleviated LPS-induced inflammatory mediator and cytokine levels in RAW 264.7 macrophages by inhibiting the NF-κB signaling pathway. Fisetin is also effective at protecting against metabolic dysfunction (Shi et al., 2018), UVB (Wu et al., 2017), cardiac ischemic injury (Garg et al., 2019), and brain disorders (Singh et al., 2018). Furthermore, fisetin was also shown to inhibit LPS-induced macrophage activation and functional maturation of dendritic cells (Liu et al., 2010) as well as LPS-induced -acute lung injury (Feng et al., 2016b) via suppressing TLR4 mediated NF-

kB cell signaling pathway. Nevertheless, the precious molecular mechanism of fisetin-mediatedendotoxic shock has not been elucidated. In the current study, using a zebrafish larva model, we proved that fisetin attenuated LPS-induced mortality and abnormality and caused a significant decrease in macrophage and neutrophil recruitment at the inflammatory site. Meanwhile, fisetin restored the heart rate up to the normal level along with the downregulation of proinflammatory genes during LPS stimulation, indicating that fisetin is a promising pharmacological candidate against LPS-induced endotoxic shock. Inhibitors of the TLR4/NF-κB have been shown to associate with the attenuation of LPS-induced acute kidney injury (Shi et al., 2017); indicating that fisetin also would be an interesting drug candidate in the acute kidney injury models and further studies are warranted in this regard. Furthermore, whether fisetin protects against endotoxic shock in preclinical studies is yet to be elucidated.

As the canonical Wnt/β-catenin signaling pathway plays a crucial role in the development of cancer through chronic inflammation, non-steroidal anti-inflammatory drugs, such as PPARγ agonists, might serve as potent therapeutic agents to treat cancers as they inhibit the Wnt/β-catenin pathway (Vallee and Lecarpentier, 2018; Vallee et al., 2019). Alternatively, Swafford et al. reported that the deletion of Wnt receptors reduced histopathological severity and inflammation in the colon, along with high expression of anti-inflammatory cytokines such as IL-10, through the conditional activation of β-catenin (Swafford et al., 2018). Such findings suggest that the canonical Wnt/β-catenin pathway negatively regulates inflammation. Despite the dual regulation of Wnt/β-catenin in inflammation, in this study, fisetin increased total β-catenin and promoted its nuclear translocation in RAW 264.7 macrophages. Further, an increased expression of inactive GSK-3β (phosphorylated at Ser9) was observed. The inhibition of the Wnt/β-catenin signaling pathway by inhibitors of both Wnt/β-catenin and PPAR exacerbated the mortality and abnormality in zebrafish

larvae. This was accompanied by a further accumulation of macrophages and neutrophils at the LPS-microinjected inflammatory site and a significant expression of proinflammatory genes. Interestingly, Deng et al. reported that β-catenin physically interacts with NF-κB to form a complex, and thereby reduces the DNA-binding ability of NF-κB (Deng et al., 2002). Jun et al. also reported that gram-negative *Salmonella* infection constitutively activated β-catenin and thereby stabilized IκBα, which subsequently repressed the activity of NF-κB in HCT116 colon cancer cells (Sun et al., 2005), indicating that the crosstalk between the Wnt/β-catenin and NF-κB pathways is linked to the regulation of inflammation. In agreement with the above studies, we found that fisetin-induced β-catenin attenuated LPS-induced inflammation and endotoxic shock by inhibiting NF-κB activation. Nevertheless, the discrepancy between the positive and negative regulatory role of the Wnt/β-catenin pathway in inflammatory disorders may be investigated in the context of NF-κB, even though NF-κB is a key activator of inflammation.

Our previous research predicted that fisetin directly binds to GSK-3β at the noncompetitive ATP-binding site and promotes β-catenin stabilization and nuclear translocation (Molagoda et al., 2020b). GSK-3β is a ubiquitous serine/threonine kinase involved in the molecular pathogenesis of severe disorders in humans, including inflammation, tumorigenesis, and neurological disorders (Beurel et al., 2015). In particular, Medunjanin et al. identified that GSK-3β directly phosphorylates NEMO, which is an essential activator of NF-κB and consequently activates NF-κB, indicating that GSK-3β stimulates a non-canonical NF-κB signaling pathway (Medunjanin et al., 2016). Ougolkov et al. also revealed that the inhibition or genetic depletion of GSK-3β inhibits NF-κB-induced gene transcription and subsequently leads to pancreatic cancer cell proliferation and survival by activating the NF-κB signaling pathway (Ougolkov et al., 2005). Based on our data, we deduced that the targeting of GSK-3β by fisetin inactivates the non-canonical NF-κB

pathway and stabilizes β-catenin to inhibit LPS-induced inflammation and endotoxic shock. However, a recent study proposed the dual effect of GSK-3β on the anti-inflammatory and inflammatory response depending on the virulence factors, cell types, and physiological state of cells (Cortes-Vieyra et al., 2012). Therefore, the significance of the crosstalk between the GSK-3β/β-catenin and NF-κB signaling pathways needs to be persistently investigated in the pathogenesis of inflammatory disorders such as septic shock.

2.5 Conclusions

In conclusion, our findings suggest that fisetin attenuates LPS-induced inflammation and endotoxic shock by suppressing the β-catenin-mediated NF-κB signaling pathway. Fisetin can thus be considered as a potential anti-inflammatory drug for systemic inflammation.

3 Chapter3

Fisetin inhibits NLRP3 inflammasome by suppressing mitochondrial ROS production, resulting from the inhibition of the TLR4-MD2 signaling pathway

Abstract

Fisetin possesses numerous pharmaceutical benefits such as anti-inflammatory antioxidant and anticancer activities. However, it remains unclear the way in which fisetin inhibits NLRP3 inflammasome. In this study, we found that fisetin binds to Toll-like receptor 4 (TLR4) and fits into the hydrophobic pocket of myloid differentiation factor 2 (MD2), which blocks LPS binding to TLR4/MD2 complex. The antagonistic effect of fisetin subsequently prevents the initiation of scaffold formation of myeloid differentiation primary response 88 (MYD88)/Interleukin-1 receptor-associated kinase 4 (IRAK4), which consequently downregulated the nuclear factor kappa B (NF-κB) cell signaling pathway. Moreover, fisetin inhibits LPS plus ATP (LPS/ATP)-induced NLRP3 inflammasome and consequent expression of interleukin-1β (IL-1β). Additionally, fisetin activates mitophagy by inhibiting depolarization of mitochondrial membrane potential and the generation of excessive mitochondrial reactive oxygen (mtROS) accompanied by accumulation of p62. Transient knockdown of *p62* using specific silencing RNA (sip62) reversed fisetin-induced antagonistic activity on NLRP3 inflammasome formation induced by LPS/ATP, which indicates that fisetin stimulates p62-mediated mitophagy to eliminate damaged mitochondria. In the LPS/ATP-stimulated zebrafish model, fisetin recovered the impaired heart rate and decreased the recruitment of macrophage in the brain accompanied by gradual downregulation of inflammasome-related gene expression. These results indicate that fisetin inhibits NLRP3 inflammasome formation by eliminating damaged mitochondria in a p62-dependent manner.

Key words: Fisetin; NLRP3 inflammasome; Nuclear factor kappa B; Mitochondria reactive oxygen species; p62

3.1 Introduction

Fisetin (3,7,3′,4′-tetrahydroxy flavone) is a member of flavonoids and ubiquitously exists in plants such as smoke trees, fruits, and vegetables (Feng et al., 2016; Kicinska and Jarmuszkiewicz, 2020). The biological effects of fisetin has been reported on a wide range of pharmacological aspects such as anticancer (Suh et al., 2010), antioxidant (Hanneken et al., 2005), melanogenesis (Molagoda et al., 2020) and anti-inflammation (Kim et al., 2012). Nevertheless, the detail molecular mechanisms fisetin on inflammasome is unclear.

Microglia are a resident myeloid derived cells in the central nervous system (CSN) (Das et al., 2016) and is considered as the primary mediators of neuroinflammation, since the cells are the most dominant resident immune cells in the brain (Korin et al., 2017). Among the developed murine microglia cell lines, BV2 microglia cells that are derived from raf/myc-immortalized murine neonatal microglia are regarded as most frequently used substitute for the primary microglia (Henn et al., 2009). Over activation of microglia under the infectious conditions is severely associated with neuronal death, that ultimately leads to neurodegenerative diseases such as Alzheimer's disease (AD), Parkinson's disease (PD) and multiple sclerosis through the massive production of reactive oxygen species and pro-inflammatory cytokines such as interleukin-1β (IL-1β), IL-18, IL-6 and tumor necrosis factor-α (TNF-α) (Cappellano et al., 2013; Stansley et al., 2012). Especially, IL-1β and IL-18 are considered as key proinflammatory cytokines in the progression of neuroinflammation (Allan et al., 2005). In this regard, intracellular multi-protein complex referred as inflammasome is consider as the major cause of triggering the mature IL-1β and IL-18 release (Hanamsagar et al., 2011). To the date, the most well-known inflammasome pathway is nucleotide-binding domain. leucine-rich-containing family, pyrin domain-containing 3 (NLRP3) inflammasome (de Zoete et al., 2014) which is consisted of NLRP3, the adaptor protein

apoptosis-associated speck-like protein containing a caspase recruitment domain (ASC) and the effector cysteine protease, caspase 1 (Tschopp and Schroder, 2010). Although the precious molecular mechanism of NLRP3 activation remains to be elucidated, a variety of stimulants including ATP, nigericin, pore-forming toxins and particulate matter trigger the activation of NLRP3 inflammasome (Bauernfeind et al., 2011). Furthermore, the generation of mitochondrial reactive oxygen species (mtROS) stimulates NLRP3-dependent inflammasome activation in response to LPS and ATP by losing mitochondrial membrane potential (Heid et al., 2013; Nakahira et al., 2011). Additionally, the excessive production of mtROS is limited by promoting autophagic clearance (mitophagy) of ROS-mediated damaged mitochondria (Vernucci et al., 2019). During the process malfunctioning mitochondria are recognized by microtubule-associated protein light chain 3 (LC3) to fuse with autophagosome through PINK1-Parkin-p62-mediated ubiquitin dependent pathway or BCL2/adenovirus E1B 19 kDa protein-interacting protein 3 (BNIP3), FUN14 domain containing 1 (FUNDC1) and cardiolipin-mediated ubiquitin-independent pathway (Zhang, 2015). Therefore, the elimination of damaged mitochondria to lower the excessive production of mtROS is a potent strategy to inhibit NLRP3 inflammasome mediated IL-1β and IL-18 formation (Chen et al., 2019; Guo et al., 2014).

In this study, we elucidated anti-NLRP3 inflammasome activity of fisetin in LPS plus ATP (LPS/ATP)-treated conditions in BV2 microglia cells. We found that fisetin inhibits LPS/ATP-induced NLRP3 inflammasome through the elimination of damaged mitochondria.

3.2 Materials and methods

3.2.1 Reagents and antibody

Fisetin, 3-(4,5-dimethylthiazol-2-yl)-2,5- diphenyl-tetrazolium bromide (MTT), LPS from *Escherichia coli* O111:B4, and adenosine 5′-triphosphate (ATP) disodium salt hydrate were obtained from Sigma (St. Louis, MO, USA). Fetal bovine serum (FBS), antibiotic mixture and Dulbecco's Modified Eagle's Medium (DMEM) were obtained from WelGENE (Gyeongsan-si, Gyeongsangbuk-do, Republic of Korea). Antibodies against ASC (sc-22514), caspase-1 (sc-65036), p50 (sc-8414), p65 (sc-8008), LC3 (sc-376404), p62/SQSTM1 (sc-480402), nucleolin (sc-13057) and β-actin (sc-69879), and peroxidase labelled anti-mouse immunoglobulins (sc-16102) were purchased from Santa Cruz Biotechnology (Santa Cruz, CA). Antibodies against NLRP3 (15101S) was purchased from Cell Signaling Technology (Beverly, MA, USA). Thermo Fisher Scientific (Waltham, MA, USA) and GenTex (Zeeland, MI, USA) supplied specific antibodies against IRAK (PA5-20018) and MYD88 (GTX-112987), respectively. Koma Biotechnology (Seoul, Republic of Korea) provided peroxidase-labeled anti-rabbit immunoglobulins (KO211708). Alexa Fluor 647 was purchased from Abcam (Cambridge, MA, UK). Dako Faramount Aqueous Mounting Media was obtained from Dako (Carpinteria, CA, USA). All other chemicals were purchased from Sigma grades.

3.2.2 Cell culture and viability assay

BV2 microglial cells were cultured at 37°C in 5% CO_2 in DMEM supplemented with 5% FBS. The cells (1×10^5 cells/mL) were pretreated with the indicated concentrations of fisetin (0-20 μM) for 2 h and primed with 1 μg/mL LPS for 2 h and 1 mM ATP for another 24 h. Then, MTT assay was performed to measure the cell viability (Berridge et al., 2005). Dissolved formazan intensities

were measured at 540 nm using an ELISA microplate reader (BioTek Instruments Inc.; Winooski, VT, USA).

3.2.3 Analysis of viability and dead cells populations

Total populations of viable cells and dead cells were measured by flow cytometry (Muse Cell Analyzer, Luminex Corp., Austin, TX, USA). Briefly, BV2 cells were pretreated with fisetin (0–20 μM) for 2 h prior to stimulation with 1 μg/mL LPS for 2 h and 1 mM ATP for another 24 h. Then, the harvested cells were stained with Muse Count & Viability Kit (MCH100102, Luminex Corp.). Cell viability% and dead cell% were measured using Muse Cell Analyzer.

3.2.4 Measurement of IL-1β by ELISA

BV2 microglia cells were pretreated with fisetin (0–5 μM) for 2 h. Then, the cells were stimulated with 1 μg/mL LPS for 2 h and then, primed with 1 mM ATP for another 48 h. Extracellular IL-1β was detected by a ELISA Assay Kit (BMS6002, Thermo Fisher Scientific).

3.2.5 Western blotting

After BV2 microglial cells were pretreated with fisetin (0–5 μM) for 2 h and then stimulated with 1 μg/mL LPS for 2 h and then, 1 mM ATP for another 9 h. Total protein was extracted using PRO-PREP protein extraction solution (iNtRON Biotechnology, Sungnam, Republic of Korea) and the total protein concentrations were determined using a Bio-Rad Protein Assay Kit (Bio-Rad, Hercules, CA). Western blotting was performed to detect the expression of indicated proteins.

3.2.6 Reverse transcriptase polymerase chain reactions (RT-PCR) using mouse specific primers

Easy-Blue Reagent (iNtRON Biotechnology) was used to extract total RNA according to the manufacturer's instructions. Target genes were amplified using the One-Step RT-PCR Premix

(iNtRON Biotechnology). The specific primers and PCR conditions were shown in Table. 1 (Molagoda et al., 2019).

Table 2. Primers and PCR conditions for BV2 microglial cells.

Gene*	Primer sequence(5′-3′)	Size	T_m	Cycle No.
NLRP3	F: 5′- ATTACCCGCCCGAGAAAGG-3′ R: 5′- TCGCAGCAAAGATCCACACAG-3′	120 bp	58℃	27
ASC	F: 5′- GCAACTGCGAGAAGGCTAT-3′ R: 5′- CTGGTCCACAAAGTGTCCTG-3′	236 bp	58℃	27
IL-1β	F: 5′- GCCCATCCTCTGTGACTCAT -3′ R: 5′- AGGCCACAGGTATTTTGTCG -3′	210 bp	65℃	27
Caspase 1	F: 5′- CTGACTGGGACCCTCAAG -3′ R: 5′- CCTCTTCAGAGTCTCTTACTG -3′	100 bp	63℃	27
GAPDH	F: 5′- CACCACCCTGTTGCTGTAGC -3′ R: 5′- ACCACAGTCCATGCCATCAC -3′	123 bp	63℃	23

Bp; base pair, T_m; melting temperature.

***** *NLRP3; nucleotide-binding domain. leucine-rich-containing family, pyrin domain-containing 3, ASC; adaptor protein apoptosis-associated speck-like protein containing a caspase recruitment domain, IL-1β; Interleukin 1β, GAPDH; glyceraldehyde 3-phosphate dehydrogenase.*

3.2.7 Immunostaining of p65 and p62/SQSTM1

BV2 microglial cells (1×10^4 cells/mL) were cultured on 3% gelatin-coated coverslips in the indicated concentrations of fisetin (0–5 μM) for 2 h, and then, 1 μg/mL LPS was treated for 2 h. After 1 mM ATP treatment for additional 1 h, the cells were fixed with 4% paraformaldehyde and permeabilized with 0.1% Triton X-100. The cells were incubated with p65 and p62/SQSTM1 antibody (1:100 in 10% donkey serum) and Alexa Fluor 647 secondary antibody was incubated for 2 h. Then, nuclear counterstaining using DAPI (300 nM) was performed, and the slide was mounted with Dako Faramount Aqueous Mounting Media. Fluorescence images were captured by

a CELENA S Digital Imaging System (Logos Biosystems, Anyang, Gyeonggi-do, Republic of Korea).

3.2.8 Analysis of mtROS

Generation of mtROS was detected by both live cell imaging and fluorometer. BV2 microglial cells were treated with indicated concentrations of fisetin for 2h. Then, 1 μg/mL LPS was treated 2 h before treatment with 1 mM ATP for 1 h. After washing the cells with PBS cells were loaded with 2 μM MitoSOX Red (Thermo Fisher Scientific) for 10 min. Fluorescence intensities were measured by GloMax 96 Microplate Luminometer (Promega) and live cell imaging was performed by a CELENA S digital imaging system.

3.2.9 Mitochondrial depolarization

BV2 microglial cells were treated with the indicated concentrations of fisetin (0–5 μM) for 2 h followed by exposure with 1 μg/mL LPS for 1 h and then 1 mM ATP for additional 1 h. The cells were stained with a Muse MitoPotential Kit (MCH100110, Luminex Corp.), and mitochondrial membrane depolarization was measured using Muse Cell Analyzer.

3.2.10 Transfection of p62 small interfering RNA (siRNA)

BV2 microglia cells were seeded at a density of 1×10^4 cells/mL and transiently transfected with 10 nM siRNA duplex (Santa Cruz, CA) with G-fectin transfection reagent (Genolution Pharmaceuticals Inc., Seoul, Republic of Korea) according to the manufacturer's protocol.

3.2.11 Maintenance of zebrafish embryo and larvae

Zebrafish study was approved the Animal Care and Use Committee of Jeju National University (Jeju Special Self-governing Province, Republic of Korea; approval No.: 2020-0013), and all methods were carried out in accordance with the approved guideline (Percie du Sert et al., 2020).

Fertilized embryos were collected through natural spawning and cultured at 28.5℃ in E3 embryo media containing 2 mg/L methylene blue.

3.2.12 Cardiac toxicity evaluation

Three days post fertilized (dpf) zebrafish larvae were pretreated with the indicated concentrations of fisetin (0-400 μM) for 2 h prior to treatment with 5 μg/mL LPS for 2 h followed by 2 mM ATP for another 24 h. Each group of larvae (*n=20*) was cultured at 28.5℃ and observed for the mortality. The heart rate of the larvae was manually counted using an Olympus SZ2-ILST stereomicroscope (Tokyo, Japan) for two minutes and used as an indicator for the cardiac toxicity evaluations (Karunarathne et al., 2020). The values were expressed as heart beats/min.

3.2.13 Neutral red staining

Macrophage staining in live zebrafish larvae was conducted using neutral red 24 h after LPS plus ATP treatment. Briefly, zebrafish larvae were immersed in 2.5 μg/mL neutral read solution containing 0.003% PTU at 28.5℃ in the dark for 6-8 h (Karunarathne et al., 2020). After staining, macrophages in the brain area were observed using an Olympus SZ2-ILST stereomicroscope.

3.2.14 Isolation of total zebrafish mRNA and RT-PCR

Total RNA was extracted from zebrafish larvae 18 h after LPS plus ATP treatment using Easy-Blue Reagent (iNtRON Biotechnology). The RNA was reverse-transcribed and amplified the One-Step RT-PCR Premix (iNtRON Biotechnology) The specific primer sequences for *IL-1β* and *β-actin* were obtained from a previous study (Liu et al., 2014) and the sequences of *ACS*, *Caspase A*, and *Caspase B* were designed based on the NCBI gene database in this study (Table 2).

Table 3. Primers and PCR conditions for zebrafish.

Gene*	Primer sequence(5′-3′)	Size	T_m	Cycle No.	NCBI accession No.
IL-1β	F 5′-TGGACTTCGCAGCACAAAATG-3′ R 5′-GTTCACTTCACGCTCTTGGATG-3′	149 bp	59℃	27	
ASC	F 5′-GGCGGAATCTTTCAAGGAGC-3′ R 5′-ACGCCGACCATTAAATCAGC-3′	171 bp	58℃	27	NM_131495
Caspase A	F 5′-GAGAATTGTCCAGCTCTGCG-3′ R 5′-GCCGGTAAGATTTGGTGTCC-3′	198 bp	58℃	27	NM_131505
Caspase B	F 5′-CCTCGAGGATCTTGTGGAGT-3′ R 5′-GCTTGATTTTGCGCAGTGTC-3′	184 bp	58℃	27	NM_152884
β-actin	F 5′-CGAGCGTGGCTACAGCTTCA-3′ R 5′-GACCGTCAGGCAGCTCATAG-3′	155 bp	61℃	23	

Bp; base pair, T_m; melting temperature.

***** *IL-1β; interleukin-1β, ASC; adaptor protein apoptosis-associated speck-like protein containing a caspase recruitment domain, GAPDH; glyceraldehyde 3-phosphate dehydrogenase*.

3.2.15 Statistical analysis

All the western blots and RT-PCR bands were quantified by ImageJ 1.50i (National Institute of Health, Manassas, VA, USA, www.imagej.net) and then statistically analyzed by Sigma plot 12.0 (Systat Software, San Jose, CA, USA, www.systatsoftware.com). All data represented the mean of at least three independent experiments. Significant differences between groups were determined using a Student *t* test and an unpaired one-way ANOVA test with Bonferroni correction. Statistical significance was set at *** and $^{###}$ $p < 0.001$, ** and $^{##}$ $p < 0.01$, * and $^{#}$ $p < 0.05$.

3.3 RESULTS

3.3.1 High concentrations of fisetin possess cytotoxicity in BV2 microglia cells at

In order to evaluate the cytotoxic effect of fisetin (Figure 19A), we treated BV2 microglia cells with fisetin for 24 h in the presence and absence of LPS plus ATP (LPS/ATP). We found that fisetin possesses significantly higher cytotoxicity from 10 µM onward (89.7 ± 1.7% and 70.9 ± 0.6% at 10 µM and 20 µM fisetin, respectively, compared with that in the untreated cells, Figure 19B). In LPS/ATP-treated conditions (89.2 ± 1.7%), the cytotoxicity notably decreased to 67.1 ± 3.4% and 52.9 ± 1.4% at 10 µM and 20 µM fisetin. Treatment with fisetin in the absence of LPS/ATP possessed no cytotoxic hall marks such as cell swelling, cell debris or floating cells (Figure 19C); however, LPS/ATP treatment resulted in low number of cells and fisetin above 10 µM strongly diminished total number of cells. According to flow cytometry data (Figure 19D), fisetin induced 18.7% ± 1.1% and 25.8% ± 0.4% of dead cell populations at 10 µM and 20 µM (Figure 19E) along with the 81.3% ± 1.1% and 75.5% ± 0.4% of viable cell populations (Figure 19F), respectively, in the absence of LPS/ATP. Align with the MTT and microscopic data, 10 µM and 20 µM fisetin further intensified cytotoxic effect of LPS/ATP to 24.5% ± 1.2% and 54.5 ± 1.4% of dead cell populations and 75.5% ± 1.2% and 46.2% ± 1.4% of viable cell populations.

Altogether these results indicate that fisetin possess no cytotoxic effect below 10 μM in BV2 microglia cells.

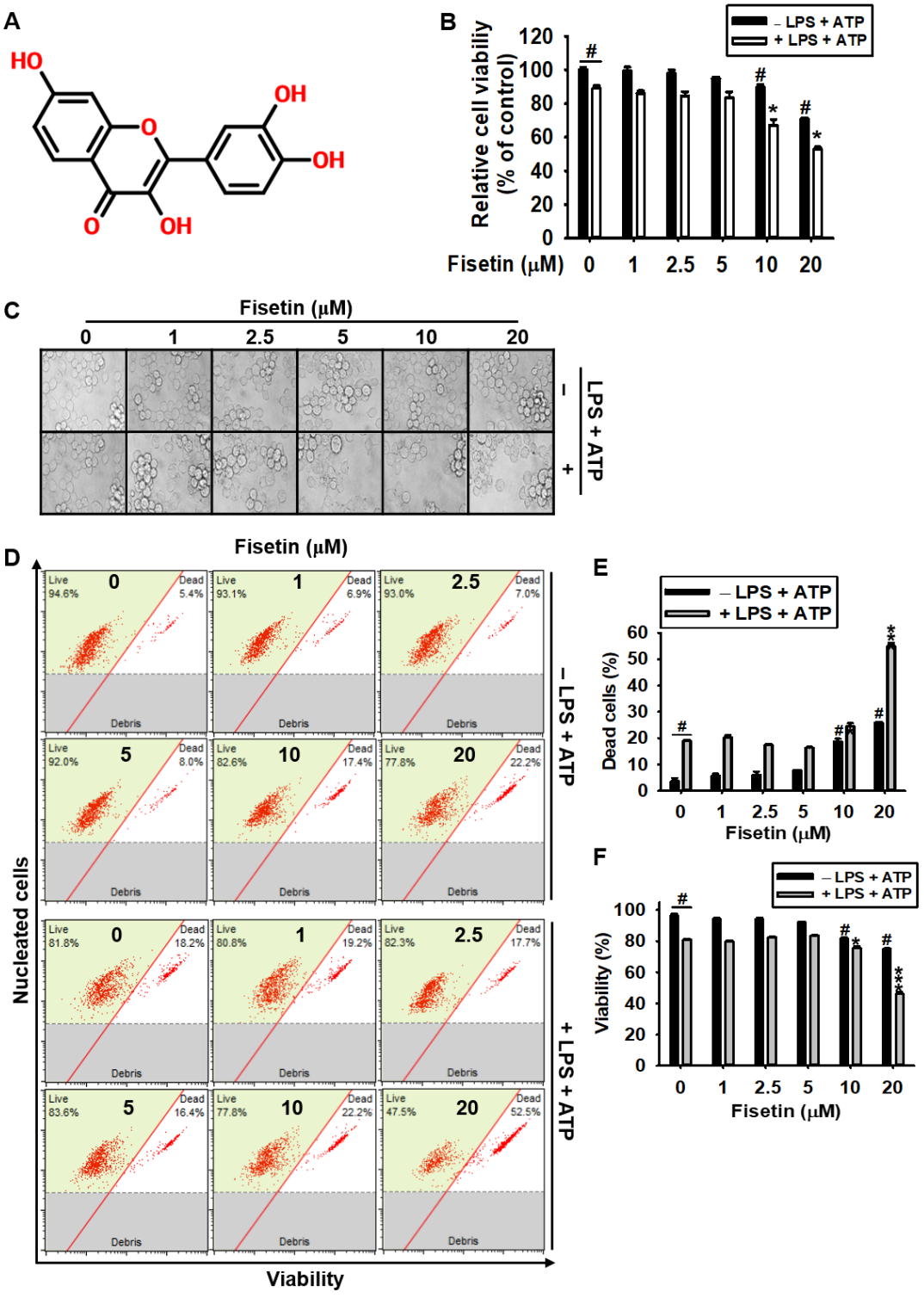

Figure 19. Fisetin exhibits cytotoxic effect at high concentrations in BV2 microglia cells. (A) Chemical structure of fisetin. BV2 microglia cells were seeded at a density of 1×10^5 cells/mL in 24 well plates and pretreated with indicated concentrations (0-20 μM) of fisetin for 2 h in the presence and absence of 1 μg/mL LPS for 2 h followed with 1 mM ATP (LPS/ATP) for another 2 h. After 24h after chemical treatment (B) Cell viability was analyzed by MTT assay. (C) Live images of the cells were taken with Ezscope i900PH phase contrast microscope (x10). (D) Cell viability and the dead cell population were measured using a Muse Cell Viability Kit. Cell viability percentage and dead cell population are shown. Significant differences among the groups were determined using the one-way ANOVA followed by Bonferroni correction. All data are the average of three independent experiments and presented as mean ± standard error of the median. $^{\#}$ $p < 0.05$ vs. untreated cells, *** $p < 0.001$ and * $p < 0.05$ vs. LPS/ATP treated cells.

3.3.2 Fisetin possibly binds to TLR4/MD2 complex and inhibits the LPS-induced downstream signaling pathway

LPS binds to Toll-like receptor 4 (TLR4)/Myeloid Differentiation factor 2 (MD2) complex and stimulates MYD88-IRAK4 axis, causing inflammatory disorders (Maeshima and Fernandez, 2013). The molecular docking data predicted four strong binding activity of fisetin to TLR4/MD2 complex. The strongest binding activity (pose 1) of fisetin showed binding score of -6.6 binding to serine 438 in TLR4 with a hydrogen bonding distance of 2.472Å and 3.218 Å, which hinders the LPS binding hydrophobic pockets of MD2 (Figure 20A and Table 3). The other 3 poses also predicted to bind to TLR4 and to block the LPS-binding pocket of MD2 with different binding scores and amino acid (Supplementary Fig. 1 and Table 3). Next, we verified whether fisetin inhibits the LPS-induced TLR4/MD2 signaling pathway by binding to TLR4/MD2 complex. Immunostaining revealed that TLR4 fluorescence was intensified in the plasma membrane by

LPS/ATP; however, it was effectively blocked in the presence fisetin (Figure 20B). Since fisetin binds to TLR4/MD2 complex and inhibits its expression on the plasma membrane, we investigated whether fisetin inhibits the recruitment of the adopter proteins such as MyD88 and IRAK4. As expected, fisetin prevented the expression of MyD88 and IRAK4 induced by LPS plus ATP treatment in a concentration-dependent manner (Figure 20C). These results indicate that fisetin interacts with TLR4/MD2 complex and consequently blocks LPS binding to the complex, which restrained the LPS-mediated TLR4/MD2 signaling.

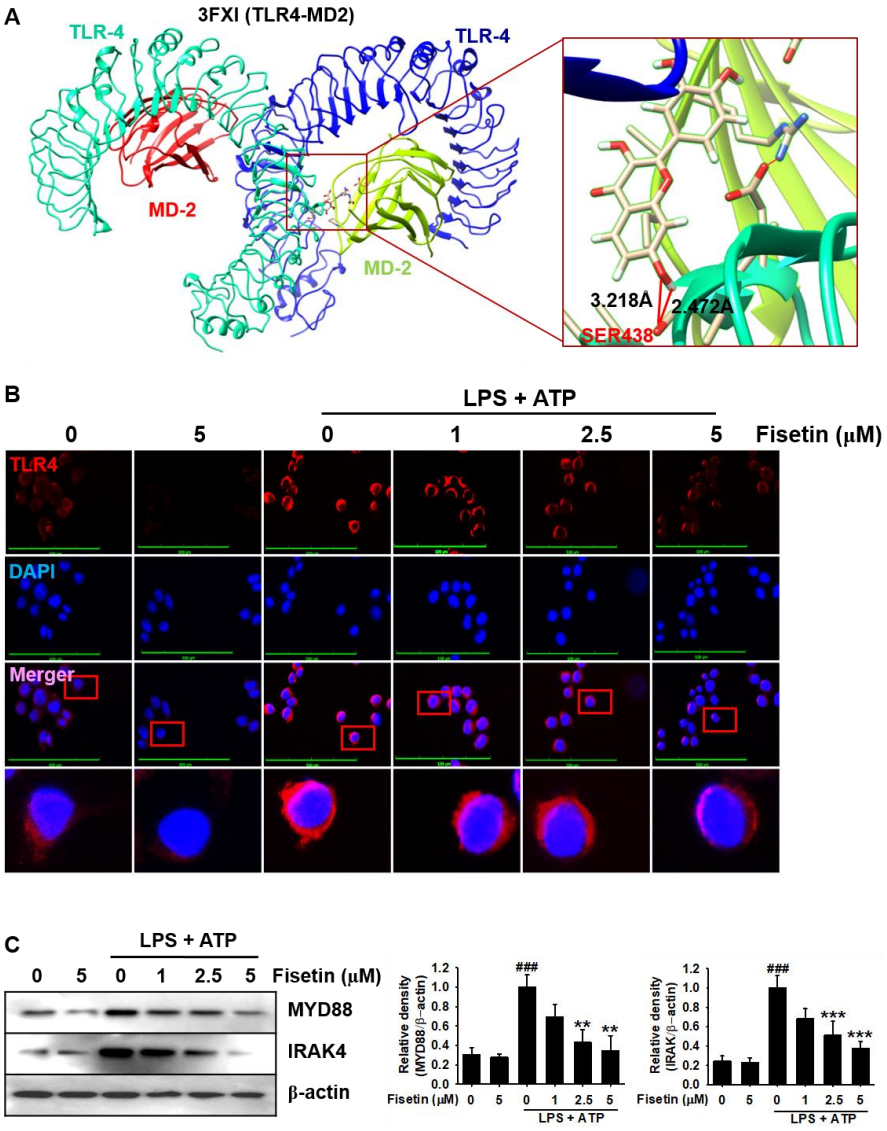

Figure 20. Fisetin mediated anti-inflammatory responses are mediated through TLR4-related cell signaling pathway. (A) Molecular docking of fisetin and TLR4/MD2. (B) BV2 microglia cells were seeded at a density of 1 x 10^4 cells/mL in 3% gelatin coated cover slips and pretreated with indicated concentrations of fisetin 2 h prior to the stimulation with 1 μg/mL LPS for 2 h followed with 1mM ATP (LPS/ATP) for another 2 h. Cells were fixed with 4% paraformaldehyde and immunostained for TLR4 with Alexa Fluor® 448 and images were taken with CELENA®S digital imaging system. (C) In a parallel experiment, cells were seeded in a density of 1 x 10^4 cells/mL in 6 well plates and total proteins were extracted 2 h after chemical treatment and western blotting was performed to detect IRAK and MYD88 protein expressions. β-Actin was used as the internal control. Significant differences among the groups were determined using the one-way ANOVA followed by Bonferroni correction. All data are the average of three independent experiments and presented as mean ± standard error of the median. $^{###}p < 0.001$ vs. untreated cells, $^{***}p < 0.001$ and $^{**}p < 0.01$ vs. LPS/ATP treated cells.

Table 4. The docking of fisetin to TLR4-MD2 (PDB: 3FX1).

Binding pose	binding score	Binding to TLR4	
		Binding AA[1]	H-bond[2] distance (Å)
1	-6.6	SER438 (OG)[3]	3.218
		SER438 (OG)	2.472
2	-6.3	LYS435 (NZ)	3.440
		SER438 (N)	2.862
		SER438 (OG)	3.250
3	-5.5	HIS431 (ND1)	2.250
		HIS456 (O)	2.608
4	-5.4	SER455 (OG)	2.932

	SER528 (OG)	2.699
	SER528 (OG)	1.863
	SER528 (OG)	3.087

[1] A.A.; Amino acids.

[2] H-bond; Hydrogen bond.

[3] Binding position at each amino acid.

3.3.3 Fisetin inhibits the NF-κB cell signaling pathway.

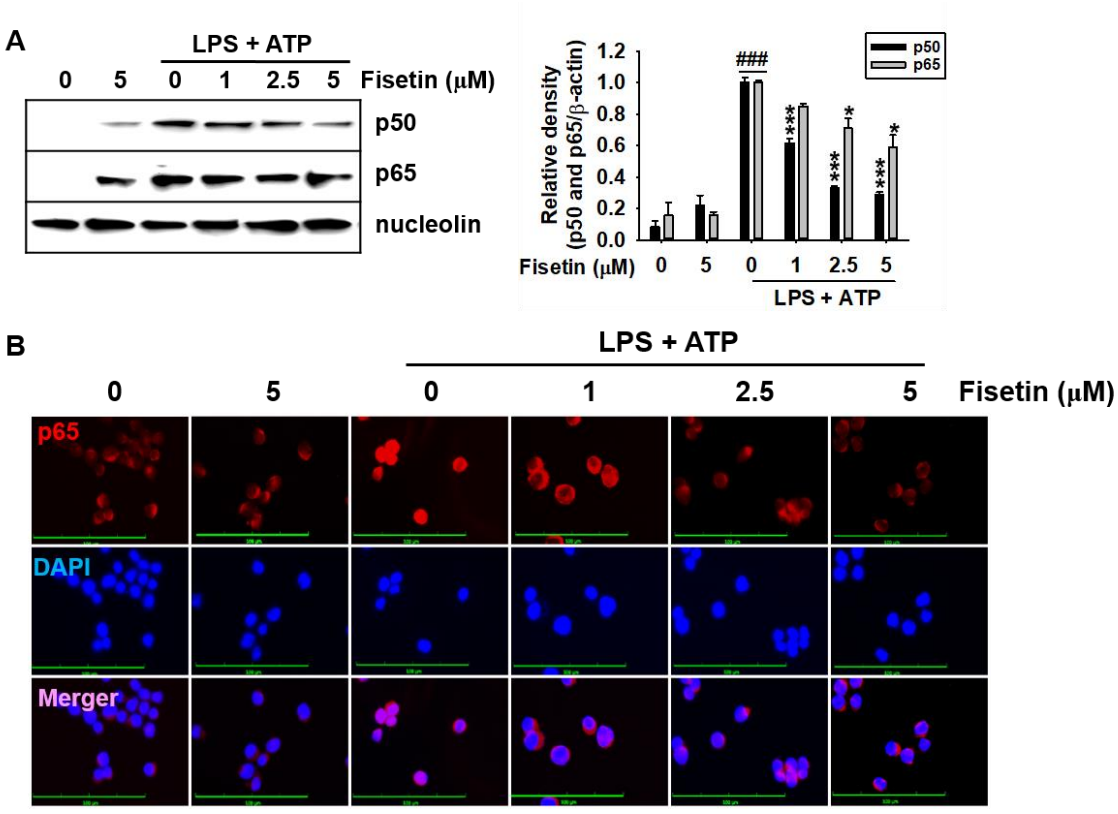

Figure 21. Fisetin inhibits the activation of NF-κB cell signaling pathway. BV2 microglial cells were seeded at a density of 1 x 10^5 cells/mL and pretreated with the indicated concentrations of fisetin for 2 h prior to stimulation with 1 μg/mL LPS for 2 h, followed with 1 mM ATP (LPS/ATP). (A) Nuclear proteins were extracted 1 h after ATP treatment and western blotting was

performed. Nucleolin was used as the internal control. (B) In a parallel experiment, the cells were fixed with 4% paraformaldehyde, immunostained for NF-κB p65 with Alexa Fluor 647 and imaged by the CELENA S digital imaging system. Significant differences among the groups were determined using the one-way ANOVA followed by Bonferroni correction. All data are the average of three independent experiments and presented as mean ± standard error of the median $^{###}$ $p < 0.001$ vs. untreated cells, *** $p < 0.001$ and * $p < 0.05$ vs. LPS/ATP treated cells.

Nuclear translocation of NF-κB results in the transcriptional initiation of the target genes including *NLRP3, ASC, Caspase 1* and *IL-1β* to trigger inflammatory immune responses (Yang et al., 2019), we examined whether fisetin could downregulates LPS/ATP-induced nuclear translocation of NF-κB. As shown in Figure 21A, fisetin concentration-dependently decreased LPS/ATP-induced nuclear expression of NF-κB p50 and p65. Additionally, the inhibitory effect was further validated with the immunostaining of p65 with Alexa Fluor 647 secondary antibody. As shown in Figure 21B, LPS/ATP remarkably intensified p65 nuclear translocation, which was strongly alleviated in the presence of fisetin in a concentration-dependent manner. Taken together, these results indicate that fisetin inhibits LPS/ATP-mediated nuclear translocation of NF-κB.

3.3.4 Fisetin inhibits the expression of NLRP3 inflammasome components

Next, we assessed the effect of fisetin on the expression of NLRP3 inflammasome components such as NLRP3, ASC, Caspase 1 and IL-1β both at the transcriptional and translational levels. Both ASC and NLRP3 were transcriptionally (Figure 22A, *top*) and translationally (Figure 22A, *bottom*) upregulated in response to LPS/ATP treatment. However, fisetin effectively blocked the LPS/ATP-induced ASC and NLRP3 expression at the transcriptional and translational levels. Additionally, LPS/ATP-induced Caspase 1 expression was markedly inhibited by fisetin both at

transcriptional and translational levels (Figure 22B). Finally, we measured the expression of IL-1β in LPS/ATP-treated cells. Fisetin effectively blocked LPS/ATP-induced IL-1β expression at the transcriptional level (Figure 22C). Moreover, LPS/ATP treatment resulted in a significant increase of secretory IL-1β (688.24 ± 108.97 pg/mL) and fisetin inhibited the extracellular IL-1β secretion in a concentration-dependent manner (603.6 ± 72.8, 469.8 ± 28.0 and 413.9 ± 44.3 pg/mL at 1, 3 and 5 μM fisetin, respectively, Figure 22D). These results indicate that fisetin inhibits LPS/ATP-induced IL-1β secretion by inhibiting the expression of NLRP3 inflammasome components.

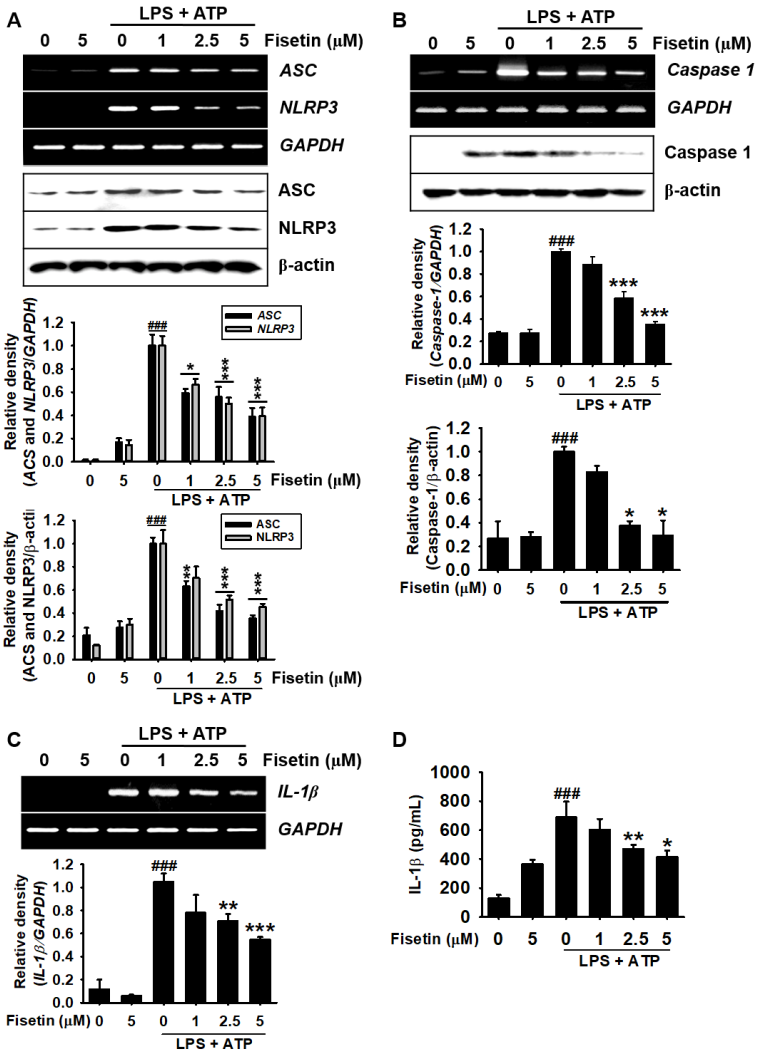

Figure 22. Fisetin inhibits IL-1β maturation by inhibiting NLRP3 inflammasome formation. BV2 microglia cells were seeded at a density of 1 x 10^5 cells/mL and treated with indicated concentrations of fisetin (0-5 µM) for 2 h prior to stimulate with 1 µg/mL LPS 2 h followed with 1mM ATP. (A) Cell culture media was collected 48 h ATP treatment and IL-1β levels were quantified using ELISA assay. (B) Total mRNA was collected 3 h after ATP treatment and RT-PCR was performed for caspase1 (upper) and total proteins were collected and western blotting was performed against caspase-1 protein (lower). (C) NLRP3 and ASC gene (upper) and protein (lower) expressions were analyzed using RTPCR and western blotting respectively. Densitometric analysis of each figure shown. Significant differences among the groups were determined using the one-way ANOVA followed by Bonferroni correction. All data are the average of three independent experiments and presented as mean ± standard error of the median $^{###}p < 0.001$ vs. untreated cells, $^{***}p < 0.001$, $^{**}p < 0.01$ and $^{*}p < 0.05$ vs. LPS/ATP treated cells.

3.3.5 Fisetin inhibits mitophagy by downregulating mitochondria depolarization and mtROS production.

Damaged mitochondria upregulate the formation of NLRP3 inflammasome complex through the release of mtROS, mtDNA and cardiolipin I to the cytosolic compartment (Kelley et al., 2019); hence, the clearance of the damaged mitochondria could be a promising strategy to prevent NLRP3 inflammasome-mediated inflammation. Therefore, we hypothesized that fisetin could inhibit the formation of NLRP3 inflammasome through the elimination of damaged mitochondria. Confirming the hypothesis, we confirmed that LPS/ATP increased the damaged mitochondria population (depolarized mitochondrial membrane potential) to 41.0% ± 1.1%, whereas fisetin effectively reduced the damaged mitochondria in the cells to 36.4% ± 2.0%, 31.0% ± 3.0% and 25.5% ± 4.0% from 1, 2.5 and 5 µM fisetin (Figure 23A). Since the damaged mitochondria

population decreased by treatment of fisetin, we analyzed the effect of fisetin on mtROS generation. As shown in Figure 23B, LPS/ATP treatment resulted in a significant increase of MitoSOX Red intensity (EX/EM 510/580 nm) from 298 ± 4.1 to 409.1 ± 3.9, whereas the LPS/ATP-induced intensity gradually decreased to 342.3 ± 5.2, 302.2 ± 6.4 and 292.5 ± 2.6 at 1, 2.5 and 5 μM fisetin. Fluorescence microscopic data also confirmed that fisetin inhibits LPS/ATP-induced mtROS production in a concentration-dependent manner (Figure 23C). Mitophagy plays an important role in eliminating damaged mitochondria from the cells; hence, we investigated whether fisetin inhibits the expression LC3 cleavage which is used as a mitophagy marker. As shown in Figure 23D, we could observed that fisetin promoted LC3 cleavage in a concentration-dependent manner. Furthermore, immunostaining of p62, another marker for mitophagy activation, also confirmed that fisetin could effectively promote the clearance of LPS/ATP-mediated damage mitochondria in BV2 microglia cells (Figure 23E). These results suggest that fisetin activates mitophagy accompanied by inhibiting mitochondrial membrane depolarization and mtROS production.

Figure 23. Fisetin Inhibits LPS/ATP induced mitochondrial depolarization and p62 expression in BV2 microglia cells. BV2 microglia cells were seeded at a density of 1 x 10^5 cells/mL in 6 well plates and pretreated with indicated concentrations of PS 2 h prior to the stimulation with 1 μg/mL LPS for 2 h followed with 1mM ATP (LPS/ATP) for another 2 h. (A) Depolarized mitochondria populations were measured by flow cytometry using Muse® MitoPotential Kit. (B-C) Cells were stained with 2 μM Mitosox red for 10 min and (B) fluorescence intensities were measured using Promega fluorometer (C) live images were taken by CELENA®S digital imaging system. (D) In a parallel experiment total proteins were extracted 9 h after LPS/ATP treatment. Western blotting was performed to detect p62 and LC3 expressions. β-

Actin was used as the internal control. (D) Cells were fixed with 4% paraformaldehyde and immunostained for p62 with Alexa Fluor® 448 and images were taken with CELENA®S digital imaging system. Significant differences among the groups were determined using the one-way ANOVA followed by Bonferroni correction. All data are the average of three independent experiments and presented as mean ± standard error of the median $^{###}p < 0.001$ vs. untreated cells, $^{***}p < 0.001$, $^{**}p < 0.01$ and $^{*}p < 0.05$ vs. LPS/ATP treated cells.

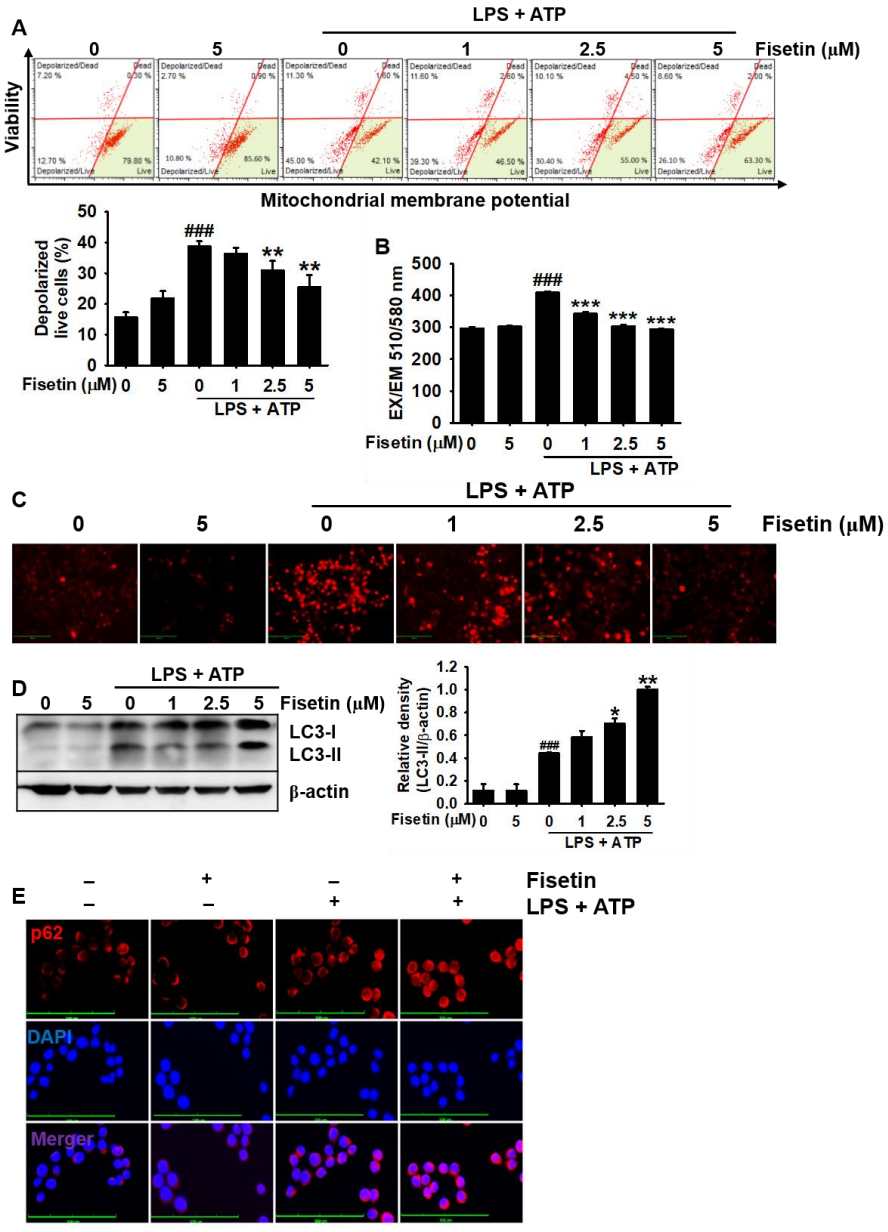

3.3.6 Silencing of p62 reverses fisetin-mediated mitophagy and NLRP3 inflammasome formation.

Since p62 plays a pivotal role in the clearance of damaged mitochondria, we examined whether fisetin-induced p62 inhibits LPS/ATP-stimulated NLRP3 inflammasome formation. Transient knockdown of *p62* resulted in an increase of total live cell population with depolarized mitochondrial membrane potential from 14.1% ± 1.1% to 24.7% ± 2.1% compared with that in the untreated cells (Figure 24A, *bottom left*) and decreased the healthy cell population from 67.6% ± 3.6% to 60.6 ± 2.8% (Figure 24A, *bottom right*). Moreover, the silencing of p62 reversed the effect of fisetin on LPS/ATP-induced mitochondria-depolarized cell population from 28.3 ± 1.9% to 42.9 ± 1.2% and decreased the healthy cell populations from 42.7 ± 1.2% to 32.6 ± 1.1%. Aligned with flow cytometry data, silencing of *p62* associated with a higher amount of mtROS production compared with that in the untreated cells and also reversed antioxidant activity of fisetin in LPS/ATP-treated cells (Figure 24B). Finally, we examined extracellular IL-1β secretion in p62-silencing condition. Transition knockdown of p62 significantly upregulated IL-1β secretion (369.4 ± 13.0 pg/mL) compared with that in the untreated cells (139.1 ± 13.5 pg/mL, Figure 24C). Furthermore, LPS/ATP-induced IL-1β level (693.2 ± 89.0 pg/mL) was strongly intensified by sip62 transfection to 830.6 ± 72.8 pg/mL. In LPS/ATP condition, fisetin-mediated IL-1β inhibition (452.8 ± 38.0 pg/mL) was also reversed by silencing of p62 to 623.9 ± 104.3 pg/mL. Altogether, these results indicated that, fisetin inhibits NLRP3 inflammasome formation in BV2 microglia cells by eliminating damaged mitochondria in p62 dependent manner.

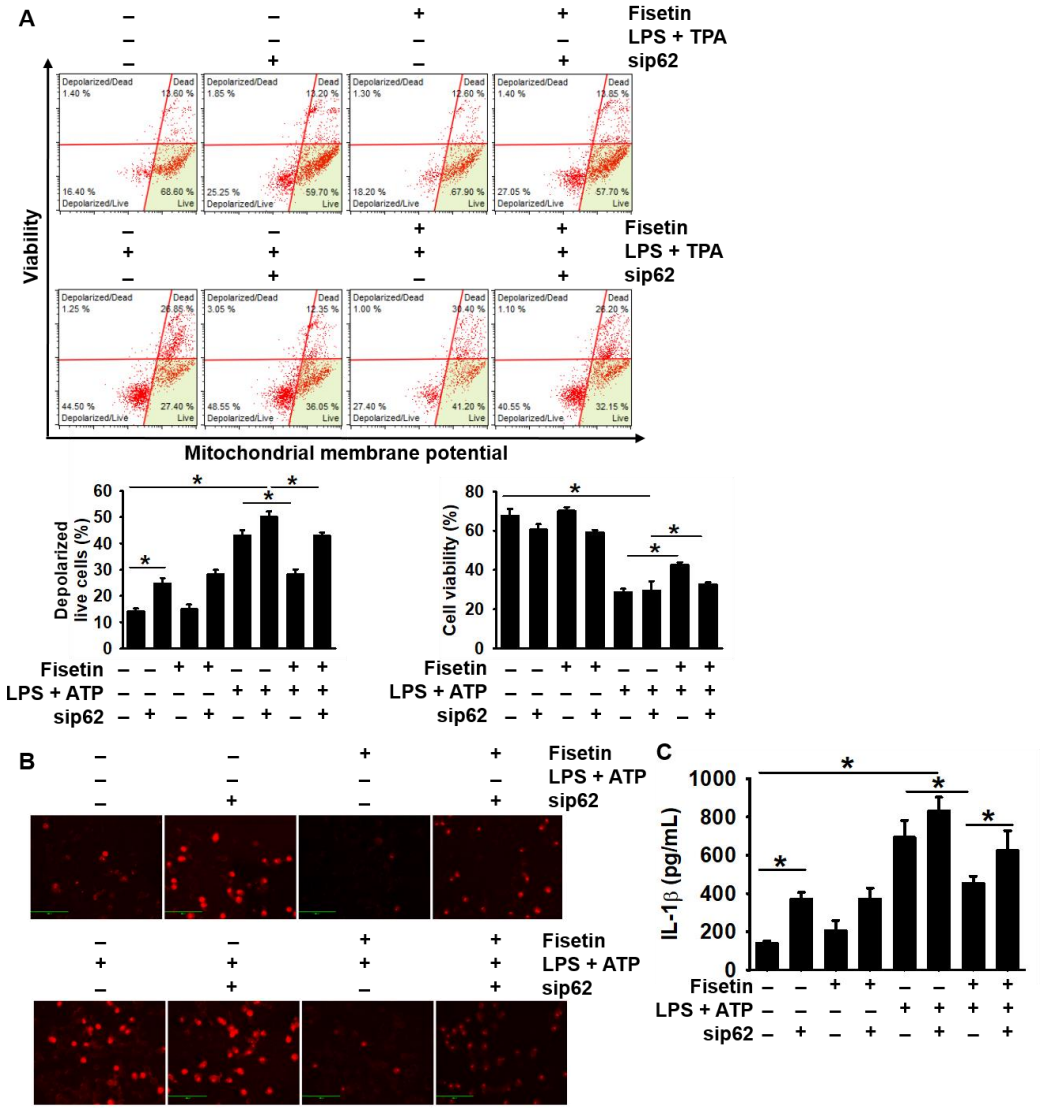

Figure 24. Transient knockdown of p62 resulted inhibition of fisetin mediated mitochondrial depolarization. BV2 microglia cells were seeded at a density of 1 x 10^4 cells/mL in 6-well plates and transiently transfected with CHOP siRNA for 48 h. The cells were treated with 1 µg/mL LPS for 2 h, followed with 1 mM ATP (LPS/ATP) for 2 h. (A) Depolarized mitochondria populations were measured by flow cytometry using Muse MitoPotential Kit. (B) In a parallel experiment cells were seeded in 8 well chamber slides and 2 h after LPS/ATP treatment cells were stained with 2 µM MitoSOX Red to identify mtROS. Live cellular images were captured using the CELENA S

digital imaging system. (C) Extracellular IL-1β levels were quantified using an ELISA assay 48 h after LPS/ATP treatment. Significant differences among the groups were determined using the one-way ANOVA followed by Bonferroni correction. All data are the average of three independent experiments and presented as mean ± standard error of the median $^{*}p < 0.05$.

3.3.7 Fisetin inhibits NLRP3 inflammasome formation in zebrafish larvae.

In order to identify the anti-inflammatory effect of fisetin in zebrafish larvae, the indicated concentrations of fisetin (0-400 μM) were pretreated for 2 h prior to the treatment with 5 μg/mL of LPS for 2 h and then, 2 mM ATP for another 24 h. Stimulation with LPS/ATP was not associated with fish death; however, significant lowering of the heart rate was observed (88.4 ± 4.3% heart rate/min) compared with that in the untreated zebrafish larvae (185.5 ± 2.4 heart beats/min, Figure 25A). LPS/ATP-induced heart rate was significantly recovered by fisetin in a concentration-dependent manner (148.7 ± 3.0 and 173.6 ± 1.7 heart beats/min at 200 μM and 400 μM fisetin, respectively). The macrophage staining also showed that treatment with LPS/ATP resulted in the higher density of macrophage population in the brain compared with that in the untreated zebrafish and fisetin mitigated LPS/ATP-induced macrophage migration in the brain (Figure 25B). Additionally, fisetin concentration-dependently inhibited the expression of NLRP inflammasome-related genes such as *IL-1β*, *ASC*, *Caspase A* and *Caspase B* (Figure 25C). These results suggest that fisetin inhibits LPS/ATP- induced NLRP-mediated inflammatory responses and macrophage recruitment to the brain in zebrafish larvae.

Figure 25. Fisetin inhibits the inflammasome formation in zebrafish larvae. Three days post fertilized (dpf) larvae were pretreated with the indicated concentrations of fisetin for 2 h prior to the treatment with 5 μg/mL LPS for 2 h, followed by 2 mM ATP (LPS/ATP) for indicated period of time. (A) Heart beat rate was counted 24 h after LPS/ATP treatment for 2 min and expressed as heart beat/min. (B) Total RNA was extracted 18 h after LPS/ATP treatment and the expression of zIL-1β, zASC, zCaspA and zCasB was assessed by RT-PCR. zβ-Actin was used as the internal control. (C) Neutral red staining was conducted for the macrophage staining at 24 after LPS/ATP treatment. All data are the average of three independent experiments and presented as mean ± standard error of the median $^{\#}p < 0.05$ vs. untreated cells, $^{***}p < 0.001$ and $^{*}p < 0.05$ vs. LPS/ATP treated cells.

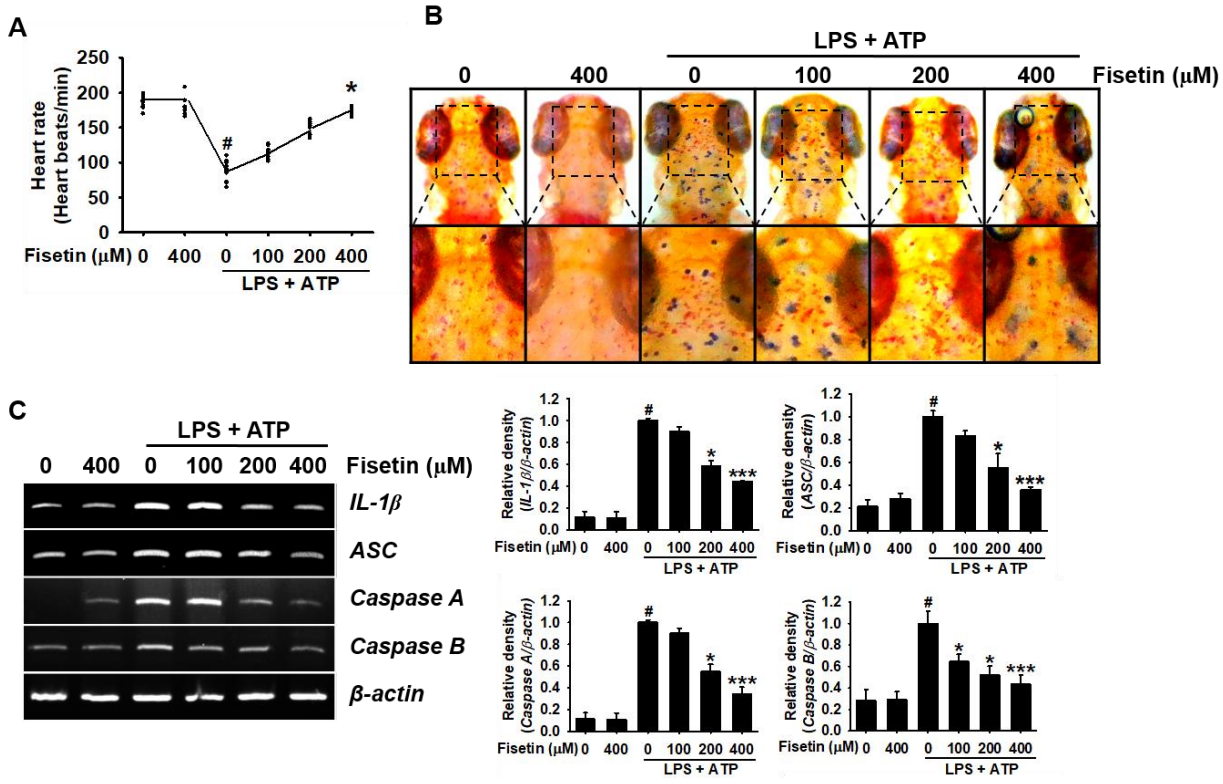

3.4 Discussion

Fisetin is a ubiquitously existing flavonol in strawberry, apple, grape and onion and is associated with anti-inflammatory, anticancer and antioxidant effects (Kicinska and Jarmuszkiewicz, 2020). Nevertheless, none of the study has focused to elucidate the effect of fisetin on NLRP3 inflammasome formation. In this study, we found that fisetin inhibits NLRP3 inflammasome formation by inhibiting the TLR4/MD2 signaling pathway and excessive mtROS production. Additionally, we found that p62-meditated mitophagy plays a crucial role in fisetin-mediated NLRP3 inflammasome inhibition (Figure. 26.).

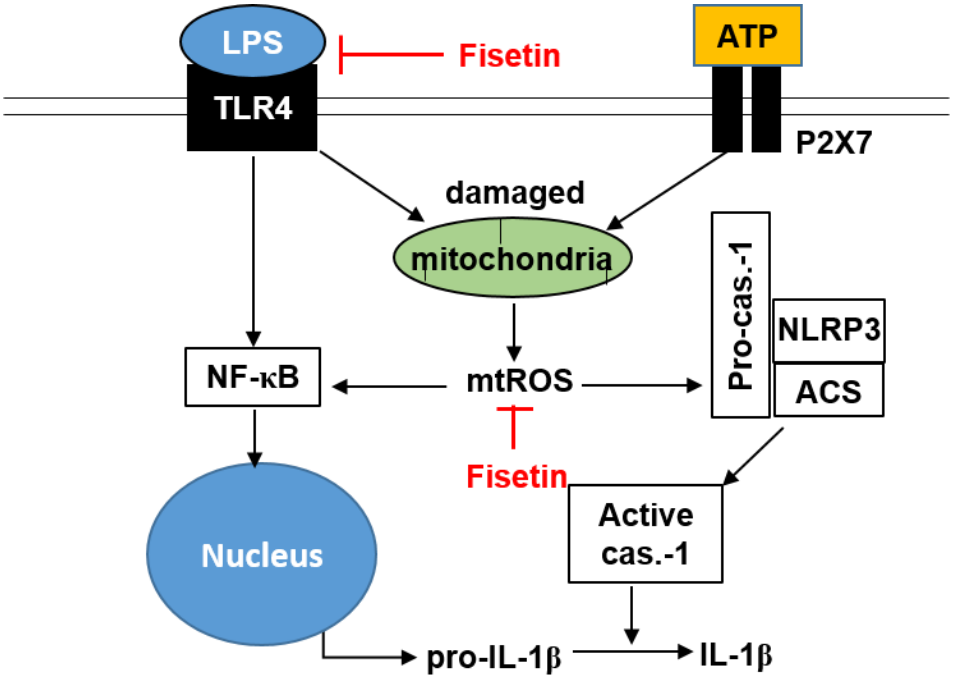

Figure 26. Graphical representation of the anti-inflammasome effect of fisetin in BV2 microglia cells. Fisetin inhibits inflammasome formation via two main cell signaling pathways. Firstly, Fisetin antagonizes the LPS recognition of TLR4 via competitively binding to the hydrophobic pockets of MD2 which consequently prevent the stimulation of canonical NF-κB cell signaling pathway to inhibit the transcription of IL-1β. Secondly, fisetin inhibits the formation of

mtROS by promoting the elimination of damaged mitochondria in a p62 dependent manner. Inhibition of mtROS generation associate with the downregulation of NLRP3 inflammasome formation which will subsequently inhibits the cleavage of pro-IL-1β in to active IL-1β.

NLRP3 inflammasome provides a critical molecular platform for the maturation of IL-1β and IL-18 to stimulates the innate immune responses, which protect the body from the various types of pathogens and host-derived danger signals (Block and Hong, 2005). However, unregulated activation of NLRP3 inflammasome leads to the pathological concerns such as Alzheimer's disease (AD), Parkinson's disease (PD) and multiple sclerosis (Cappellano et al., 2013; Stansley et al., 2012). In previous studies, the LPS-induced NF-κB signaling pathway associated with a significant increase of IL-1β and IL-18 maturation by promoting NLRP3 inflammasome component synthesis; hence, antagonizing the recognition of LPS by TLR4/MD2 complex has become a promising therapeutic strategy to cure NLRP3-mediated inflammatory disorders (Karunarathne et al., 2020; Lima et al., 2015). Previously, intravenous injection of fisetin resulted in the alleviation of acute lung injury in LPS-treated mice via the inhibition of the TLR4-NF-κB signaling pathway (Feng et al., 2016). Since fisetin inhibits the TLR4-NF-κB signaling pathway, none of study determined whether fisetin directly binds to TLR4/MD2 complex, leading to the inhibition of the NF-κB signaling pathway. Therefore, we, in this study, focused whether fisetin prevents the recognition of LPS to TLR4/MD2 complex. Interestingly, molecular docking data predicted that fisetin binds to TLR4 and blocked the hydrophobic pockets of MD2, which prevents the dimerization of TLR4/MD2 complex by inhibiting its LPS recognition. In a previous study, MD2 mimetics resulted in the inhibition of LPS-induced downstream signaling by preventing the dimerization of TLR4/MD2 complex, which, in turn, inhibited the MYD88/IRAK4-NF-κB signaling pathway (Kuzmich et al., 2017). In this study, we also found that the inhibition of the

TLR4/MD2 signaling pathway by fisetin resulted in the downregulation of MYD88 and IRAK4, which consequently inhibited the nuclear translocation of NF-κB. These results indicate that fisetin could prevent LPS- and TLR4/MD2-induced inflammatory disorders by downregulating the NF-κB signaling pathway.

Several possible mechanisms have been proposed for the assembly of NLRP3 inflammasome complex. Especially, excessive mtROS production from the damaged mitochondria-related oxidative stress is sought to be a key regulator for NLRP3 inflammasome activation (Chen et al., 2019; Guo et al., 2014). The proposed mechanism is further strengthen due to the localization of NLRP3 inflammasome in the vicinity of mitochondria (Hamilton and Anand, 2019), which helps mtROS production to prime the NLRP3 inflammasome formation. On the other hand, Yu et al, (Yu et al., 2014) elucidated that the knockout of *NLRP3* and *Caspase 1* in mice resulted in the inhibition of mtROS production in response to the ATP and nigericin, indicating that activation of NLRP3 inflammasome resulted a positive regulatory loop with the perturbation of mitochondrial physiology. Additionally, excessive mtROS production involve in various pathological concerns such as inflammatory disorders and cancers (Li et al., 2013); hence, targeting mtROS by eliminating damaged-mitochondria could be a promising strategy for the treatment of NLRP3 inflammasome-related disorders. Interestingly, a previous study showed that fisetin prevented intracellular ROS formation in RANKL-induced osteoclast differentiation (Sakai et al., 2013) and protected cardiac cell death (Rodius et al., 2020), which imply that fisetin plays in antioxidant. In this study, we addressed that LPS/ATP stimulated mitochondrial depolarization and mtROS production and, in turn, promoted the activation of NLRP3 inflammasome. However, fisetin inhibited the activation of LPS/ATP-induced NLRP3 inflammasome by inhibiting depolarization of mitochondrial membrane potential and consequent mtROS production.

p62 is a LC3-binding cargo protein and transfers ubiquitinated damaged-mitochondria to the autophagosome, causing the degradation of the damaged mitochondria (Zhang, 2015). Previous studies on p62 revealed that silencing of *p62* in THP-1 macrophages resulted in the elevation of LPS/ATP-mediated inflammasome and subsequent IL-1β maturation through the Nrf2-Keap1-ARE axis (Ko et al., 2017). Furthermore, $p62^{-/-}$-ablated mice associated with the suppression of inclusion body formation compared to that in the wildtype (Komatsu et al., 2007). In this study, we found that transient knockdown of *p62* using siRNA upregulated the depolarized mitochondrial membrane potential along with elevated mtROS production. Aligned with these data, the transition knockdown of *p62* reversed the inhibitory effect of fisetin on NLRP3 inflammasome complex formation by inhibiting the mitophagy. However, in the contrary, Zhong et al. demonstrated that activation of NF-κB can restrict the NLRP3 inflammasome activation via eliminating damaged mitochondria in a p62 dependent manner. (Zhong et al., 2016). Therefore further studies are needed to warrant the way in which fisetin-inhibited NF-κB upregulate p62 in BV2 microglia cells.

In this study, we elucidated that fisetin binds to TLR4/MD2 complex and subsequently inhibits the NF-κB signaling pathway. Furthermore, fisetin stabilized mitochondrial membrane potential irritated by LPS/ATP treatment and downregulated mtROS production, resulting in the inhibition of NLRP3 inflammasome. In this regards, fisetin may be an influential bioactive for the treatment of NLRP3 inflammasome-induced inflammatory disorder.

4 Chapter4

Fisetin promotes osteoblast differentiation and bone formation through GSK-3β Ser9 phosphorylation and consequent β-catenin activation

Abstract

Fisetin is a bioactive flavonol, and inhibits osteoclastogenesis and promotes osteoblastogenesis. However, the osteogenic activities of fisetin has not extensively studied. In this study, we found that fisetin significantly increased alkaline phosphatase (ALP) activity and bone mineralization in MC3T3-E1 preosteoblasts accompanied by a significant increase of runt-related transcription factor 2 (RUNX2), ALP, collagen type I alpha 1 (Col1α1), osterix (OSX), Osteocalcin (OCN) and bone morphogenetic protein 4 (BMP4) expression. In addition, fisetin promoted vertebrae formation in zebrafish larvae; high concentration of fisetin were comparable to β-glycerophosphate treatment. Furthermore, fisetin inhibited prednisolone-induced bone resorption genes such as *nuclear factor of activated T-cells (NFATc1), tartrate-resistant acid phosphatase-6 (ACP6), dendrocyte expressed seven transmembrane protein (DC-STAMP)* and *Cathepsin K (CTSK)* while the inhibition of ALP activity, bone mineralization and zebrafish bone loss was also restored. Finally, we confirmed that fisetin-mediated osteogenic activities are related to the phosphorylation of GSK-3β at ser9 which consequently release β-catenin from destructive complex to promote its nuclear translocation. Inhibition of β-catenin by FH535 and stabilization of GSK-3β by DOI hydrochloride reverse the fisetin mediated osteogenic activities confirming the significance of GSK-3β/β-catenin cell signaling pathway in fisetin mediated osteogenic activities. Therefore, collectively, our study suggests that stimulation of osteogenic activities by fisetin is an effective strategy to prevent osteoporosis.

Key words: Fisetin, osteoblast differentiation, osteoporosis, GSK-3β, β-catenin

4.1 Introduction

Fine-tuning of osteoclast-induced bone resorption and osteoblast-mediated bone formation is indispensable for dynamic bone metabolism (Chen et al., 2018). The process is comprised of three key events, namely, osteogenesis, modeling and remodeling. Synthesis of the extracellular matrix is taken place during the osteogenesis, leading to large amounts of bone, and carving out the shape to fit to the physical environment and adjusting to the body growth are happened during the modeling and remodeling process (Katsimbri, 2017). However, the disruption of balance between bone resorption and bone formation causes the bone metabolic diseases such as osteoporosis, rickets, renal osteodystrophy, osteopetrosis and Paget's disease of bone (Feng and McDonald, 2011). Out of them, osteoporosis is well characterized by the reduction of bone mass and alteration in bone architecture, resulting in increased risk such as bone fragility and fractures and the risk is greater in postmenopausal women and elderly men (Akkawi and Zmerly, 2018). According to the clinical research, the majority of patient are suffering not only from lifelong pain but also from a great financial burden (Hernlund et al., 2013). In the regard, several studies have suggested that stimulation of osteoblast differentiation may be an effective strategy to prevent osteoporosis (Kassem and Marie, 2011; Qin et al., 2016).

Receptor activator of nuclear factor-κB (RANK) ligand (RANKL) plays an important role on osteoclast precursors for the onset of osteoclastogenesis through the upregulation of osteoclast specific genes such as *acid phosphatase* (*ACP*), *dendritic cell-specific transmembrane protein* (*DC-STAMP*) and *Cathepsin K (CTSK)* (Ono et al., 2020). Binding of RANKL to RANK receptor, resulted the recruitment of adaptor molecules such tumor necrosis factor receptor-associated factor 6 (TRAF6) on the cytoplasmic tails of a trimetric RANK, which stimulates mitogen-activated protein kinase (MAPKs) and nuclear transcription factor-κB (NF-κB) (Wada et al., 2006).

Activated NF-κB subsequently translocates to the nucleus and induces nuclear factor of activated T cells cytoplasmic 1 (NFATc1) through the activation of Ca^{2+}-dependent calcineurin (Kim and Kim, 2014). Especially, the induction of NFATc1 is required for the transcription of osteoclast specific genes such as *ACP, DC-STAMP* and *OSCAR* (Sitara and Aliprantis, 2010). In contrary, Runt-related transcription factor 2 (RUNX2) is considered as a key transcription factor to promote the expression of osteogenic genes such as *alkaline phosphate* (*ALP*), *osterix* (*OSX*), *osteocalcin* (*OCN*), *collagen type 1 alph-1* (*Col1α1*), which regulate the osteoblast differentiation (Komori, 2019). Bone morphogenetic proteins (BMPs) that belong to the transforming growth factor β (TGF-β) superfamily also act as osteogenic stimulators by stimulating RUNX2 expression (Phimphilai et al., 2006). Additionally, the Wingless-related integration site (Wnt)/β-catenin pathway triggers bone anabolism by inhibiting glycogen synthase kinase-3β (GSK-3β) (Bertacchini et al., 2018).

Fisetin (3,3′,4′,7-tetrahydroxyflavone) is a bioactive flavonol found in fruits and vegetables such as apple, grape, and strawberry (Kashyap et al., 2019). Fisetin is associate with a number of potent biological effects such as antiinflammatory (Kim et al., 2015), antioxidative (Khan et al., 2013) and anticarcinogenic (Syed et al., 2016) effects. Fisetin also inhibits RANKL-induced osteoclast differentiation by inhibiting the NFATc1 signaling pathway (Choi et al., 2012) and stimulates osteoblast differentiation by increasing RUNX2 expression (Leotoing et al., 2014), which indicates that fisetin may be used to cure bone resorption disorders such as osteoporosis. Nevertheless, whether fisetin directly promotes bone formation at juvenile stage remains unclear. In this study, we found that fisetin accelerates vertebrae formation and restores prednisolone-mediated bone resorption.

4.2 Materials and method

4.2.1 Reagents and antibody

Fisetin, 3-(4,5-dimethylthiazol-2-yl)-2,5-diphenyltetrazolium bromide (MTT), calcein, alizarin red, gelatin, donkey serum, 4′6-diamidino-2-phenylindole (DAPI) and β-glycerophosphate (GP) were purchased from Sigma-Aldrich Chemical Co. (St. Louis, MO, USA). Specific antibodies against RUNX2 (sc-101145), ALP (sc-398461), Col1α1 (sc-293182), OSX (sc-393325), OCN (sc-390877), BMP4 (sc-393329), GSK-3β (sc-81462), phospho (p)-GSK-3β Ser9 (sc-37800), β-catenin (sc-59737), β-actin (sc-69879) and nucleolin (sc-13057), and peroxidase-labeled anti-mouse immunoglobulins (sc-516102) were purchased from Santa Cruz Biotechnology (Santa Cruz, CA, USA). Peroxidase-labeled anti-rabbit immunoglobulins (KO211708) were obtained from KOMA BIOTECH (Seoul, Republic of Korea). Alexa Fluor 647- and Alexa Fluor 488-conjugated secondary antibodies were purchased from Abcam (Cambridge, MA, USA). Dako faramount aqueous mounting media was purchased from Dako (Carpinteria, CA, USA). DOI hydrochloride (DOI) and 2,5-dichloro-N-(2-methyl-4-nitrophenyl)benzenesulfonamide (FH535) were obtained from Tocris (Bristol, UK). Minimum essential medium alpha modification (α-MEM), fetal bovine serum (FBS), and antibiotics mixture were obtained from WelGENE (Gyeongsan-si, Gyeongsangbuk-do, Republic of Korea). All other chemicals were supplied from Sigma-Aldrich Chemical Co.

4.2.2 Cell culture and MTT activity

Mouse preosteoblast MC3T3-E1 cells were obtained from the American Type Culture Collection (ATCC, Manassas, VA, USA) and maintained in α-MEM supplemented with 10% FBS and antibiotics mixture in a humidified incubator at 5% CO_2 and 37°C. Relative cell viability was measured by an MTT assay. Briefly, MC3T3-E1 cells were seeded into 24-well plates at a density

of 1×10^4 cells/mL and incubated with different concentrations (0–1000 nM) of fisetin for 14 days. The media was replaced every 3 days with fisetin. The viability was measured by incubating the cells with 0.5 mg/mL MTT. Formazan was dissolved with dimethyl sulfoxide (DMSO) and absorbance was measured at 540 nm using a microplate reader (BioTek Instruments Inc., Winooski, VT, USA).

4.2.3 Analysis of viability and dead cells populations

Cell viability and dead cell populations were measured by flow cytometry. Briefly, MC3T3-E1 cells were seeded at a density of 1×10^4 cells/mL in 12-well plates and treated with the indicated concentrations of fisetin (0–1000 nM) for 14 days. The media was replaced every 3 days with fisetin. Then, the harvested cells were washed with ice-cold phosphate buffered saline (PBS) and stained with Muse Count & Viability Kit (MCH100102, EMD Millipore, Billerica, MA, USA) for 5 min. Cell viability and dead cell populations were measured by Muse Cell Analyzer (EMD Millipore).

4.2.4 Alizarin red staining

In vitro calcium deposition was measured using 2% alizarin red staining. Briefly, MC3T3-E1 cells were seeded at a density of 1×10^4 cells/mL in a 24 well-plate and then treated with the indicated concentrations of fisetin (0–800 nM) for 14 days. In order to evaluate the effect of fisetin under prednisolone treated conditions, cells were pretreated with 10 μM prednisolone for 2 days prior to expose with 0-800 nM fisetin for another 12 days. The media was replaced every 3 days with fisetin. GP (2 mM) was used as a positive control. The cells were washed with PBS and fixed with 4% paraformaldehyde for 10 min at 37°C. Then, the cells were stained with 2% alizarin red

solution for 30 min. Images of each wells were taken by phase contrast microscopy (Ezscope i900PH, Macrotech; Goyang-si, Gyeonggi-do, Korea.

4.2.5 ALP assay

MC3T3-E1 cells were seeded at a density of 1×10^4 cells/mL in 24-well plates and then treated with the different concentrations of fisetin (0–800 nM) for 14 days in the presence and absence of prednisolone. The media was replaced every 3 days with fisetin. GP (2 mM) was used as a positive control. ALP activity was measured by a TRACP & ALP double-staining Kit (Takara Bio Inc., Kusatsu, Shiga, Japan) according to the manufacture's protocol. Briefly, the cells were rinsed three times with PBS and incubated with fixation buffer for 5 min. Then, ALP substrate was added into each well and incubated at 37°C for 45 min. The images of each well were taken by phase contrast microscopy.

4.2.6 Reverse transcription polymerase chain reaction (RT-PCR)

MC3T3-E1 cells were treated with the different concentrations of fisetin (0–800 nM) for 14 days in the presence and absence of prednisolone. The media was replaced every 3 days with fisetin. GP (2 mM) was used as a positive control. Total RNA was extracted using easy-BLUE total RNA extraction kit (iNtRON Biotechnology, Sungnam-si, Gyeonggi-do, Republic of Korea) according to the manufacturer's instruction. Two micrograms of RNA were reverse-transcribed using specific primers (Table 1). Osteoblast related primers were selected based on our previous studies (Molagoda et al., 2019) while osteoclast-related primer were specifically design for the current study. All PCR contained same conditions of denaturation at 94°C for 30 s and extension at 72°C for 30 s during the PCR amplification. *Glyceraldehyde 3-phosphate dehydrogenase* (*GAPDH*) was

used as an internal control to evaluate the relative expression of *RUNX2*, *ALP*, *Col1α1*, *OCN*, *OSX*, *BMP4*, *NFATc1*, *ACP*, *DC-STAMP* and *OSCAR*.

Table 5. Mouse primers and PCR conditions used in this experiment.

Gene*	Primer sequence(5′-3′)	Size	T_m	Cycle No.
RUNX2	F 5′-CATGGTGGAGATCATCGCGG-3′ R 5′-GGCCATGACGGTAACCACAG-3′	171 bp	60℃	30
ALP	F 5′-TTGTGGCCCTCTCCAAGACA-3′ R 5′-GACTTCCCAGCATCCTTGGC-3′	198 bp	60℃	30
Col1α1	F 5′-GACGCATGGCCAAGAAGACA-3′ R 5′-TCTTTGGGGGTTGGGACAGT-3′	174 bp	56℃	30
OSX	F 5′-AAGGCGGTTGGCAATAGTGG-3′ R 5′-GCAGCTGTGAATGGGCTTCT-3′	194 bp	60℃	30
OCN	F 5′-GCCCTGAGTCTGACAAAGCC-3′ R 5′-GCGTTTGTAGGCGGTCTTCA-3′	187 bp	60℃	30
BMP4	F 5′-GACTTCACTGACGTGGGCTG-3′ R 5′-TGGGGACACAACAGGCCTFTA-3′	142 bp	60℃	30
NFATc1	F 5′-TATCGAGTGTTCCCAGCGGT-3′ R 5′-CCCGGTCAGTCTTTGCTTCC-3′	193 bp	60℃	30
ACP5	F 5′-TTCACTGGAGTGCACGATGC-3′ R 5′-CGGTAGTAAGGGCTGGGGAA-3′	190 bp	60℃	30
DC-STAMP	F 5′-ACCCTTGGGCTGTTCTTCCT-3′ R 5′-CGATCCCTTGGGTTCCTTGC-3′	172 bp	60℃	30
CTSK	F 5′- GCGGCTATATGACCACTGCC-3′ R 5′- GCTTTCTCGTTCCCCACAGG-3′	166 bp	60℃	30
GAPDH	F 5′-CGATGCCCCCATGTTTGTTGTGA-3′ R 5′-ACAGTCTTCTGGGTGGCAGT-3′	185 bp	60℃	30

Bp; base pair, T_m; melting temperature.

**RUNX2, Runt-related transcription factor 2*; *ALP*, Alkaline phosphatase; *Col1α1*, collagen, type I alpha 1; *OCN*, *osteocalcin*; *OSX*, *osterix*; *BMP4*, *bone morphogenetic protein 4*; *NFATc1*, *nuclear factor of activated T-cells cytoplasmic 1*; *ACP5*, *acid phosphatase 5*; *DC-STAMP*,

dendritic cell-specific transmembrane protein; *CTSK, cathepsin K*; *GAPDH, glyceraldehyde 3-phosphate dehydrogenase*.

4.2.7 Western Blotting Analysis

MC3T3-E1 cells with indicated concentrations of fisetin (0–800 nM) for 14 days in the presence and absence of prednisolone. The media was replaced every 3 days with fisetin. GP (2 mM) was used as a positive control. Total proteins were extracted with radioimmunoprecipitation assay lysis buffer (iNtRON biotechnology). After cleaning lysates by centrifugation, protein was quantified by the Bio-Rad protein assay reagents (Bio-Rad, Hercules, CA, USA). In a parallel experiment, the cells were washed with ice-cold PBS, and cytosolic and nuclear proteins were separately extracted using NE-PER Nuclear and Cytoplasmic Extraction Reagents (Pierce, Rockford, IL, USA). An equal amount of protein was separated on SDS-polyacrylamide gel, transferred onto polyvinylidene fluoride membrane (Thermo Fisher Scientific, Waltham, MA, USA) and then immunoblotted with indicated antibodies. Bound antibodies were detected using an enhanced chemiluminescence plus kit (Thermo Fisher Scientific). The images were captured by ImageQuant LAS 500 (GE Healthcare Bio-Sciences AB, Uppsala, Sweden). β-Actin and nucleolin were used as the loading control for cytosolic and nuclear proteins, respectively.

4.2.8 Immunostaining

MC3T3-E1 cells (5×10^3 cells/mL) were seeded on 3% gelatin-coated coverslips and then treated with 800 nM fisetin and 2 mM GP for 14 d. The cells were fixed with 4% paraformaldehyde for 10 min at 37°C and permeabilized with 0.1% Triton X-100 for 10 min at room. The cells were blocked with 10% donkey serum and incubated with anti-β-catenin antibody for 18 at 4°C. After washing with ice-cold PBST, the cells were incubated with Alexa Fluor 647 fluorescent dye-

conjugated secondary antibody for 1 h at room temperature followed by counter stained with DAPI (300 nM) for 10 min. The coverslips were mounted onto glass slides with Dako faramount aqueous mounting media and fluorescence images were captured by CELENA S digital imaging system (Logos biosystems, Anyang-si, Gyeonggi-do, Republic of Korea).

4.2.9 Vertebrae formation in zebrafish larvae

Zebrafish was raised and handled according to standard guidelines of the Animal Care and Use Committee of Jeju National University (Jeju-do, Republic of Korea). Three-days post fertilized (dpf) zebrafish larvae were treated with 0-200 μM for 6 more days. In order to evaluate the effect of fisetin under prednisolone treated conditions, zebrafish larvae were pretreated with 20 μM prednisolone for 2 days prior to expose with 0-200 μM fisetin for another 4 days. Media was changed every 2 days. Vertebrae formation was visualize using 0.05% calcein green fluorescent marker. GP (4 mM) was used as the positive control. After extensive rinsing, the larvae were anesthetized in 0.04% tricaine methanesulfonate solution and mounted on depression slides using 3% methylcellulose before imaging and fluorescence images were captured by CELENA S digital imaging system (Logos biosystems, Anyang-si, Gyeonggi-do, Republic of Korea).

4.2.10 RT-PCR of zebrafish larvae

Zebrafish larvae at 3 days postfertilization (dpf) were treated with the indicated concentrations of fisetin in the presence and absence of prednisolone and mRNA was extracted using an easy-BLUE™ kit (iNtRON Biotechnology) at 9 dpf. Two micrograms of RNA were reverse-transcribed using MMLV reverse transcriptase (iNtRON Biotechnology). All PCR contained same conditions of denaturation at 94°C for 30 s and extension at 72°C for 30 s during the PCR amplification. *β-Actin* was used as an internal control to evaluate the relative expression. The target cDNA was

amplified using specific zebrafish primers (Table 2) according to the previous studies (Chen et al., 2017; Kitamura et al., 2013).

Table 6. Zebrafish primers and PCR conditions used in this experiment.

Gene*	Primer sequence(5′-3′)	size	T_m	Cycle No.
RUNX2a	F 5′-GACGGTGGTGACGGTAATGG-3′ R 5′-TGCGGTGGGTTCGTGAATA-3′	173 bp	58°C	30
RUNX2b	F 5′-CGGCTCCTACCAGTTCTCCA-3′ R 5′-CCATCTCCCTCCACTCCTCC-3′	149 bp	59°C	30
Col1a1	F 5′-CTGTGCCAATCCCATCATTTC -3′ R 5′-ATATCGCCTGGTTCTCCTTTC-3′	110 bp	56°C	30
OSX	F 5'-GGCTATGCTAACTGCGACCTG-3' R 5'GCTTTCATTGCGTCCGTTTT-3'	153 bp	56°C	30
OCN	F 5′-TGGCCTCTATCATCATGAGACA-3′ R 5′-CTCTCGAGCTGAAATGGAGTC-3′	72 bp	59°C	30
BMP4	F 5′-TTGTGCTGTGCATGTTTGAA-3′ R 5′- GGTCGCTTGGCTATGTGTTT-3′	174 bp	56°C	30
NFATc1	F 5′-AACCTTCCTCGTTCCCTCAA-3′ F 5′-CGCTGTTATCCTCCACCTCA-3′	152 bp	57°C	30
ACP5b	F 5′-GCTGCTGCTAACAAACAAT-3′ F 5′-GACCAACCACGATGACAA-3′	78 bp	56°C	30
DC-STAMP	F 5′-GCGCATCTCTTTCATCAACA-3′ F 5′-CATTGTGCAACCCACAGAAC-3′	186 bp	56°C	30
CTSK	F 5′-GGACTCAATCACTATCACT-3′ R 5′-AGAACAAGACATCTAAGACA-3′	117 bp	56°C	30
β-actin	F 5′-CGAGCGTGGCTACAGCTTCA-3′ R 5′-GACCGTCAGGCAGCTCATAG-3′	154 bp	61°C	30

Bp; base pair, T_m; melting temperature.

**RUNX2a/b*, *runt-related transcription factor 2a/b*; *Col1α1*; collagen type I alpha 1; *OSX*, *osterix*; *OCN*, *osteocalcin*; *BMP4*, *bone morphogenetic protein 4; NFATc1*, *nuclear factor of activated T-*

cells cytoplasmic 1; ACP5b, acid phosphatase 5b; DC-STAMP, dendritic cell-specific transmembrane protein; CTSK, cathepsin K.

4.2.11 Statistical Analysis

All the western blots and RT-PCR bands were quantified by ImageJ 1.50i (National Institute of Health, Manassas, VA, USA) and then statistically analyzed by Sigma plot 12.0. All data represented the mean of at least three independent experiments. Significant differences between groups were determined using a Student *t* test and an unpaired one-way ANOVA test with Bonferroni correction. Statistical significance was set at *** and $^{###}$ $p < 0.001$, ** and $^{##}$ $p < 0.01$, * and $^{\#}$ $p < 0.05$.

4.3 Results

4.3.1 Fisetin shows no cytotoxicity at low concentrations

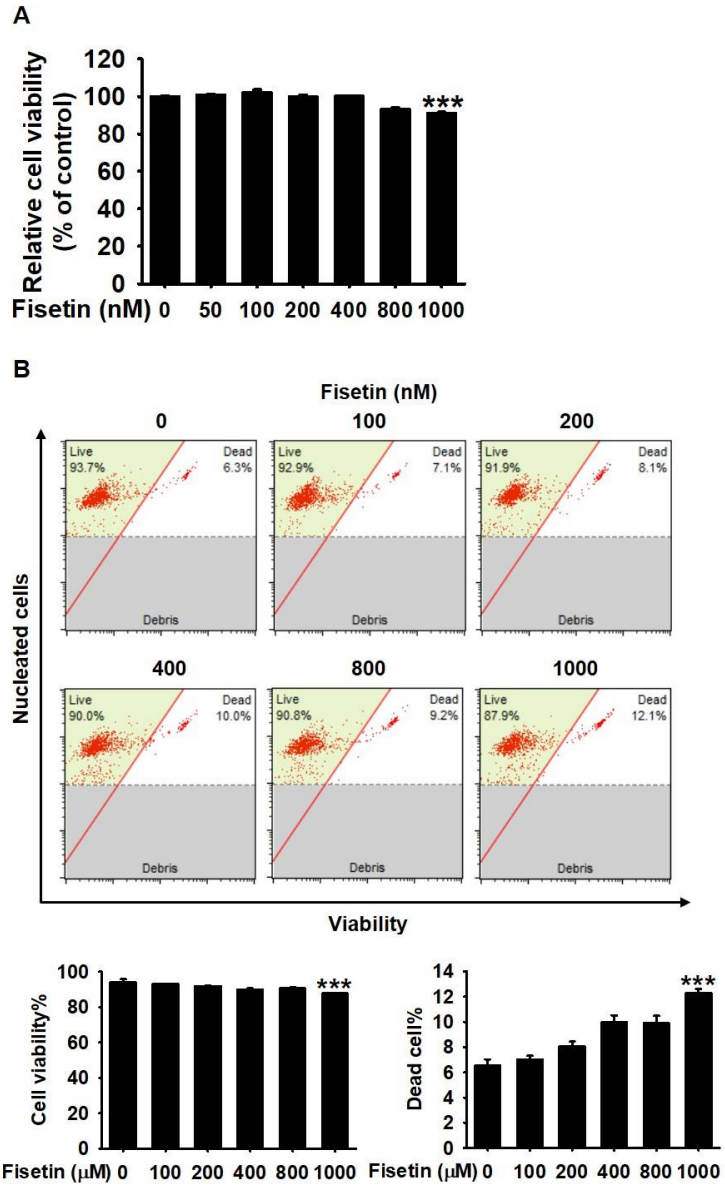

Figure 27. Fisetin possess no toxicity at low concentrations. MC3T3E1 cells were seeded at 1 x 104 cells/mL and treated with 0-1000 nM fisetin for 14 days. (A) Cell viability was measured using MTT assay. Viability was expressed as a % of control. (B) In a parallel experiment Cell viability and the dead cell population were measured using a Muse® Cell Viability Kit. Cell

viability percentage and dead cell population are shown. Significant differences among the groups were determined using the one-way ANOVA followed by Bonferroni correction. All data are presented as the standard error of the median from three independent experiments (*** $p < 0.001$, ** $p < 0.01$, and * $p < 0.05$ vs the untreated cells).

In order to identify the cytotoxic effect of fisetin (Figure 27A) on MC3T3-E1 cells, we treated the indicated concentrations (0–1000 nM) for 14 d. We could not able to see a cytotoxic effect of fisetin at indicated concentrations up to day 11 (data not shown). However, the highest concentration (1000 nM) of fisetin used in this experiment showed a significant cytotoxicity at day14, as lower as 91.1 ± 0.6% compared with that in the untreated cells (Figure 27B). The cytotoxic effect of fisetin was further validated using flow cytometery in the same experimental condition at day 14 (Figure 27C). As shown in Figure 27C and Figure 27D, compared with those in the untreated cells (93.8% ± 1.9% of viability and 6.1% ± 2.8% of dead cells), the highest concentration of fisetin significantly reduced the cell viability to 87.7% ± 0.3% and dead cell populations to 12.3% ± 0.3%. However, no significant effect was found below 800 nM fisetin. Altogether, these results indicated that low concentrations of fisetin possess no cytotoxicity in MC3T3-E1 cells.

4.3.2 Fisetin induces osteoblast differentiation accompanied by osteoblast-specific gene expression

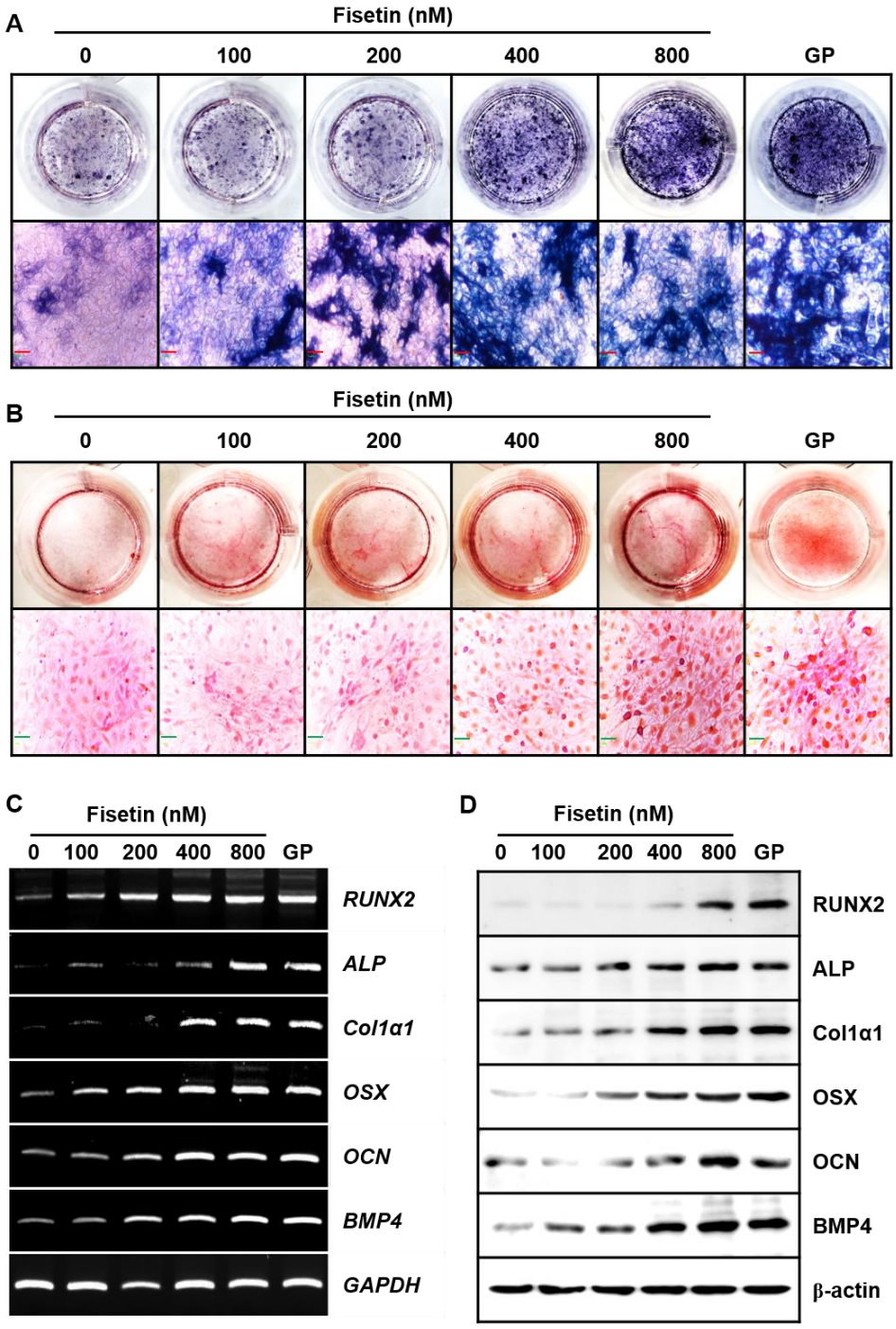

Figure 28. Fisetin promote the osteoblast differentiation in MC3T3E1 cells. MC3T3E1 cells were seeded at a density of 1 x 10^4 cells/mL and treated with 0-800 nM fisetin for 14 days. GP (2

mM) was used as the positive control. (A) Cells were stained for ALP activity using ALP staining assay kit and (B) stained with 2% alizarin red for the mineralization. Representative images were taken with Ezscope i900PH phase contrast microscope (x10). Scale bar = 40 μm. (C) In a parallel experiment cells were treated with fisetin for 14 days and total mRNA was extracted and RTPCR was performed to detect the expression of *mRUNX2, mALP, mCol1α1, mOSX, mOCN, mBMP4. mGAPDH* was used as the house keeping gene. (D) Total protein was isolated and western blotting was performed to detect the effect of fisetin on osteoblast marker genes such as RUNX2, ALP, Col1α1, OSX, OCN, BMP4 protein expression. β-actin was used as the house keeping protein. Each value indicates the mean ± standard error median (SEM) and is representative of the results obtained from three independent experiments. Significant differences among the groups were determined using the Student's *t*-test ($^{###}$, $p < 0.001$, $^{##}$, $p < 0.01$, and $^{#}$, $p < 0.05$ vs. the untreated larvae) and one-way ANOVA with Bonferroni correction (***, $p < 0.001$, **, $p < 0.01$, and *, $p < 0.05$ vs. the LPS-treated larvae).

We investigated whether that fisetin promotes osteoblast differentiation, fisetin was treated in MC3T3-E1 cells for 14 days, and the media was replaced every 3 days with fisetin. ALP staining indicated that fisetin significantly induced ALP activity in MC3T3-E1 cells in a concentration-dependent manner (Figure 28A). Alizarin red staining also confirmed that fisetin concentration-dependently increased bone mineralization (Figure 28B). Especially, the osteogenic ALP activity and mineralization at 800 nM fisetin was comparable to GP-treated cells. We, next, tried to elaborate the effect of fisetin on osteoblast-specific marker gene expression at the transcriptional and the translational levels. The expression of osteoblast-specific marker genes such as *RUNX2, ALP*, *Colo1α1, OSX*, *OCN* and *BMP4* was upregulated at day14 in a concentration dependent manner (Figure 28C). As shown in Figure 28D, all the tested target proteins such as RUNX2, ALP,

Col1α1, OSX, OCN and BMP4 were also highly upregulated in response to fisetin in a concentration dependent manner at day 14. Aligned with the ALP activity and alizarin red-based mineralization results, treatment with GP remarkably increased the osteoblast-specific genes and proteins, comparable to those in the presence of 800 nM fisetin. Altogether, these results confirmed that fisetin promotes ALP activity and bone mineralization accompanied by upregulation of the osteoblast-specific genes and proteins.

4.3.3 Fisetin promotes vertebrae formation in zebrafish larvae along with the upregulation of osteoblast-specific gene expression.

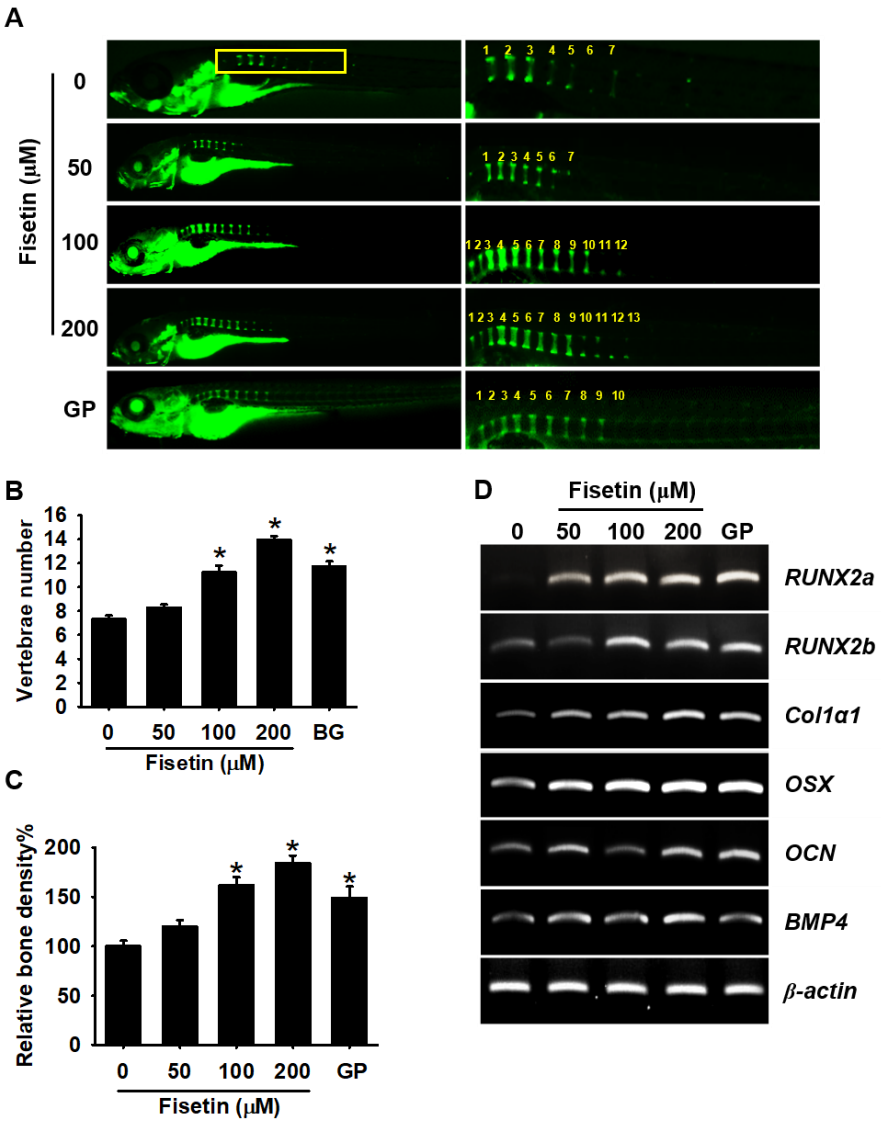

Figure 29. Fisetin promotes bone formation in zebrafish larvae. Three days post fertilized (3 dpf) zebrafish larvae were treated with 0-200 µM fisetin for 6 days. GP (4 mM) was used as the positive control. (A) Zebrafish larvae at 9 dpf were stained with 0.05% calcein to visualize the vertebrae formation. (B) The number of vertebrae were manually counted. (C) Relative bone densities were measured by imageJ software and normalized against to the untreated conditions. (D) In a parallel experiment total mRNA was extracted and RT-PCR was performed to detect the expression of *zRUNX2a, zRUNX2b, zCol1a1, zOSX, zOCN, and zBMP4. zβ-actin* was used as the house keeping gene. Each value indicates the mean ± standard error median (SEM) and is representative of the results obtained from three independent experiments. Significant differences among the groups were determined using the Student's *t*-test ($^{###}$, $p < 0.001$, $^{##}$, $p < 0.01$, and $^{#}$, $p < 0.05$ vs. the untreated larvae) and one-way ANOVA with Bonferroni correction (***, $p < 0.001$, **, $p < 0.01$, and *, $p < 0.05$ vs. the LPS-treated larvae).

In order to elaborate the effect of fisetin on the *in vivo* vertebrae formation, 3 dpf zebrafish larvae were treated with 0-200 µM fisetin until 9 dpf and investigated total number of vertebrae. As shown in Figure 29A-29C, fisetin promote the bone formation in zebrafish larvae in a concentration-dependent manner (8.29 ± 0.27, 11.2 ± 0.5 and 13.9 ± 0.4 respectively in 50, 100 and 200 µM fisetin). Interestingly, the effect of fisetin even at 100 µM concentration was comparable to the GP-treated zebrafish larvae (11.7 ± 0.4). We further noticed that, fluorescence intensities of vertebrae were also significantly increased in a concentration dependent manner (120.14 ± 6.2%, 162.16 ± 7.9% and 184.04 ± 7.9% respectively by 50, 100 and 200 µM fisetin compared to the untreated control group) while the effect of fisetin at 100 µM was comparable to the GP-treated larvae (149.17 ± 11.3%). Furthermore, the effect of fisetin was assessed in the mRNA level at the zebrafish larvae. All the tested marker genes such as *RUNX2a, RUNX2b,*

Col1α1, OSX, OCN and *BMP4* were significantly upregulated in response to fisetin (Figure 29D). Treatment with GP was comparable to 100 μM fisetin on the osteoblast-specific gene expression, and the effect of fisetin at 200 μM was more prominent than that to the GP-treated zebrafish larvae. Altogether these results suggest that fisetin promotes vertebrae formation in zebrafish larvae accompanied by osteoblast-specific gene expression.

4.3.4 Fisetin mitigates PDS-induced anti-osteogenic activity

We, next, investigated whether fisetin restores PDS-induced anti-osteogenic activity. Pretreatment with PDS sustained the lower expression of all the tested osteoblast-specific genes such as *RUNX2*, *ALP, Colo1α1, OSX, OCN* and *BMP4* than the untreated cells (Figure 30A). However, fisetin concentration-dependently restored osteoblast-specific genes even in the presence of PDS. Aligned with the RT-PCR results, PDS did not stimulate the expression of osteoblast-specific proteins such as RUNX2, ALP, Colo1α1, OSX, OCN and BMP4, whereas fisetin restored the inhibitory effect of PDS in a concentration-dependent manner (Figure 30C). Additionally, PDS dramatically increased the expression of osteoclast-specific genes such as *NFATc1, ACP, DC-STAMP* and *CTSK* (Figure 30B); however; fisetin concentration-dependently downregulated those gene expression (Figure 30B). Aligned with the RT-PCR and western blot data, pretreatment with PDS markedly decreased ALP activity (Figure 30D) and mineralization (Figure 30E) to the lower level than the untreated cells. As expected, treatment with fisetin activated ALP activity and mineralization in the presence of PDS, which indicated that fisetin can cure PDS-induced bone

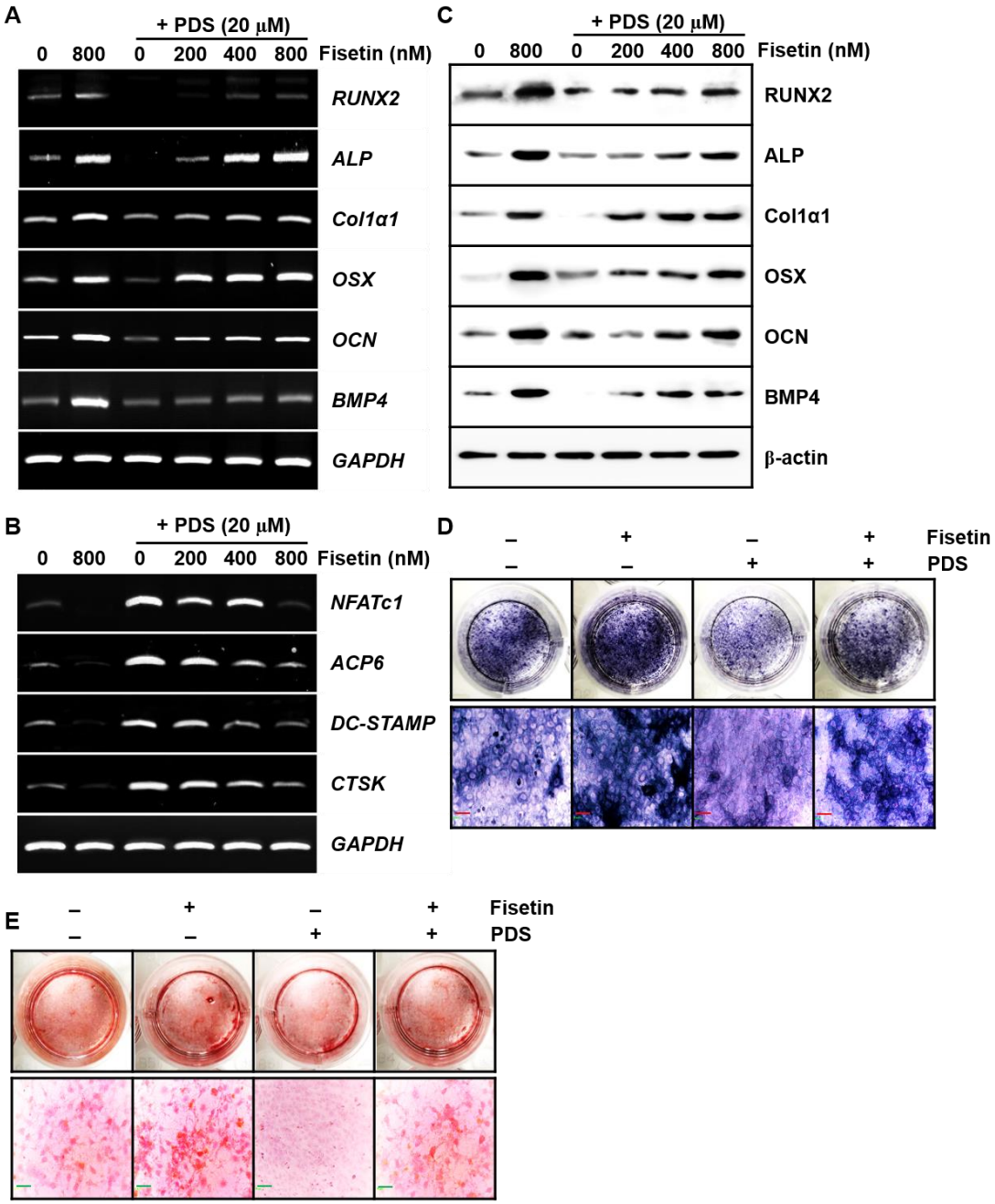

Figure 30. Fisetin alleviate prednisolone mediated osteoporosis in MC3T3E1 cells. MC3T3E1 cells were seeded at a density of 1 x 104 cells/mL and pretreated with 10 μM prednisolone for 2 days. Then the cells were replaced with 0-800 nM fisetin for another 12 days. (A-B) Total RNA was extracted and RT-PCR was performed to detect the expression of (A) osteoblast marker genes such as mRUNX2, mALP, mCol1α1, mOSX, mOCN, mBMP4 and (B) osteoclast specific marker

genes such as mNFATc1, mACP6, mDC-STAMP, mOSX, , mCTSK. mGAPDH was used as the house keeping gene. (C) In a parallel experiment total protein was extracted and western blotting was performed to detect the expression osteoblast specific marker proteins such as RUNX2, ALP, Col1α1, OSX, OCN and BMP4. β-actin was used as the house keeping protein. (D-E) Cells were stained for (D) ALP activity using ALP staining assay kit and (E) 2% alizarin red for the mineralization. Representative images were taken with Ezscope i900PH phase contrast microscope (x10). Scale bar = 40 μm. Each value indicates the mean ± standard error median (SEM) and is representative of the results obtained from three independent experiments. Significant differences among the groups were determined using the Student's t-test (###, $p < 0.001$, ##, $p < 0.01$, and #, $p < 0.05$ vs. the untreated larvae) and one-way ANOVA with Bonferroni correction (***, $p < 0.001$, **, $p < 0.01$, and *, $p < 0.05$ vs. the LPS-treated larvae).

4.3.5 Fisetin alleviates PDS-induced delay in vertebrae formation of zebrafish larvae

In order to evaluate whether fisetin could inhibits PDS-induced osteoporosis in zebrafish larvae, PDS was pretreated for 2 days prior to fisetin treatment. We confirmed that fisetin could relieve PDS-induced osteoporosis in zebrafish larvae (Figure 31A). We found that pretreatment with PDS resulted in a significant lowering of vertebrae number (3.2 ± 1.0, Figure 31B) and bone mineral intensities (38.09 ± 11.5%, Figure 31C) compared with those in the untreated zebrafish larvae (8.1 ± 0.4 of vertebrae number and 100 ± 6.6% of relative bone intensity); however, fisetin treatment significantly restored total vertebrae number in the presence of PDS to 5.2 ± 0.7, 8.5 ± 0.2 and 9.3 ± 0.9 and a decrease of relative bone density to 64.7 ± 6.6%, 97.5 ± 7.5% and 122.7 ± 13.7% at 50, 100 and 200 μM fisetin, respectively. As expected, fisetin remarkably upregulated the expression of osteoblast-specific marker genes such as *RUNX2a, RUNX2b, Col1α1, OSX, OCN* and *BMP4*; even in the presence of PDS, fisetin effectively increased those gene expression (Figure

31D). Furthermore, we verified the effect of fisetin on the osteoclast-specific marker genes such as *NFATc1, zACP5b and zDC-STAMP and zCTSK* in the PDS-pretreated conditions. PDS remarkably increase the osteoclast-specific gene expression; however, as expected, fisetin effectively downregulated their expression in a concentration-dependent manner (Figure 31E). Taken together, these results indicated that fisetin is a potent pharmacological agent to inhibit glucocorticoid-induced osteoporosis.

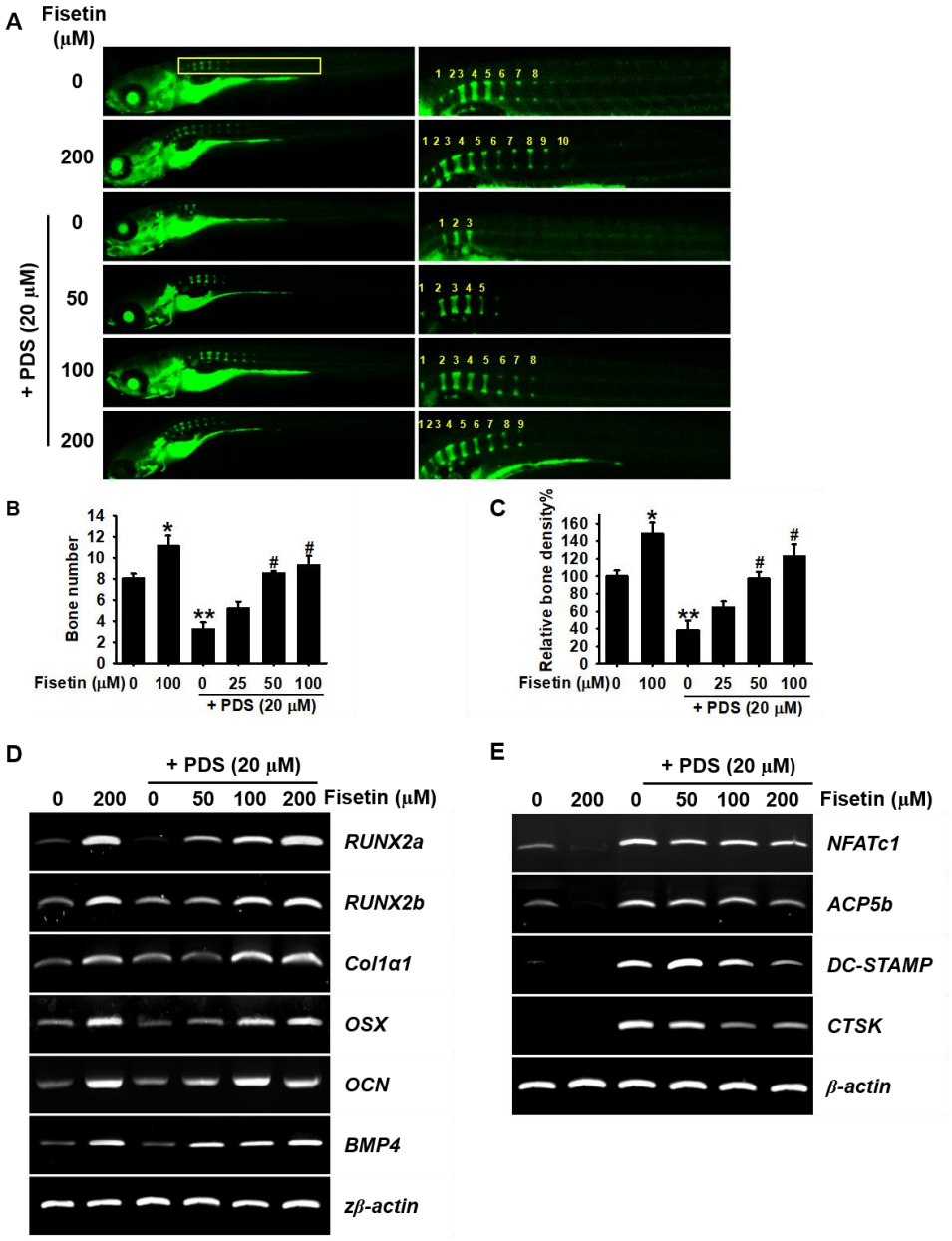

Figure 31. Fisetin alleviate the prednisolone mediated osteoporosis in zebrafish larvae. Zebrafish larvae at 3 dpf were pretreated with 20 μM fisetin for 2 days. Then the media was replaced with 0-200 μM fisetin for another 4 days. (A) Zebrafish larvae at 9 dpf were stained with 0.05% calcein to visualize the vertebrae formation. (B-C) The number of vertebrae were manually counted and relative bone densities were measured by imageJ software. (C-D) In a parallel experiment total mRNA was extracted and RT-PCR was performed to detect the expression of (C) osteoblast specific marker genes such as *zRUNX2a, zRUNX2b, zCol1a1, zOSX, zOCN, zBMP4* and (C) osteoclast specific marker genes such as (C) *zNFATc1, zACP6, zSC-STMAP and zCTSK. zβ-actin* was used as the house keeping gene. Each value indicates the mean ± standard error median (SEM) and is representative of the results obtained from three independent experiments. Significant differences among the groups were determined using the Student's t-test (###, $p < 0.001$, ##, $p < 0.01$, and #, $p < 0.05$ vs. the untreated larvae) and one-way ANOVA with Bonferroni.

4.3.6 Fisetin promotes osteoblast differentiation and mineralization through the phosphorylation of GSK-3β at Ser9

Since the significance of GSK-3β and β-catenin was reported for osteoblast differentiation in both in *vitro* and *in vivo* (Bertacchini et al., 2018), we, in this study, investigated that fisetin upregulates phosphorylation of GSK-3β at Ser9 and nuclear translocation of β-catenin for ALP activity and mineralization. As shown in Figure 32A, fisetin upregulated GSK-3β phosphorylation at Ser9 and promotes nuclear translocation of β-catenin. Immunostaining of β-catenin was also confirmed that fisetin promoted nuclear translocation of β-catenin and the effect was comparable to that in the GP-treated cells (Figure 32B). Then, we pretreated the cells with a GSK-3β stabilizer, DOI, and a specific β-catenin inhibitor, FH535, for 2 h prior to fisetin treatment. Both DOI and FH535 remarkably downregulated fisetin-induced ALP activity (Figure 32C) and mineralization (Figure

32D). Especially, the inhibitory effect of DOI was more prominent than that in the FH535-treated cells under fisetin-treated conditions. Taken together, these results suggest that fisetin promotes osteoblast differentiation and mineralization through phosphorylation GSK-β at Ser9 and nuclear translocation of β-catenin.

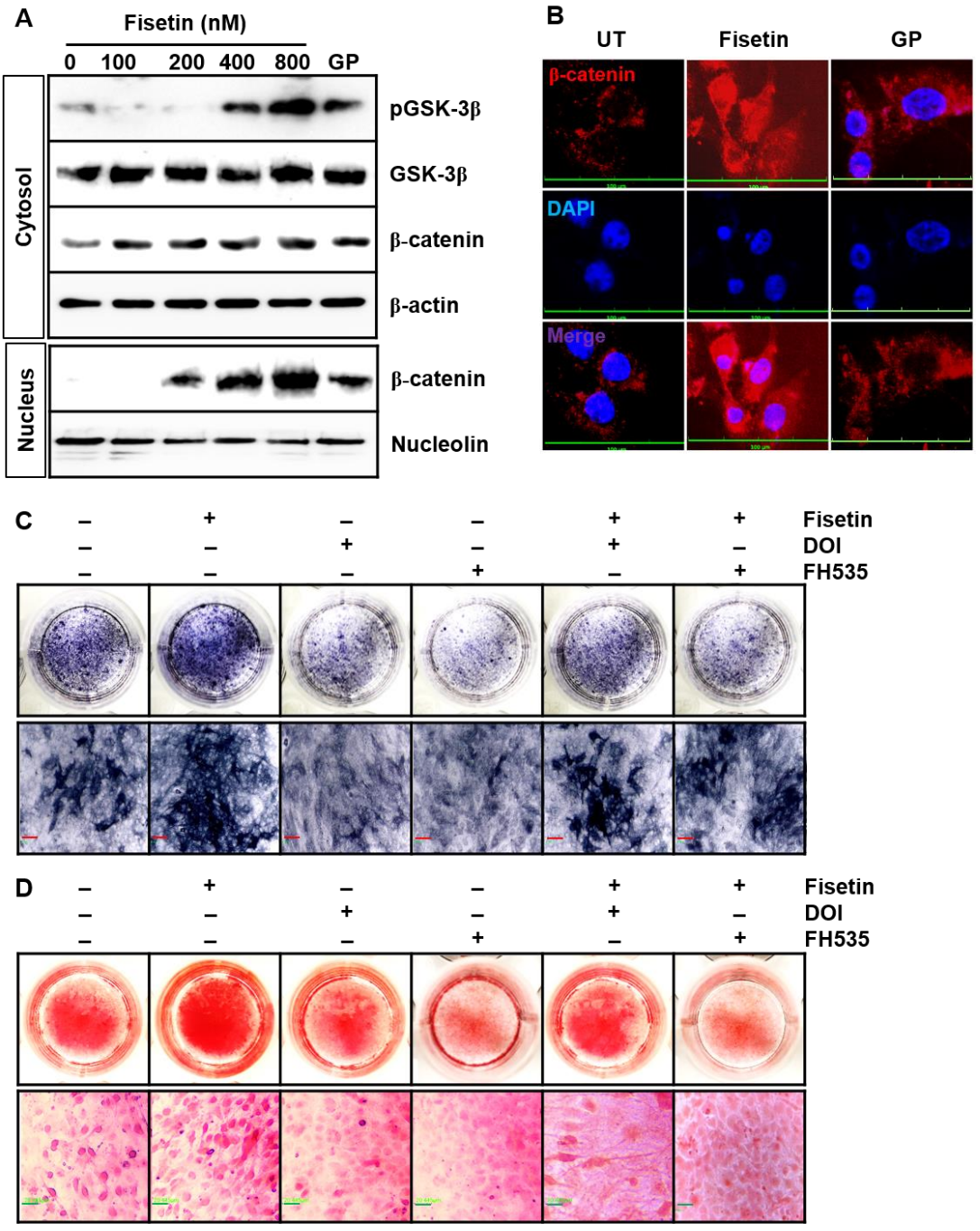

Figure 32.Fisetin promotes osteoblast differentiation via phosphorylation of GSK-3β at ser9. MC3T3E1 cells were seeded at a density of 1 x 10^4 cells/mL and with 0-800 nM fisetin for another 14 days. GP (4 mM) was used as the positive control. (A) Nuclear protein were isolated from NE-PER^{TM} nuclear and cytoplasmic extraction reagents and western blotting was performed to detect the expression of GSK-3β, GSK-3β (ser9) and β-catenin. β-actin and nucleolin was used as the house keeping proteins for cytosolic and nuclear proteins respectively. (B) In a parallel experiment, 3 x 10^3 cells/mL cells were seeded on 3% gelatin coated cover slips and immunostained for β-catenin nuclear translocalization. Scale bar = 100 μm (C-D) Cells were pretreated with 10 μM FH535 and 30 μM DOI for 2 h prior to the exposer with 800 nM fisetin and stained for (C) ALP activity using ALP staining assay kit and (D) 2% alizarin red for the mineralization. Representative images were taken with Ezscope i900PH phase contrast microscope (x10). Scale bar = 40 μm. Each value indicates the mean ± standard error median (SEM) and is representative of the results obtained from three independent experiments. Significant differences among the groups were determined using the Student's *t*-test ($^{###}$, $p < 0.001$, $^{##}$, $p < 0.01$, and $^{#}$, $p < 0.05$ vs. the untreated larvae) and one-way ANOVA with Bonferroni correction (***, $p < 0.001$, **, $p < 0.01$, and *, $p < 0.05$ vs. the LPS-treated larvae).

4.4 Discussion

Bone resorption disorders such as osteoporosis is characterized by thin and brittle bones and consequently increase the incident of bone fractures accompanied by a significant increase of osteoclast activity and the physiological decrease of osteoblast activity (Guido et al., 2009). Clinical data investigated that most of bone resorption-treatment drugs such as estrogen, selective estrogen receptor modulators, bisphosphonate and calcitonin are capable of inhibiting osteoclast formation and their functions; however, the drugs are proven to associate with serious side effects

and moderate drug efficacy especially, among the postmenopausal women (Premaor et al., 2010). Therefore, natural bioactive compounds would be preferred to cure bone resorption through promotion of osteoblast differentiation with minimum side effects. In previous studies, fisetin showed the possibility to cure bone resorption disorders (Choi et al., 2012; Leotoing et al., 2014); however, the underlying signaling mechanisms are not observed. In this study, we found that fisetin promotes osteoblastic differentiation in MC3T3-E1 cells and vertebrae formation in zebrafish larvae via the Wnt/β-catenin cell signaling pathway. Furthermore, fisetin alleviate PDS-induced bone resorption both *in vitro* and *in vivo*.

RUNX2 and OSX are essential for osteoblast differentiation: RUNX2 is a key transcription factor in the early stage differentiation from bone marrow mesenchymal stem cell to preosteoblast, OSX stimulates preosteoblast into the functional osteoblast, leading to osteoblast-specific gene expression such as *ALP*, *Col1α1*, and *OCN*, and mineralization of bone nodules (Galindo et al., 2005; Zhang et al., 2010). Therefore, bioactive compounds that regulates the expression of RUNX2 and OSX provide the possibility for clinical application as new drugs for treatment of osteoporosis (An et al., 2016). In the regards, we found that fisetin promotes the expression of RUNX2 and OSX, as well as mineralization in preosteoblast cells and stimulates vertebrae formation in zebrafish larvae. In addition, the Wnt/β-catenin signaling plays a vital role in osteoblast differentiation and anabolism for bone formation (Buckland, 2015). Activation of canonical Wnt signaling pathway liberates β-catenin from its destructive complex with GSK-3β, β-catenin translocates to the nucleus and interacts with transcription factor of T cell factor 1 (TCF1), resulting in the activation of downstream target genes such as RUNX2 and OSX (MacDonald et al., 2009; Zhang et al., 2010). In our previous study, we found that fisetin could effectively promote the β-catenin nuclear translocalization during melanogenesis by

phosphorylating GSK-3β at Ser9 (Molagoda et al., 2020). Therefore, we hypothesized the possibility that fisetin stimulates β-catenin-mediated bone formation. In the present study, we confirmed that fisetin significantly increased GSK-3β Ser9 phosphorylation, and β-catenin nuclear translocation in preosteoblast MC3T3-E1 cells, resulting in a significant increase of ALP activity and mineralization of osteoblast nodule. Furthermore, specific inhibition of β-catenin by FH535 and GSK-3β stabilization by DOI hydrochloride aggravated fisetin-induced osteogenic effect and vertebrae formation in both preosteoblast MC3T3-E1 cells and zebrafish larvae. Above results indicates that fisetin blocked GSK-3β-mediated β-catenin degradation, and liberated β-catenin promotes transcription of RUNX2, leading to stimulation of osteogenesis.

The binding of RANKL to its receptor RANK stimulates differentiation from osteoclast precursors to mature osteoclasts by activating NF-κB and c-Fos via the recruitment of adaptor molecules such as TRAF6 (Kim et al., 2015). Nuclear translocation of NF-κB and c-FOS transactivates *NFATc1* that is indispensable for osteoclast differentiation, resulting in the robust expression of OSCAR and CTSK (Kim and Kim, 2014; Tobeiha et al., 2020). In detail, Takyanagi et al. (Takayanagi et al., 2002) showed that, in the *NFATc1*-deficient condition, embryonic stem cells are unable to differentiate into mature osteoclast; whereas the overexpression of NFATc1 leads to the osteoclast maturation even in the absence of RANKL through the upregulation of OSCAR and CTSK (Charles et al., 2012). Glucocorticoids such as PDS are one of most powerful anti-inflammatory and immunosuppressive drugs for the treatment of chronic inflammatory disease (Becker, 2013); however, their long-term treatment causes severe bond loss and side effects in both time- and dose-dependent manner, resulting in osteoporosis (Nishimura and Ikuyama, 2000, LoCascio, 1990). Humphrey et al. (Humphrey et al., 2006) reported that PDS induces the expression of RANKL and osteoprotegerin (OPG) to severely aggravate bone resorption by increasing osteoclast

differentiation. In this study, we also found that fisetin mitigates PDS-induced antiosteogenic activity and vertebrae formation both *in vivo* and *in vitro*. This result indicates that fisetin may be a potential drug against bone resorption disorders such as osteoporosis.

In conclusion, our results demonstrated that fisetin promotes osteoblast differentiation and vertebrae formation in preosteoblast MC3T3-E1 cells and zebrafish larvae. During this study, we noticed that fisetin stimulates GSK-3β ser9 phosphorylation and subsequent liberation of β-catenin, and thereby upregulate the osteoblast differentiation and bone formation. Furthermore, fisetin could alleviate PDS-induced osteoporosis by inhibiting osteoclast differentiation. Nevertheless, osteogenic and antiosteoclastogenic effects of fisetin will be investigated in the clinical stage for human.

5 Chapter5

Fisetin protects HaCaT human keratinocytes from fine particulate matter ($PM_{2.5}$)-induced oxidative stress and apoptosis via inhibiting endoplasmic reticulum stress response

Abstract

Fine particulate matter ($PM_{2.5}$) originated from coal combustion and diesel vehicle exhaust. $PM_{2.5}$ readily penetrates the skin through aryl hydrocarbon receptors, causing skin senescence, inflammatory skin diseases, DNA damages and carcinogenesis. In this study, we investigated whether a bioactive flavonoid, fisetin, prevents HaCaT human keratinocytes from $PM_{2.5}$-induced cell death. Fisetin (below 10 μM) significantly downregulated $PM_{2.5}$-induced apoptosis accompanied by a strongly inhibition of reactive oxygen species production and proapoptotic protein expression. Additionally, $PM_{2.5}$-induced apoptosis was associated with endoplasmic reticulum (ER) stress responses through the PERK-eIF2α-ATF4-CHOP axis concomitantly with a remarkable increase of cytosolic calcium. In contrary, fisetin inhibited the expression of ER stress-related proteins such as GRP78, p-eIF2α, ATF4 and CHOP accompanied by low levels of cytosolic calcium accumulation. The data supports that fisetin inhibits $PM_{2.5}$-induced apoptosis by alleviating ER stress responses and ROS production.

Key words: Fisetin; $PM_{2.5}$; Apoptosis, endoplasmic reticulum stress; Reactive oxygen species

5.1 Introduction

Most fine particulate matter ($PM_{2.5}$) originated from coal combustion and diesel vehicle exhaust causes serious pathological disease, including lung cancer, chronic airway inflammation, cardiovascular dysfunction, diabetes mellitus and genotoxicity (Cho et al., 2018). Aerodynamic diameter of $PM_{2.5}$ is below 2.5 μM (Shi et al., 2015); hence, largest fraction of $PM_{2.5}$ is deposited in the lungs and subsequently penetrates to the deepest regions of the lungs, causing respiratory system damage (Marshall, 2013). In spite of the lungs, toxicological and epidemiological investigations revealed that inhaled $PM_{2.5}$ enters in to the systemic circulation and potentially causes severe life-threatening disorders in nervous system (Sram et al., 2017), respiratory system (Xing et al., 2016), immune system (Wei and Tang, 2018) and cardiovascular system (Du et al., 2016). $PM_{2.5}$ is a mixture of hundreds of different chemicals such as metals, allergens, toxic products of combustion of fossil fuels and endotoxins; especially, the compounds such as polycyclic organic hydrocarbons readily penetrate the skin through aryl hydrocarbon receptors (AhR) (Xu et al., 2019), which results excessive generation of reactive oxygen species (Komatsu et al.) consequently causes skin senescence, inflammatory skin diseases, DNA damage and carcinogenesis (Piao et al., 2018; Ryu et al., 2019).

Piao et al. (Piao et al., 2018) demonstrated that $PM_{2.5}$ induces oxidative stress-related endoplasmic reticulum (ER) stress in HaCaT human keratinocytes. Excessive ROS production in the adverse physiological conditions is directly linked with the induction of ER stress responses and Ca^{2+} release from the ER lumen in HaCaT keratinocytes (Farrukh et al., 2014). Disruption of the ER membrane results in the lowering of protein folding capacity, leading to the unfolded protein response (UPR) (Lin et al., 2008). Especially, protein kinase R-like ER kinase (PERK) (Zhong et al.) bears an ER luminal domain that monitors the protein-folding imbalance in the ER by binding

to 78-kDA glucose-regulated protein (GRP78) (Adams et al., 2019). Phosphorylation of eukaryotic initiation factor 2α (eIF2α) by PERK inhibits the assembly of 80s ribosomes at the initiation codon of mRNA to commence protein synthesis (Harding et al., 1999). Concurrently, eIF2α is allowed to interact with the coding region of activating transcription factor 4 (ATF4) that ultimately result in the upregulation of CCAAT-enhancer-binding protein (C/EBP) homologous protein (CHOP), which subsequently results in the initiation of cell death signals (Pakos-Zebrucka et al., 2016). As a transcription factor, CHOP regulates the expression of many anti-apoptotic and pro-apoptotic genes, including Bcl-2 family proteins (Pihán et al., 2017). Impairment of the Bcl-2 to Bax ratio in the mitochondrial membrane consequently open the mitochondrial permeability transition (MPT) hole, which enables the release of apoptotic active substances such as cytochrome *c* and eventually causes cell death via caspase dependent manner (Sharpe et al., 2004).

Fisetin is a bioactive flavonoid and exists in many fruits and vegetables such as grape, onion and strawberry (Khan et al., 2013). Fisetin is associated with a number of potent biological effects such as anti-inflammatory (Kim et al., 2015), antioxidant (Naeimi and Alizadeh, 2017) and anticarcinogenic (Jia et al., 2019) effects. Nevertheless, protective effect of fisetin against $PM_{2.5}$-induced damage in keratinocytes remains unclear. In this study, we investigated whether fisetin prevents HaCaT keratinocytes against $PM_{2.5}$-induced oxidative stress and apoptosis by inhibiting ER stress responses.

5.2 Material and Method

5.2.1 Regent and antibodies

Diesel particulate matter ($PM_{2.5}$), 3-(4,5-dimethylthiazol-2-yl)-2,5-diphenyltetrazolium bromide (MTT) and salubrinal were purchased from Sigma Aldrich (St. Louis, MO, USA). 2′,7′-

Dichlorodihydrofluorescein diacetate (DCFDA) was purchased from Molecular Probes (Eugene, OR, USA). Antibodies against Bid (sc-11423), cytochrome *c* (sc-13560), Bax (sc-7480), PARP (sc-7150), caspase-3 (sc-7272), caspase-8 (sc-1637), caspase-9 (sc-70507), GRP78 (sc-13968), CHOP (sc-575), β-actin (sc-69879) and peroxidase labelled anti-mouse immunoglobulins (sc-16102) were purchased from Santa Cruz Biotechnology (Santa Cruz, CA, USA). Antibodies against Bcl-2 (MA5-15046), eIF2α (PA5-27366), phospho (p)-eIF2α (MA5-15133), ATF4 (PA5-19521) were purchased from Thermo Fisher Scientific (Waltham, MA, USA). Peroxidase-labeled anti-rabbit immunoglobulins (KO211708) was obtained from Koma Biotechnology (Seoul, Republic of Korea). Dulbecco's modified eagle medium (DMEM), antibiotic mixtures, fetal bovine serum (FBS) and trypsin-EDTA solution were purchased from WELGENE (Gyeongsan, Gyeongsangbuk-do, Republic of Korea). All other chemicals were purchased from Sigma grades.

5.2.2 Cell culture and cell viability

Immortalized HaCaT keratinocytes were obtained from American Type Cell Culture Collection (ATCC, Manassas, VA, USA) and maintained in DMEM containing 10% FBS and antibiotic mixture. In detail, HaCaT keratinocytes were fisetin (0–20 μM) for 24 h and stained with Muse Count & Viability Kit (Luminex Corp., Austin, TX, USA) for 5 min. Viability and dead cell populations were measured by Muse Cell Analyzer (Luminex Corp.).

5.2.3 Annexin V staining for apoptosis detection

HaCaT keratinocytes were seeded at a density of 1×10^4 cell/mL and treated with fisetin (0–20 μM) for 2 h prior to stimulation with 100 μg/mL $PM_{2.5}$ for 24 h. The cells were collected and incubated with a Muse Annexin V & Dead Cell Kit (Luminex Corp.) for 30 min. Apoptotic cell populations were measured by Muse Cell Analyzer (Luminex Corp.).

5.2.4 Protein extraction and western blotting

HaCaT keratinocytes were seeded at 1×10^4 cells/mL and pretreated with fisetin (0–10 μM) for 2 h prior to exposure to 100 μg/mL $PM_{2.5}$. Then, the cells were lysed with RIPA lysis buffer (iNtRON Biotechnology, Seongnam, Gyeonggi-do, Republic of Korea) and the proteins were quantified by Bio-Rad Protein Assay Reagents (Bio-Rad, Hercules, CA, USA). Then, western blotting was performed and protein expression was captured by ImageQuant LAS 500 (GE Healthcare Bio-Sciences AB; Uppsala, Sweden). β-Actin was used as the loading control.

5.2.5 Caspase3/7 activity

HaCaT keratinocytes were treated with fisetin (0–10 μM) for 2 h prior to exposure to 100 μg/mL $PM_{2.5}$ for 24 h. Then, the cells were harvested and stained with Fluorogenic Muse Caspase-3/7 Reagent (Luminex Corp.) followed by incubation with cell death dye, 7-AAD. Caspase-$3/7^+$ apoptotic cell populations were measured using Muse Cell Analyzer (Luminex Corp.).

5.2.6 Quantification of intracellular ROS

HaCaT keratinocytes were treated with fisetin (0–10 μM) and then stimulated with 100 μg/mL $PM_{2.5}$ for 2 h. ROS^+ cell populations were measured by Muse Oxidative Stress Kit (Luminex Corp.).

5.2.7 Intracellular ROS

HaCaT keratinocytes were treated with 10 μM fisetin in the presence and absence of 100 μg/mL $PM_{2.5}$ for 2 h. The cells were incubated with 10 μM DCFDA for 10 min and cell images were captured using a CELENA S digital imaging system (Logos Biosystems, Anyang, Gyeonggi-do, Republic of Korea).

5.2.8 Cytosolic calcium

HaCaT keratinocytes were treated with 10 μM fisetin and 20 μM salubrinal in the presence and absence of 100 μg/mL $PM_{2.5}$ for 24 h. The cells were incubated with 1 μM Fluo-4 AM for 10 min and cell images were captured by a CELENA S digital imaging system (Logos Biosystems).

5.2.9 ROS staining in live zebrafish larvae

Zebrafish were maintained and raised according to standard guidelines of the Animal Care and Use Committee of Jeju National University (Jeju, Jeju Special Self-governing Province, Republic of Korea; approval No.:000000). Fertilized embryos were cultured in E3 embryo media containing with 2 mg/L methylene blue. Three days post fertilized (dpf) zebrafish larvae (*n=20* for each group) were pretreated with 0–400 μM fisetin for 2 h followed by treatment with 50 μg/mL $PM_{2.5}$ for 24 h. Zebrafish embryos (4 dpf) were incubated with 20 μM DCFDA for 30 min and visualized using a CELENA S digital imaging system (Logos Biosystems). Fluorescence intensities were calculated using ImageJ software (Wayne Rasband, National Institute of Health) and relative intensity was represented.

5.2.10 Statistical Analysis

All western blots were quantified by Image J software and then statistically analyzed by Sigma plot 12.0. All data represented the mean of at least triplicate experiments, and were expressed as ± the standard error of the median. Significant differences between groups were determined using an unpaired one-way ANOVA test with Bonferroni correction. Statistical significance was set at *** and $^{\#\#\#}p < 0.001$, ** and $^{\#\#}p < 0.01$, * and $^{\#}p < 0.05$. The results shown in each of the figures are representative of at least three independent experiments.

5.3 Results

5.3.1 Fisetin protects HaCaT keratinocytes from $PM_{2.5}$-induced apoptosis.

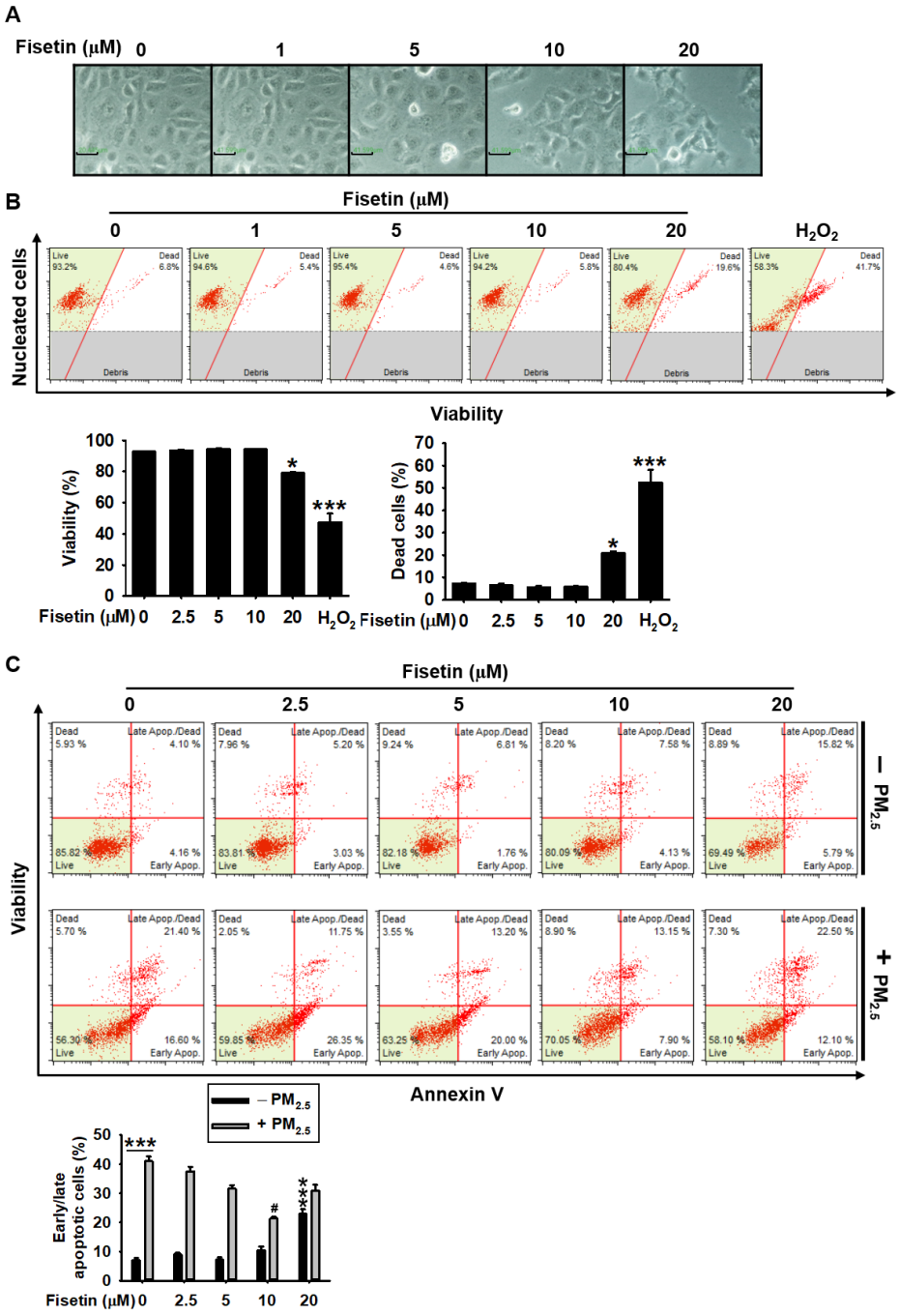

Figure 33. Fisetin protects HaCaT keratinocytes from PM2.5-induced apoptosis. HaCaT keratinocytes treated with 0–20 μM fisetin for 24 h. (A) Morphological changes observed using

phase contrast microscopy (×10). Scale bar = 40 μm. (B) Cell viability was measured Muse Count & Viability Kit. Viability and dead cell population are shown. (C) Fisetin (0–20 μM) was pretreated for 2 h prior to stimulation with 100 μg/mL $PM_{2.5}$ for 24 h. Cell viability and early/late apoptosis were measured using Muse Annexin V & Dead Cell Assay Kit. Early/late apoptosis populations are shown. $^{***}p < 0.001$ and $^{*}p < 0.05$ vs. untreated cells and $^{###}p < 0.001$ and $^{#}p < 0.05$ vs. $PM_{2.5}$-treated cells.

In order to evaluate the cytotoxic effect of fisetin, we first treated with fisetin for 24 h and evaluated cellular morphology and viability. Morphological observation revealed that the highest concentration of fisetin (20 μM) increased a significant amount of apoptosis-related cellular marks such as shrunk cells and floating cells; however, below 10 μM fisetin, none of apoptotic morphology was observed (Figure 33A). Further, flow cytometry data showed that 20 μM fisetin significantly decreased cell viability (79.0% ± 0.7%, Figure 33B., *bottom left*) and increased dead cell populations (21.0% ± 0.6%, Figure 33B., *bottom right*) compared with those in the untreated cells (92.7% ± 0.3% and 7.3% ± 0.3% in cell viability and dead cell populations, respectively) (Figure 33B). In detail, 20 μM fisetin increased total apoptotic cell population from 7.02 ± 0.79% to 22.9 ± 1.6% and fisetin did not upregulated the apoptotic cells below 10 μM (Figure 33C). Furthermore, $PM_{2.5}$ significantly sensitized apoptotic death (41.0% ± 1.6%); however, fisetin alleviated $PM_{2.5}$-induced apoptosis in a concentration dependent manner (37.5% ± 1.5%, 31.6% ± 1.1% and 21.4 ± 0.6% at 2.5, 5 and 10 μM, respectively). Additionally, the anti-apoptotic effect of fisetin at 20 μM (30.8% ± 2.1%) was significant but lower than 10 μM treatment. These results indicate that low concentrations of fisetin possess no cytotoxicity and protects $PM_{2.5}$-induced apoptosis in HaCaT keratinocytes.

5.3.2 Fisetin inhibits $PM_{2.5}$- induced apoptosis through modulating apoptosis-related proteins

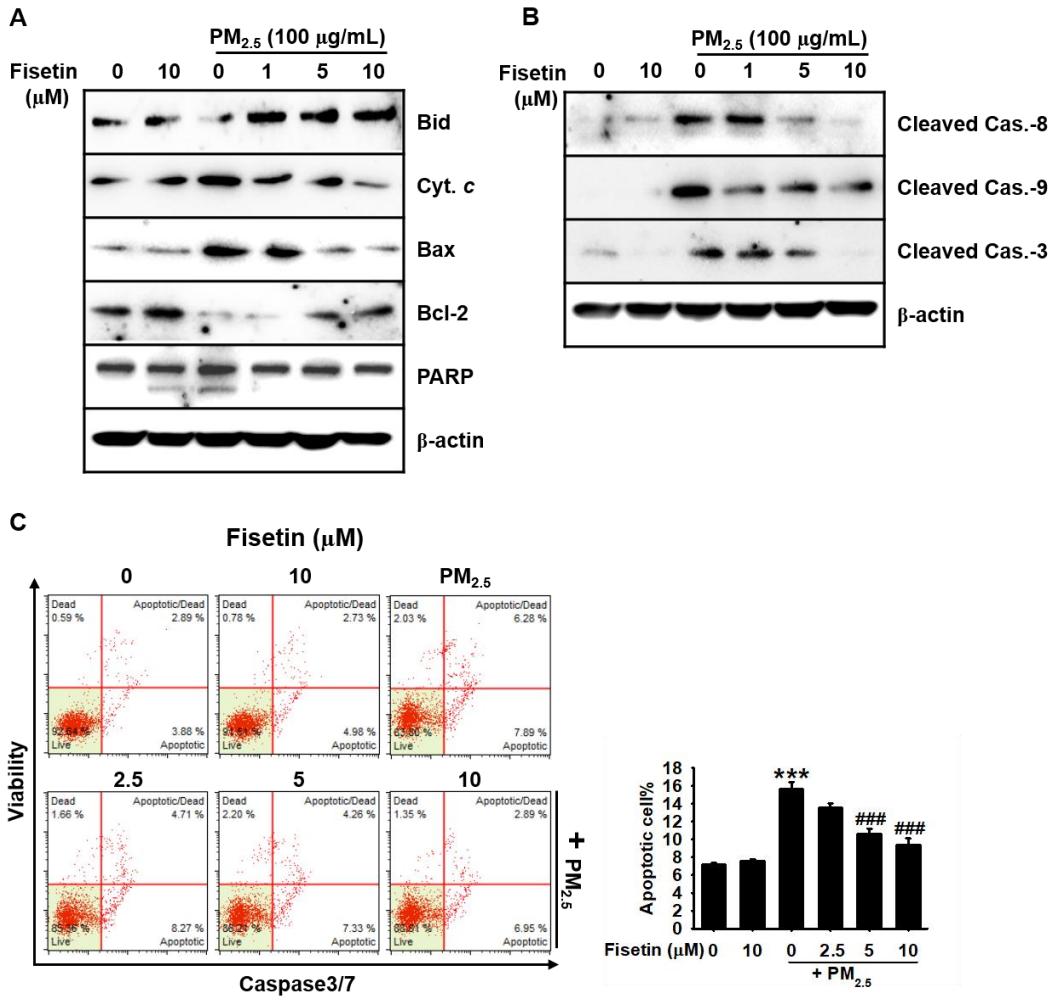

Figure 34. Fisetin downregulates $PM_{2.5}$-induced proapoptotic activity in HaCaT keratinocytes. HaCaT keratinocytes were treated with 0–10 μM fisetin for 2 h prior to stimulation with 100 μg/mL $PM_{2.5}$ for 24 h. (A and B) Total proteins were extracted and western blotting was performed: (B) Bid, cytochrome *c* (Cyt. *c*). Bax, Bcl-2 and PARP, and (C) cleaved caspase (Cas.)-8, cleaved caspase-9 and cleaved caspase-3. (C) β-actin was used as the loading control. *** $p < 0.001$ vs. untreated cells and $^{###}$ $p < 0.001$ and $^{#}$ $p < 0.05$ vs. the $PM_{2.5}$-treated cells.

Since Bcl-2 family proteins are considered as main apoptosis-regulating key in response to the mitochondria-derived apoptotic signals, the protein expression was investigated. As shown in Fig. 2A, fisetin effectively increased total Bid expression along with Bcl-2 in the presence of $PM_{2.5}$ and downregulated cytochrome c and Bax expression accompanied by the cleavage of PARP (Figure 34A). As expected, $PM_{2.5}$-induced cleavage of capase-3, -8 and -9 was significant and fisetin effectively blocked the cleavage of both initiator caspases such as caspase-8 and -9, and an executioner caspase such as caspase-3 in a concentration-dependent manner (Figure 34B). To further validate the inhibition of active caspase expression by fisetin, caspase 3/7 activity was measured using flow cytometry (Figure 34C, *left*). $PM_{2.5}$ significantly triggered caspase-$3/7^+$ apoptotic cell populations from 6.3% ± 0.3% to 15.7% ± 0.8%, whereas fisetin inhibits $PM_{2.5}$-induced caspase-$3/7^+$ population to 13.5 ± 0.4, 10.1 ± 0.6 and 9.4 ± 0.7% at 2.5, 5 and 10 μM respectively.

5.3.3 Fisetin inhibits $PM_{2.5}$-induced ROS formation.

Since excessive ROS production promotes the initiation of the apoptosis pathways, we, next, investigated whether fisetin alleviates $PM_{2.5}$-induced ROS production in both HaCaT keratinocytes and zebrafish larvae. As expected, flow cytometry data (Figure. 35A, *left*) showed that $PM_{2.5}$ markedly increased ROS^+ cell populations to 54.9% ± 2.0% compared that in the untreated cells (10.8% ± 2.8%, Figure. 35A, *right*). However, fisetin gradually inhibited $PM_{2.5}$-induced ROS production in a concentration-dependent manner (39.7% ± 1.1%, 33.5% ± 3.6% and 31.3% ± 5.2% at 2.5, 5 and 10 μM, respectively). Fluorescence staining using DCFDA also confirmed that fisetin effectively inhibited the $PM_{2.5}$-induced ROS production in HaCaT keratinocytes (Figure. 35B). In order to elaborate the ROS scavenging ability of fisetin in zebrafish larvae, 3 dpf zebrafish larvae were treated with fisetin for 2 h prior to stimulation with $PM_{2.5}$ for

24 h. According to the fluorescence microscopic data, $PM_{2.5}$ significantly induced higher amount of ROS compared with that in the untreated zebrafish larvae (Figure. 35C). Fisetin remarkably attenuated the $PM_{2.5}$-induced ROS production in a concentration-dependent manner. These results suggest that fisetin inhibits $PM_{2.5}$-induced ROS generation in both HaCaT keratinocytes and zebrafish larvae.

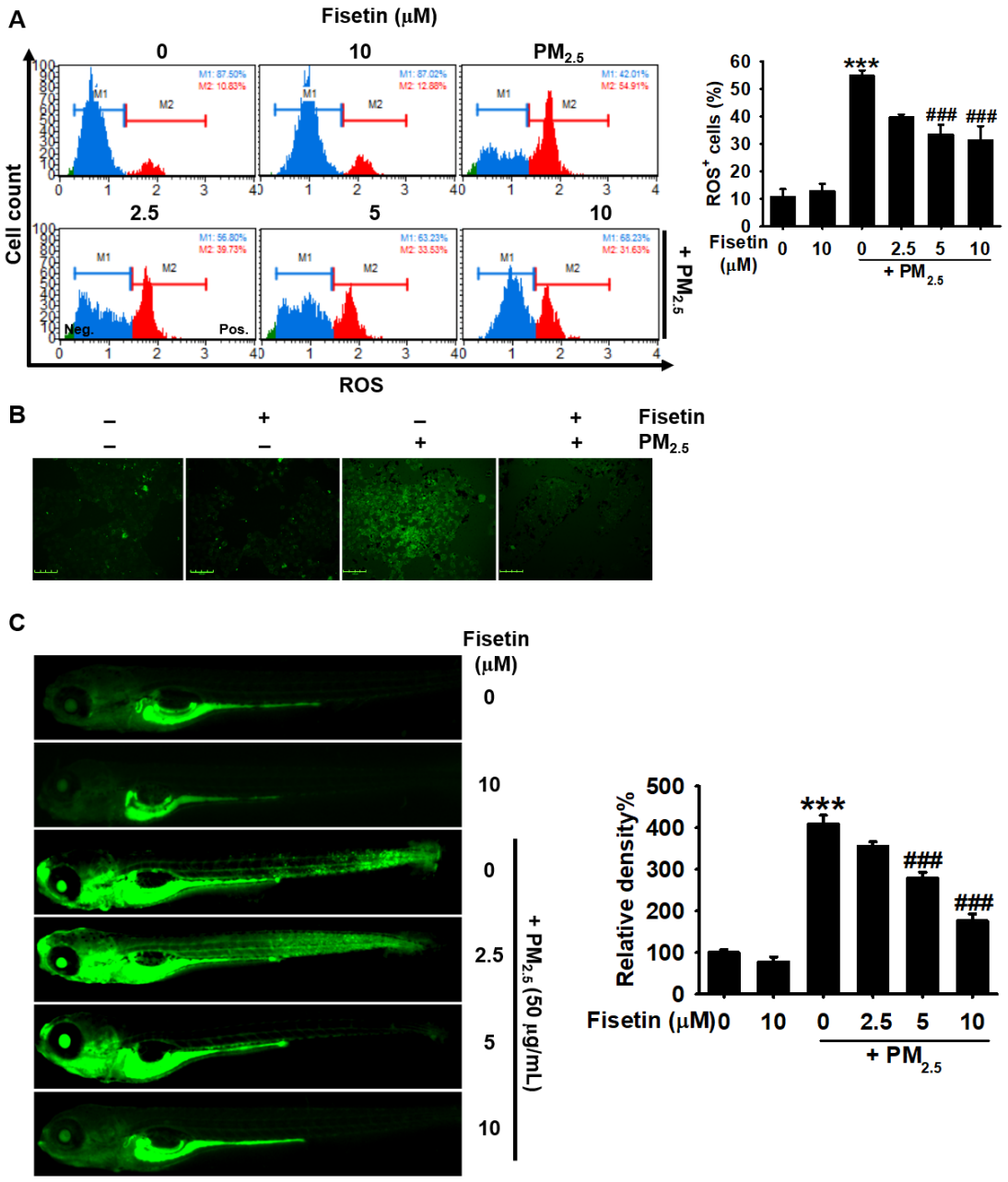

Figure 35. Fisetin inhibits PM2.5-induced ROS generation. HaCaT keratinocytes were treated with fisetin (0–10 μM) for 2 h and then, exposed with 100 μg/mL $PM_{2.5}$ for 24 h. (A) The cells were stained with Muse Oxidative Stress Assay Kit and analyzed ROS production. (B) In a parallel experiment, the cells were treated with 10 μM fisetin in the presence and absence of 100 μg/mL $PM_{2.5}$ for 24 h. Cells were washed with PBS and loaded with 10 μM DCFDA for 10 min and live imaging was performed by CELENA S digital imaging system. Scale bar = 100 μm. (C) Three days post fertilized (3 dpf) zebrafish larvae were pretreated with fisetin (0–400 μM) for 2 h and then exposed with 50 μg/mL $PM_{2.5}$ for 24 h. The larvae were stained with 20 μM DCFDA for 30 min and visualized using CELENA S digital imaging system. Fluorescence intensities were calculated using ImageJ software and expressed as a percentage comparable to the untreated control. $^{***}p < 0.001$ vs. untreated conditions and $^{###}p < 0.001$ vs. $PM_{2.5}$ treated conditions.

5.3.4 Fisetin inhibits $PM_{2.5}$-induced apoptosis by alleviating ER stress

In order to confirm the effect of fisetin on $PM_{2.5}$-induced ER stress, the PERK-ATF4-CHOP axis in the ER stress response was investigated. We found that $PM_{2.5}$ associated with the upregulation of ER stress marker proteins such as GRP78, p-eIF2α, ATF4 and CHOP, whereas fisetin attenuated the upregulated protein levels in a concentration-dependent manner (Fig. 4A). Induction of the ER stress responses by $PM_{2.5}$ resulted in the upregulation of cytosolic calcium levels and pretreatment with 10 μM fisetin markedly reduced the $PM_{2.5}$-induced calcium levels comparable to treatment with 20 μM salubrinal (Fig. 4B). Additionally, salubrinal inhibited the $PM_{2.5}$-induced ROS^{+} cell population from 58.5% ± 3.6% to 11.45 ± 2.56%, and 10 μM fisetin also decreased to 27.28 ± 5.46%. Aligned with the ROS production data, $PM_{2.5}$-induced apoptotic cell population (39.7% ± 3.6%) were significantly inhibited by salubrinal to 20.5% ± 5.2%, and fisetin also downregulated

to 21.1% ± 1.9%. These results indicate that fisetin inhibits $PM_{2.5}$-induced apoptosis by alleviating ER stress responses.

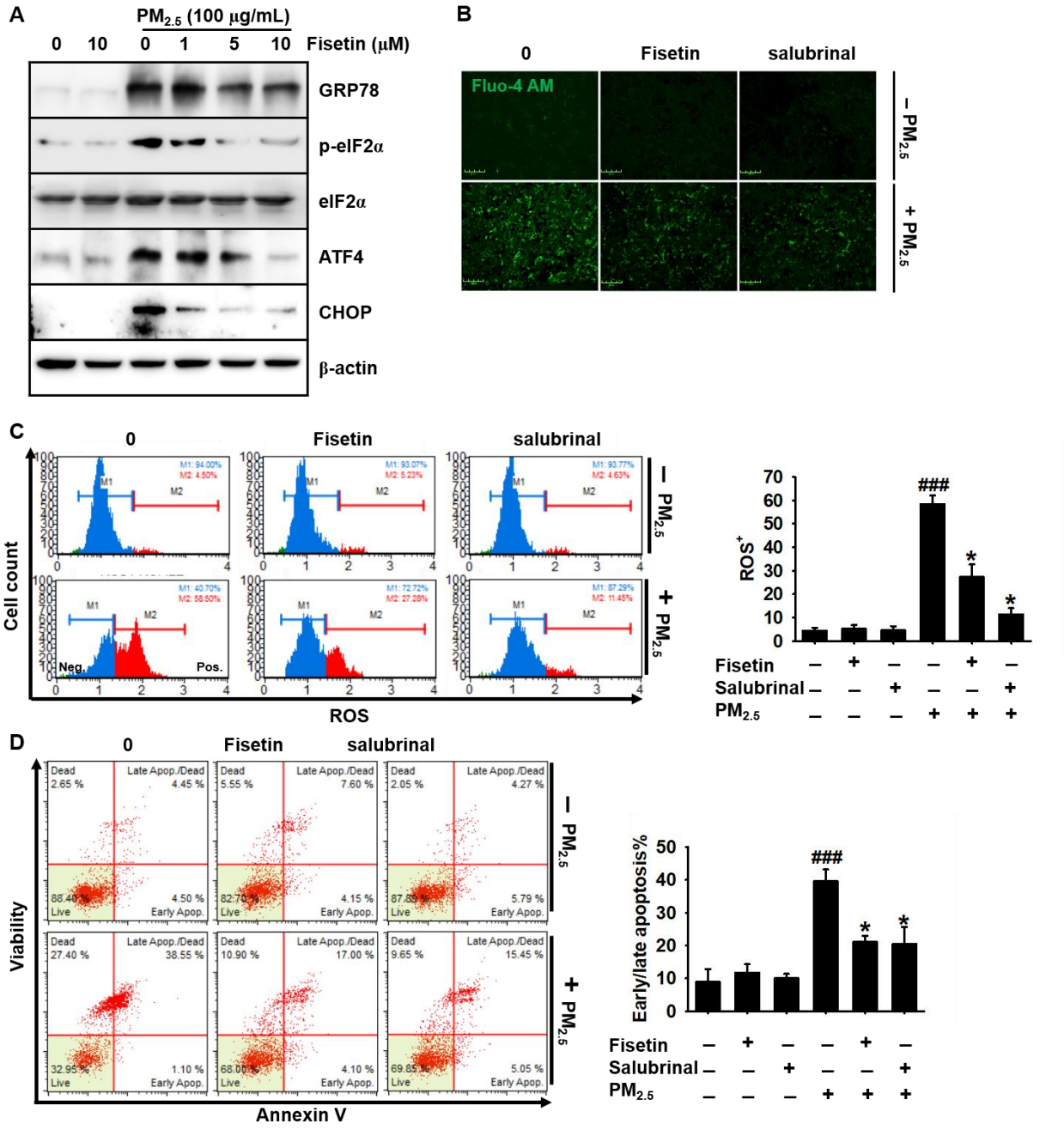

Figure 36. Fisetin inhibits PM2.5-induced apoptosis through alleviating ER stress. HaCaT keratinocytes were treated with fisetin (0-10 μM) for 2 h followed by stimulation with 100 μg/mL

$PM_{2.5}$ for 24 h. (A) Total proteins were extracted and western blotting was performed to detect the expression of GRP78, peIF2α, eIF2α and CHOP. β-actin was used as the loading control. (B) The cells were treated with 10 μM fisetin or 20 μM salubrinal in the presence and absence of 100 μg/mL $PM_{2.5}$ for 24 h. The cells were stained with Ca^{2+} sensitive Fluo-4-AM for 10 min and live images were captured using CELENA S digital imaging system. Scale bar = 100 μm. (C-D) In a parallel experiment, the cells were treated with 10 μM fisetin or 20 μM salubrinal in the presence and absence of 100 μg/mL $PM_{2.5}$ for 24 h. The cells were stained with (C) Muse Oxidative Stress Assay Kit for ROS^{+} cell populations and (D) Muse Annexin V & Dead Cell Assay Kit for the early/late apoptotic cell populations. * $p < 0.05$ vs. untreated cells and $^{###}$ $p < 0.001$ vs. $PM_{2.5}$-treated cells.

5.4 Discussion

Skin is the largest organ in the body and acts as an interface between the human body and external environment. Stratum corneum regulates the passage of electrolytes, biological substances and toxic materials through the skin; however, prolong or repeated exposer to the irritations makes skin vulnerable to the adverse pathological risks (Schwartz and Friedman, 2016). Accumulating evidences showed that $PM_{2.5}$ breaks the skin barriers and exert adverse effect on keratinocytes, resulting in oxidative stress-mediated apoptosis (Liao et al., 2020; Piao et al., 2018). Additionally, $PM_{2.5}$ contains higher levels of polycyclic organic hydrocarbons that readily penetrate the skin through AhR, which eventually promotes excessive ROS production, ER stress, mitochondrial dysfunction and apoptosis (Xu et al., 2019). Plant-derived bioactive compounds such as polyphenols may protect skin from air pollutant-induced irritation, ROS production and cell death (Boo, 2019). Fisetin is a bioactive flavonoid containing ROS scavenging, chelation of metal ions implicated in generation of free radicals or activation of antioxidant defenses (Khan et al., 2013;

Naeimi and Alizadeh, 2017). In this study, we investigated that fisetin effectively blocks $PM_{2.5}$-induced ROS formation and apoptosis in HaCaT keratinocytes by inhibiting ER stress.

$PM_{2.5}$ disrupts the skin homeostasis by damaging the nucleic acids, protein and lipid metabolism in the cells and subsequently promotes the generation of excessive ROS and cell death (Piao et al., 2018; Ryu et al., 2019). In addition, intracellular calcium is also play a crucial role in ROS production in response to $PM_{2.5}$. In spite of an enormous amount of ROS generation, $PM_{2.5}$ inhibits the filaggrin to downregulate keratin bundle aggregation in keratinocytes and thereby breaks the skin barrier functions (Li et al., 2017). In this regard, some polyphenolic bioactives strongly rescue the skin cells from $PM_{2.5}$-induced ROS generation and apoptosis, resulting in healthy skin (Boo, 2019). In this study, we also found that fisetin effectively blocked the $PM_{2.5}$-induced ROS levels in HaCaT keratinocytes. Additionally, $PM_{2.5}$-induced apoptosis was inhibited in fisetin-treated HaCaT keratinocytes accompanied by the downregulation of caspases. These data imply that fisetin possesses the protective effect against $PM_{2.5}$-mediated cell death in keratinocytes. Nevertheless, further study will be needed to evaluate whether fisetin protects human skin from $PM_{2.5}$-induced severe damages

The prolong exposer of $PM_{2.5}$ activates ER stress responses through calcium mobilization form the ER lumen, leading to the Unfolded protein response (UPR)-dependent PERK pathway and disruption of cellular homeostasis (Wang et al., 2017). Furthermore, pharmacological inhibition of ER calcium-ATPase pump by thapsigargin potently ER calcium depletion and cytosolic calcium accumulation, and UPR, causing cell death (Sehgal et al., 2017). We found that 100 μg/mL $PM_{2.5}$ increased the cytosolic calcium concurrently with upregulated levels of GRP78, causing ROS-induced apoptosis. In the contrary, high concentration of $PM_{2.5}$ (1 mg/mL) blocked the activation

of ER-stressed-induced apoptotic proteins such as ATF4 and DDIT3 in HaCaT keratinocytes (Kim et al., 2020), indicating that $PM_{2.5}$ concentration-differently gives rise to ER stress. Furthermore, in this study, we found that $PM_{2.5}$ activated the PERK-ATF4-CHOP axis; however, fisetin effectively blocked the axis of ER stress and consequently inhibited the accumulation of excessive calcium. Additionally, disruption of the ER homeostasis by $PM_{2.5}$ is linked with the mitochondrial membrane potential loss and subsequently disturb the balance between anti-apoptotic Bcl-2 proteins and pro-apoptotic Bax, causing caspase-mediated apoptosis (Piao et al., 2018). In this regard, fisetin may be a potent bioactive against PM2.5-induced apoptosis.

In conclusion, fisetin potently inhibited $PM_{2.5}$-induced ER stress response by downregulating the PERK-eIF2-ATF4 pathway accompanied by decline of ROS production and calcium accumulation. Meanwhile, fisetin stabilized mitochondrial membrane potential against $PM_{2.5}$-induced depolarization and inhibited caspase activity, leading to the protection of $PM_{2.5}$-induced apoptosis. In conclusion, the data support that fisetin potently protect skin against $PM_{2.5}$-induced damage.

Bibliography

1. D'Mello, S.A.; Finlay, G.J.; Baguley, B.C.; Askarian-Amiri, M.E. Signaling pathways in melanogenesis. Int. J. Mol. Sci. 2016, 17, 1144.
2. Bonaventure, J.; Domingues, M.J.; Larue, L. Cellular and molecular mechanisms controlling the migration of melanocytes and melanoma cells. Pigment Cell Melanoma Res. 2013, 26, 316–325.
3. Ogbechie-Godec, O.A.; Elbuluk, N. Melasma: An up-to-date comprehensive review. Dermatol. Ther. 2017, 7, 305–318.
4. Videira, I.F.; Moura, D.F.; Magina, S. Mechanisms regulating melanogenesis. An. Bras. Dermatol. 2013, 88, 76–83.
5. Graff, J.R.; McNulty, A.M.; Hanna, K.R.; Konicek, B.W.; Lynch, R.L.; Bailey, S.N.; Banks, C.; Capen, A.; Goode, R.; Lewis, J.E.; et al. The protein kinase Cb-selective inhibitor, Enzastaurin (LY317615.HCl), suppresses signaling through the AKT pathway, induces apoptosis, and suppresses growth of human colon cancer and glioblastoma xenografts. Cancer Res. 2005, 65, 7462–7469.
6. Rodriguez, C.I.; Setaluri, V. Cyclic AMP (cAMP) signaling in melanocytes and melanoma. Arch. Biochem. Biophys. 2014, 563, 22–27.
7. Rzepka, Z.; Buszman, E.; Beberok, A.; Wrzesniok, D. From tyrosine to melanin: Signaling pathways and factors regulating melanogenesis. Postepy Hig. Med Dosw. 2016, 70, 695–708.
8. Beurel, E.; Grieco, S.F.; Jope, R.S. Glycogen synthase kinase-3 (GSK3): Regulation, actions, and diseases. Pharmacol. Ther. 2015, 148, 114–131.

9. Ajmone-Cat, M.A.; D'Urso, M.C.; di Blasio, G.; Brignone, M.S.; De Simone, R.; Minghetti, L. Glycogen synthase kinase 3 is part of the molecular machinery regulating the adaptive response to LPS stimulation in microglial cells. Brain Behav. Immun. 2016, 55, 225–235.
10. Dembowy, J.; Adissu, H.A.; Liu, J.C.; Zacksenhaus, E.; Woodgett, J.R. Effect of glycogen synthase kinase-3 inactivation on mouse mammary gland development and oncogenesis. Oncogene 2015, 34, 3514–3526.
11. Maqbool, M.; Mobashir, M.; Hoda, N. Pivotal role of glycogen synthase kinase-3: A therapeutic target for Alzheimer's disease. Eur. J. Med. Chem. 2016, 107, 63–81.
12. Golpich, M.; Amini, E.; Hemmati, F.; Ibrahim, N.M.; Rahmani, B.; Mohamed, Z.; Raymond, A.A.; Dargahi, L.; Ghasemi, R.; Ahmadiani, A. Glycogen synthase kinase-3 beta (GSK-3β) signaling: Implications for Parkinson's disease. Pharmacol. Res. 2015, 97, 16–26.
13. Bartman, C.M.; Egelston, J.; Kattula, S.; Zeidner, L.C.; D'Ippolito, A.; Doble, B.W.; Phiel, C.J. Gene expression profiling in mouse embryonic stem cells reveals glycogen synthase kinase-3-dependent targets of phosphatidylinositol 3-kinase and Wnt/β-catenin signaling pathways. Front. Endocrinol. 2014, 5, 133.
14. Clevers, H.; Nusse, R. Wnt/β-catenin signaling and disease. Cell 2012, 149, 1192–1205.
15. Stamos, J.L.; Weis, W.I. The β-catenin destruction complex. Cold Spring Harb. Perspect. Biol. 2013, 5, a007898.
16. Clevers, H. Wnt/β-catenin signaling in development and disease. Cell 2006, 127, 469–480.
17. MacDonald, B.T.; Tamai, K.; He, X. Wnt/β-catenin signaling: Components, mechanisms, and diseases. Dev. Cell 2009, 17, 9–26.

18. Ma, K.; Yang, L.M.; Chen, H.Z.; Lu, Y. Activation of muscarinic receptors inhibits glutamate-induced GSK-3β overactivation in PC12 cells. Acta Pharmacol. Sin. 2013, 34, 886–892.
19. Doble, B.W.; Woodgett, J.R. GSK-3: Tricks of the trade for a multi-tasking kinase. J. Cell Sci. 2003, 116, 1175–1186.
20. Schepsky, A.; Bruser, K.; Gunnarsson, G.J.; Goodall, J.; Hallsson, J.H.; Goding, C.R.; Steingrimsson, E.; Hecht, A. The microphthalmia-associated transcription factor Mitf interacts with β-catenin to determine target gene expression. Mol. Cell. Biol. 2006, 26, 8914–8927.
21. Siegrist, W.; Eberle, A.N. In situ melanin assay for MSH using mouse B16 melanoma cells in culture. Anal. Biochem. 1986, 159, 191–197.
22. Bertolotto, C.; Bille, K.; Ortonne, J.P.; Ballotti, R. In B16 melanoma cells, the inhibition of melanogenesis by TPA results from PKC activation and diminution of microphthalmia binding to the M-box of the tyrosinase promoter. Oncogene 1998, 16, 1665–1670.
23. Prince, S.; Wiggins, T.; Hulley, P.A.; Kidson, S.H. Stimulation of melanogenesis by tetradecanoylphorbol 13-acetate (TPA) in mouse melanocytes and neural crest cells. Pigment Cell Res. 2003, 16, 26–34.
24. Chao-Hsing, K.A.; Hsin-Su, Y.U. A study of the effects of phorbol 12-myristate-13-acetate on cell differentiation of pure human melanocytes in vitro. Arch. Dermatol. Res. 1991, 283, 119–124.
25. Lajis, A.F.B. A zebrafish embryo as an animal model for the treatment of hyperpigmentation in cosmetic dermatology medicine. Medicina 2018, 54, 35.

26. Karunarathne, W.; Molagoda, I.M.N.; Park, S.R.; Kim, J.W.; Lee, O.K.; Kwon, H.Y.; Oren, M.; Choi, Y.H.; Ryu, H.W.; Oh, S.R.; et al. Anthocyanins from Hibiscus syriacus L. inhibit melanogenesis by activating the ERK signaling pathway. Biomolecules 2019, 9, 645.
27. Karunarathne, W.; Molagoda, I.M.N.; Kim, M.S.; Choi, Y.H.; Oren, M.; Park, E.K.; Kim, G.Y. Flumequine-mediated upregulation of p38 MAPK and JNK results in melanogenesis in B16F10 cells and zebrafish larvae. Biomolecules 2019, 9, 596.
28. Singh, A.P.; Nusslein-Volhard, C. Zebrafish stripes as a model for vertebrate colour pattern formation. Curr. Biol. 2015, 25, R81–R92.
29. Choi, T.Y.; Kim, J.H.; Ko, D.H.; Kim, C.H.; Hwang, J.S.; Ahn, S.; Kim, S.Y.; Kim, C.D.; Lee, J.H.; Yoon, T.J. Zebrafish as a new model for phenotype-based screening of melanogenic regulatory compounds. Pigment Cell Res. 2007, 20, 120–127.
30. Khan, H.; Marya; Amin, S.; Kamal, M.A.; Patel, S. Flavonoids as acetylcholinesterase inhibitors: Current therapeutic standing and future prospects. Biomed. Pharmacother. 2018, 101, 860–870.
31. Ahmad, A.; Ali, T.; Park, H.Y.; Badshah, H.; Rehman, S.U.; Kim, M.O. Neuroprotective effect of fisetin against amyloid-β-induced cognitive/synaptic dysfunction, neuroinflammation, and neurodegeneration in adult mice. Mol. Neurobiol. 2017, 54, 2269–2285.
32. Zheng, W.; Feng, Z.; You, S.; Zhang, H.; Tao, Z.; Wang, Q.; Chen, H.; Wu, Y. Fisetin inhibits IL-1β-induced inflammatory response in human osteoarthritis chondrocytes through activating SIRT1 and attenuates the progression of osteoarthritis in mice. Int. Immunopharmacol. 2017, 45, 135–147.

33. Jo, W.R.; Park, H.J. Antiallergic effect of fisetin on IgE-mediated mast cell activation in vitro and on passive cutaneous anaphylaxis (PCA). J. Nutr. Biochem. 2017, 48, 103–111.
34. Khan, N.; Mukhtar, H. Dietary agents for prevention and treatment of lung cancer. Cancer Lett. 2015, 359, 155–164.
35. Li, J.; Qu, W.; Cheng, Y.; Sun, Y.; Jiang, Y.; Zou, T.; Wang, Z.; Xu, Y.; Zhao, H. The inhibitory effect of intravesical fisetin against bladder cancer by induction of p53 and down-regulation of NF-κB pathways in a rat bladder carcinogenesis model. Basic Clin. Pharmacol. Toxicol. 2014, 115, 321–329.
36. Smith, M.; Murphy, K.; Doucette, C.; Greenshields, A.; Hoskin, D. The dietary flavonoid fisetin causes cell cycle arrest, caspase-dependent apoptosis, and enhanced cytotoxicity of chemotherapeutic drugs in triple-negative breast cancer cells. J. Cell. Biochem. 2016, 117, 1913–1925.
37. Mukhtar, E.; Adhami, V.M.; Siddiqui, I.A.; Verma, A.K.; Mukhtar, H. Fisetin enhances chemotherapeutic effect of cabazitaxel against human prostate cancer cells. Mol. Cancer Ther. 2016, 15, 2863–2874.
38. Chen, Y.; Wu, Q.; Song, L.; He, T.; Li, Y.; Li, L.; Su, W.; Liu, L.; Qian, Z.; Gong, C. Polymeric micelles encapsulating fisetin improve the therapeutic effect in colon cancer. ACS Appl. Mater. Interfaces 2015, 7, 534–542.
39. Youns, M.; Abdel Halim Hegazy, W. The natural flavonoid fisetin inhibits cellular rroliferation of hepatic, colorectal, and pancreatic cancer cells through modulation of multiple signaling pathways. PLoS ONE 2017, 12, e0169335.
40. Takekoshi, S.; Nagata, H.; Kitatani, K. Flavonoids enhance melanogenesis in human melanoma cells. Tokai J. Exp. Clin. Med. 2014, 39, 116–121.

41. Shon, M.S.; Kim, R.H.; Kwon, O.J.; Roh, S.S.; Kim, G.N. Beneficial role and function of fisetin in skin health via regulation of the CCN2/TGF-β signaling pathway. Food Sci. Biotechnol. 2016, 25, 133–141.
42. Curto, E.V.; Kwong, C.; Hermersdorfer, H.; Glatt, H.; Santis, C.; Virador, V.; Hearing, V.J., Jr.; Dooley, T.P. Inhibitors of mammalian melanocyte tyrosinase: In vitro comparisons of alkyl esters of gentisic acid with other putative inhibitors. Biochem. Pharmacol. 1999, 57, 663–672.
43. Tsuboi, T.; Kondoh, H.; Hiratsuka, J.; Mishima, Y. Enhanced melanogenesis induced by tyrosinase gene-transfer increases boron-uptake and killing effect of boron neutron capture therapy for amelanotic melanoma. Pigment Cell Res. 1998, 11, 275–282.
44. Agalou, A.; Thrapsianiotis, M.; Angelis, A.; Papakyriakou, A.; Skaltsounis, A.L.; Aligiannis, N.; Beis, D. Identification of novel melanin synthesis inhibitors from Crataegus pycnoloba using an in vivo zebrafish phenotypic assay. Front. Pharmacol. 2018, 9, 265.
45. Cornet, C.; Calzolari, S.; Minana-Prieto, R.; Dyballa, S.; van Doornmalen, E.; Rutjes, H.; Savy, T.; D'Amico, D.; Terriente, J. ZeGlobalTox: An innovative approach to address organ drug toxicity using zebrafish. Int. J. Mol. Sci. 2017, 18, 864.
46. Zhang, C.; Willett, C.; Fremgen, T. Zebrafish: An animal model for toxicological studies. Curr. Protoc. Toxicol. 2003, 17, doi:10.1002/0471140856.tx0107s17.
47. del Ser, T.; Steinwachs, K.C.; Gertz, H.J.; Andres, M.V.; Gomez-Carrillo, B.; Medina, M.; Vericat, J.A.; Redondo, P.; Fleet, D.; Leon, T. Treatment of Alzheimer's disease with the GSK-3 inhibitor tideglusib: A pilot study. J. Alzheimers Dis. 2013, 33, 205–215.

48. Tolosa, E.; Litvan, I.; Hoglinger, G.U.; Burn, D.; Lees, A.; Andres, M.V.; Gomez-Carrillo, B.; Leon, T.; Del Ser, T.; Investigators, T. A phase 2 trial of the GSK-3 inhibitor tideglusib in progressive supranuclear palsy. Mov. Disord. 2014, 29, 470–478.
49. Zamek-Gliszczynski, M.J.; Abraham, T.L.; Alberts, J.J.; Kulanthaivel, P.; Jackson, K.A.; Chow, K.H.; McCann, D.J.; Hu, H.; Anderson, S.; Furr, N.A.; et al. Pharmacokinetics, metabolism, and excretion of the glycogen synthase kinase-3 inhibitor LY2090314 in rats, dogs, and humans: A case study in rapid clearance by extensive metabolism with low circulating metabolite exposure. Drug Metab. Dispos. 2013, 41, 714–726.
50. Khan, N.; Syed, D.N.; Ahmad, N.; Mukhtar, H. Fisetin: A dietary antioxidant for health promotion. Antioxid. Redox Signal. 2013, 19, 151–162.
51. Kashyap, D.; Sharma, A.; Sak, K.; Tuli, H.S.; Buttar, H.S.; Bishayee, A. Fisetin: A bioactive phytochemical with potential for cancer prevention and pharmacotherapy. Life Sci. 2018, 194, 75–87.
52. He, W.B.; Abe, K.; Akaishi, T. Oral administration of fisetin promotes the induction of hippocampal long-term potentiation in vivo. J. Pharmacol. Sci. 2018, 136, 42–45.
53. Denat, L.; Kadekaro, A.L.; Marrot, L.; Leachman, S.A.; Abdel-Malek, Z.A. Melanocytes as instigators and victims of oxidative stress. J. Investig. Dermatol. 2014, 134, 1512–1518.
54. Tomita, Y.; Hariu, A.; Kato, C.; Seiji, M. Radical production during tyrosinase reaction, dopa-melanin formation, and photoirradiation of dopa-melanin. J. Investig. Dermatol. 1984, 82, 573–576.
55. Land, E.J.; Ramsden, C.A.; Riley, P.A. Quinone chemistry and melanogenesis. In Methods in Enzymology; 2004 ; Volume 378, pp. 88–109.

56. Fenoll, L.G.; Rodríguez-López, J.N.; García-Molina, F.; García-Cánovas, F.; Tudela, J. Unification for the expression of the monophenolase and diphenolase activities of tyrosinase. IUBMB Life 2002, 54, 137–141.
57. Liu-Smith, F.; Meyskens, F.L. Molecular mechanisms of flavonoids in melanin synthesis and the potential for the prevention and treatment of melanoma. Mol. Nutr. Food Res. 2016, 60, 1264–1274.
58. Kumagai, A.; Horike, N.; Satoh, Y.; Uebi, T.; Sasaki, T.; Itoh, Y.; Hirata, Y.; Uchio-Yamada, K.; Kitagawa, K.; Uesato, S.; et al. A potent inhibitor of SIK2, 3,3',7-trihydroxy-4'-methoxyflavon (4'-O-methylfisetin), promotes melanogenesis in B16F10 melanoma cells. PLoS ONE 2011, 6, e26148.
59. Widlund, H.R.; Horstmann, M.A.; Price, E.R.; Cui, J.; Lessnick, S.L.; Wu, M.; He, X.; Fisher, D.E. β-Catenin-induced melanoma growth requires the downstream target microphthalmia-associated transcription factor. J. Cell. Biol. 2002, 158, 1079–1087.
60. Eldar-Finkelman, H.; Argast, G.M.; Foord, O.; Fischer, E.H.; Krebs, E.G. Expression and characterization of glycogen synthase kinase-3 mutants and their effect on glycogen synthase activity in intact cells. Proc. Natl. Acad. Sci. USA 1996, 93, 10228–10233.
61. Kockeritz, L.; Doble, B.; Patel, S.; Woodgett, J.R. Glycogen synthase kinase-3—An overview of an over-achieving protein kinase. Curr. Drug Targets 2006, 7, 1377–1388.
62. Lei, P.; Ayton, S.; Bush, A.I.; Adlard, P.A. GSK-3 in neurodegenerative diseases. Int. J. Alzheimers Dis. 2011, 2011, 189246.
63. Pandey, M.K.; DeGrado, T.R. Glycogen synthase kinase-3 (GSK-3)-targeted therapy and imaging. Theranostics 2016, 6, 571–593.

64. Nabavi, S.F.; Braidy, N.; Habtemariam, S.; Sureda, A.; Manayi, A.; Nabavi, S.M. Neuroprotective effects of fisetin in Alzheimer's and Parkinson's diseases: From chemistry to medicine. Curr. Top. Med. Chem. 2016, 16, 1910–1915.

65. John, J.K.; Paraiso, K.H.T.; Rebecca, V.W.; Cantini, L.P.; Abel, E.V.; Pagano, N.; Meggers, E.; Mathew, R.; Krepler, C.; Izumi, V.; et al. GSK3β inhibition blocks melanoma cell/host interactions by downregulating N-cadherin expression and decreasing FAK phosphorylation. J. Investig. Dermatol. 2012, 132, 2818–2827.

66. Prame Kumar, K.; Nicholls, A.J.; Wong, C.H.Y. Partners in crime: neutrophils and monocytes/macrophages in inflammation and disease. Cell Tissue Res 2018, 371, 551-565, doi:10.1007/s00441-017-2753-2.

67. Tursi, A.; Elisei, W. Role of inflammation in the pathogenesis of diverticular disease. Mediators Inflamm 2019, 2019, 8328490, doi:10.1155/2019/8328490.

68. Rathinam, V.A.K.; Zhao, Y.; Shao, F. Innate immunity to intracellular LPS. Nature Immunology 2019, 20, 527-533, doi:10.1038/s41590-019-0368-3.

69. Munford, R.S. Sensing gram-negative bacterial lipopolysaccharides: a human disease determinant? Infection and immunity 2008, 76, 454-465, doi:10.1128/IAI.00939-07.

70. Jackie, J.; Lau, W.K.; Feng, H.-T.; Li, S.F.Y. Detection of Endotoxins: From Inferring the Responses of Biological Hosts to the Direct Chemical Analysis of Lipopolysaccharides. Critical Reviews in Analytical Chemistry 2019, 49, 126-137, doi:10.1080/10408347.2018.1479958.

71. Walsh, M.C.; Lee, J.; Choi, Y. Tumor necrosis factor receptor- associated factor 6 (TRAF6) regulation of development, function, and homeostasis of the immune system. Immunological reviews 2015, 266, 72-92, doi:10.1111/imr.12302.

72. Fang, J.; Muto, T.; Kleppe, M.; Bolanos, L.C.; Hueneman, K.M.; Walker, C.S.; Sampson, L.; Wellendorf, A.M.; Chetal, K.; Choi, K., et al. TRAF6 Mediates Basal Activation of NF-κB Necessary for Hematopoietic Stem Cell Homeostasis. Cell Reports 2018, 22, 1250-1262, doi:https://doi.org/10.1016/j.celrep.2018.01.013.
73. Lawrence, T. The nuclear factor NF-κB pathway in inflammation. Cold Spring Harb Perspect Biol 2009, 1, a001651, doi:10.1101/cshperspect.a001651.
74. Tornatore, L.; Thotakura, A.K.; Bennett, J.; Moretti, M.; Franzoso, G. The nuclear factor kappa B signaling pathway: integrating metabolism with inflammation. Trends Cell Biol 2012, 22, 557-566, doi:10.1016/j.tcb.2012.08.001.
75. Gupta, S.C.; Sundaram, C.; Reuter, S.; Aggarwal, B.B. Inhibiting NF-κB activation by small molecules as a therapeutic strategy. Biochim Biophys Acta 2010, 1799, 775-787, doi:10.1016/j.bbagrm.2010.05.004.
76. MacDonald, B.T.; He, X. Frizzled and LRP5/6 receptors for Wnt/β-catenin signaling. Cold Spring Harbor perspectives in biology 4, a007880, doi:10.1101/cshperspect.a007880.
77. Stamos, J.L.; Weis, W.I. The β-catenin destruction complex. Cold Spring Harbor perspectives in biology 2013, 5, a007898.
78. Kisoh, K.; Hayashi, H.; Itoh, T.; Asada, M.; Arai, M.; Yuan, B.; Tanonaka, K.; Takagi, N. Involvement of GSK-3β Phosphorylation Through PI3-K/Akt in Cerebral Ischemia-Induced Neurogenesis in Rats. Molecular Neurobiology 2017, 54, 7917-7927, doi:10.1007/s12035-016-0290-8.
79. Deng, J.; Miller, S.A.; Wang, H.-Y.; Xia, W.; Wen, Y.; Zhou, B.P.; Li, Y.; Lin, S.-Y.; Hung, M.-C. β-Catenin interacts with and inhibits NF-κB in human colon and breast cancer. Cancer Cell 2002, 2, 323-334, doi:https://doi.org/10.1016/S1535-6108(02)00154-X.

80. Ma, B.; Hottiger, M.O. Crosstalk between Wnt/β-catenin and NF-κB signaling pathway during inflammation. Front Immunol 2016, 7, 378, doi:10.3389/fimmu.2016.00378.

81. Kumar, S.; Pandey, A.K. Chemistry and Biological Activities of Flavonoids: An Overview. The Scientific World Journal 2013, 2013, 16, doi:10.1155/2013/162750.

82. Khan, N.; Syed, D.N.; Ahmad, N.; Mukhtar, H. Fisetin: A Dietary Antioxidant for Health Promotion. Antioxidants & Redox Signaling 2013, 19, 151-162, doi:10.1089/ars.2012.4901.

83. Sahu, B.D.; Kumar, J.M.; Sistla, R. Fisetin, a dietary flavonoid, ameliorates experimental colitis in mice: Relevance of NF-κB signaling. J Nutr Biochem 2016, 28, 171-182, doi:10.1016/j.jnutbio.2015.10.004.

84. Huang, W.; Li, M.L.; Xia, M.Y.; Shao, J.Y. Fisetin-treatment alleviates airway inflammation through inhbition of MyD88/NF-κB signaling pathway. Int J Mol Med 2018, 42, 208-218, doi:10.3892/ijmm.2018.3582.

85. Molagoda, I.M.N.; Karunarathne, W.; Park, S.R.; Choi, Y.H.; Park, E.K.; Jin, C.Y.; Yu, H.; Jo, W.S.; Lee, K.T.; Kim, G.Y. GSK-3β-targeting fisetin promotes melanogenesis in B16F10 melanoma cells and zebrafish larvae through β-catenin activation. Int J Mol Sci 2020, 21, doi:10.3390/ijms21010312.

86. Molagoda, I.M.N.; Choi, Y.H.; Jin, C.Y.; Lee, S.; Kim, G.Y. Deoxynivalenol increases the expression of pro-inflammatory genes and mediators accompanied by NF-κB activation. Lat. Am. J. Pharm. 2019, 38, 388-395.

87. Liu, X.; Chang, X.; Wu, H.; Xiao, J.; Gao, Y.; Zhang, Y. Role of intestinal inflammation in predisposition of Edwardsiella tarda infection in zebrafish (Danio rerio). Fish Shellfish Immunol 2014, 41, 271-278, doi:10.1016/j.fsi.2014.09.009.

88. Handeli, S.; Simon, J.A. A small-molecule inhibitor of Tcf/β-catenin signaling down-regulates PPARγ and PPARδ activities. Molecular Cancer Therapeutics 2008, 7, 521-529, doi:10.1158/1535-7163.mct-07-2063.
89. Werdan, K.; Hettwer, S.; Bubel, S.; Oelke, A.; Hoke, R.S.; Wimmer, R.; Ebelt, H.; Muller-Werdan, U. Septic circulatory shock and septic cardiomyopathy. Internist (Berl) 2009, 50, 799-800, 802-796, 808-799, doi:10.1007/s00108-008-2286-6.
90. Goldstein, J.L.; Cryer, B. Gastrointestinal injury associated with NSAID use: a case study and review of risk factors and preventative strategies. Drug Healthc Patient Saf 2015, 7, 31-41, doi:10.2147/DHPS.S71976.
91. Ali, S.; Singh, N.N.; Yildirim, H.; Ramji, D.P. Requirement for nuclear factor kappa B signalling in the interleukin-1-induced expression of the CCAAT/enhancer binding protein-delta gene in hepatocytes. The international journal of biochemistry & cell biology 2010, 42, 113-119, doi:10.1016/j.biocel.2009.09.018.
92. Kishimoto, T.; Tanaka, T. Interleukin 6. Encyclopedia of Inflammatory Diseases 2015, 1-8.
93. Zheng, H.; Ban, Y.; Wei, F.; Ma, X. Regulation of Interleukin-12 Production in Antigen-Presenting Cells. In Regulation of Cytokine Gene Expression in Immunity and Diseases, Ma, X., Ed. Springer Netherlands: Dordrecht, 2016; 10.1007/978-94-024-0921-5_6pp. 117-138.
94. Hop, H.T.; Reyes, A.W.B.; Huy, T.X.N.; Arayan, L.T.; Min, W.; Lee, H.J.; Rhee, M.H.; Chang, H.H.; Kim, S. Activation of NF-κB-mediated TNF-induced antimicrobial immunity is required for the efficient Brucella abortus clearance in RAW 264.7 cells. Frontiers in Cellular and Infection Microbiology 2017, 7, doi:10.3389/fcimb.2017.00437.

95. Vila-del Sol, V.; Fresno, M. Involvement of TNF and NF-κB in the Transcriptional Control of Cyclooxygenase-2 Expression by IFN-γ in Macrophages. The Journal of Immunology 2005, 174, 2825, doi:10.4049/jimmunol.174.5.2825.
96. Goh, F.Y.; Upton, N.; Guan, S.; Cheng, C.; Shanmugam, M.K.; Sethi, G.; Leung, B.P.; Wong, W.S. Fisetin, a bioactive flavonol, attenuates allergic airway inflammation through negative regulation of NF-κB. Eur J Pharmacol 2012, 679, 109-116, doi:10.1016/j.ejphar.2012.01.002.
97. Shi, Y.S.; Li, C.B.; Li, X.Y.; Wu, J.; Li, Y.; Fu, X.; Zhang, Y.; Hu, W.Z. Fisetin attenuates metabolic dysfunction in mice challenged with a high-fructose diet. J Agric Food Chem 2018, 66, 8291-8298, doi:10.1021/acs.jafc.8b02140.
98. Wu, P.Y.; Lyu, J.L.; Liu, Y.J.; Chien, T.Y.; Hsu, H.C.; Wen, K.C.; Chiang, H.M. Fisetin regulates Nrf2 expression and the inflammation-related signaling pathway to prevent UVB-induced skin damage in hairless mice. Int J Mol Sci 2017, 18, doi:10.3390/ijms18102118.
99. Garg, S.; Malhotra, R.K.; Khan, S.I.; Sarkar, S.; Susrutha, P.N.; Singh, V.; Goyal, S.; Nag, T.C.; Ray, R.; Bhatia, J., et al. Fisetin attenuates isoproterenol-induced cardiac ischemic injury in vivo by suppressing RAGE/NF-κB mediated oxidative stress, apoptosis and inflammation. Phytomedicine 2019, 56, 147-155, doi:10.1016/j.phymed.2018.09.187.
100. Singh, S.; Singh, A.K.; Garg, G.; Rizvi, S.I. Fisetin as a caloric restriction mimetic protects rat brain against aging induced oxidative stress, apoptosis and neurodegeneration. Life Sci 2018, 193, 171-179, doi:10.1016/j.lfs.2017.11.004.
101. Liu, S.H.; Lin, C.H.; Hung, S.K.; Chou, J.H.; Chi, C.W.; Fu, S.L. Fisetin inhibits lipopolysaccharide-induced macrophage activation and dendritic cell maturation. Journal of agricultural and food chemistry 2010, 58, 10831-10839, doi:10.1021/jf1017093.

102. Feng, G.; Jiang, Z.Y.; Sun, B.; Fu, J.; Li, T.Z. Fisetin Alleviates Lipopolysaccharide-Induced Acute Lung Injury via TLR4-Mediated NF-κB Signaling Pathway in Rats. Inflammation 2016, 39, 148-157, doi:10.1007/s10753-015-0233-y.
103. Shi, M.; Zeng, X.; Guo, F.; Huang, R.; Feng, Y.; Ma, L.; Zhou, L.; Fu, P. Anti-Inflammatory Pyranochalcone Derivative Attenuates LPS-Induced Acute Kidney Injury via Inhibiting TLR4/NF-κB Pathway. Molecules (Basel, Switzerland) 2017, 22, doi:10.3390/molecules22101683.
104. Vallee, A.; Lecarpentier, Y.; Vallee, J.N. Targeting the canonical WNT/β-catenin pathway in cancer treatment using non-steroidal anti-inflammatory drugs. Cells 2019, 8, doi:10.3390/cells8070726.
105. Vallee, A.; Lecarpentier, Y. Crosstalk between peroxisome proliferator-activated receptor gamma and the canonical WNT/β-catenin pathway in chronic inflammation and oxidative stress during carcinogenesis. Front Immunol 2018, 9, 745, doi:10.3389/fimmu.2018.00745.
106. Swafford, D.; Shanmugam, A.; Ranganathan, P.; Hussein, M.S.; Koni, P.A.; Prasad, P.D.; Thangaraju, M.; Manicassamy, S. Canonical Wnt signaling in CD11c+ APCs regulates microbiota-induced inflammation and immune cell homeostasis in the colon. J Immunol 2018, 200, 3259-3268, doi:10.4049/jimmunol.1701086.
107. Sun, J.; Hobert, M.E.; Duan, Y.; Rao, A.S.; He, T.-C.; Chang, E.B.; Madara, J.L. Crosstalk between NF-κB and β-catenin pathways in bacterial-colonized intestinal epithelial cells. American Journal of Physiology-Gastrointestinal and Liver Physiology 2005, 289, G129-G137, doi:10.1152/ajpgi.00515.2004.
108. Beurel, E.; Grieco, S.F.; Jope, R.S. Glycogen synthase kinase-3 (GSK3): regulation, actions, and diseases. Pharmacol Ther 2015, 148, 114-131, doi:10.1016/j.pharmthera.2014.11.016.

109. Medunjanin, S.; Schleithoff, L.; Fiegehenn, C.; Weinert, S.; Zuschratter, W.; Braun-Dullaeus, R.C. GSK-3β controls NF-κB activity via IKKγ/NEMO. Sci Rep 2016, 6, 38553, doi:10.1038/srep38553.

110. Ougolkov, A.V.; Fernandez-Zapico, M.E.; Savoy, D.N.; Urrutia, R.A.; Billadeau, D.D. Glycogen Synthase Kinase-3β Participates in Nuclear Factor κB–Mediated Gene Transcription and Cell Survival in Pancreatic Cancer Cells. Cancer Research 2005, 65, 2076-2081, doi:10.1158/0008-5472.can-04-3642.

111. Cortes-Vieyra, R.; Bravo-Patino, A.; Valdez-Alarcon, J.J.; Juarez, M.C.; Finlay, B.B.; Baizabal-Aguirre, V.M. Role of glycogen synthase kinase-3β in the inflammatory response caused by bacterial pathogens. J Inflamm (Lond) 2012, 9, 23, doi:10.1186/1476-9255-9-23.

112. Allan, S.M., Tyrrell, P.J., Rothwell, N.J., 2005. Interleukin-1 and neuronal injury. Nature Reviews Immunology 5, 629-640.

113. Bauernfeind, F., Ablasser, A., Bartok, E., Kim, S., Schmid-Burgk, J., Cavlar, T., Hornung, V., 2011. Inflammasomes: current understanding and open questions. Cellular and molecular life sciences : CMLS 68, 765-783.

114. Berridge, M.V., Herst, P.M., Tan, A.S., 2005. Tetrazolium dyes as tools in cell biology: new insights into their cellular reduction. Biotechnol Annu Rev 11, 127-152.

115. Block, M.L., Hong, J.-S., 2005. Microglia and inflammation-mediated neurodegeneration: multiple triggers with a common mechanism. Progress in neurobiology 76, 77-98.

116. Cappellano, G., Carecchio, M., Fleetwood, T., Magistrelli, L., Cantello, R., Dianzani, U., Comi, C., 2013. Immunity and inflammation in neurodegenerative diseases. Am J Neurodegener Dis 2, 89-107.

117. Chen, K., Feng, L., Hu, W., Chen, J., Wang, X., Wang, L., He, Y., 2019. Optineurin inhibits NLRP3 inflammasome activation by enhancing mitophagy of renal tubular cells in diabetic nephropathy. The FASEB Journal 33, 4571-4585.

118. Das, A., Kim, S.H., Arifuzzaman, S., Yoon, T., Chai, J.C., Lee, Y.S., Park, K.S., Jung, K.H., Chai, Y.G., 2016. Transcriptome sequencing reveals that LPS-triggered transcriptional responses in established microglia BV2 cell lines are poorly representative of primary microglia. Journal of Neuroinflammation 13, 182.

119. de Zoete, M.R., Palm, N.W., Zhu, S., Flavell, R.A., 2014. Inflammasomes. Cold Spring Harbor perspectives in biology 6, a016287.

120. Feng, G., Jiang, Z.-y., Sun, B., Fu, J., Li, T.-z., 2016. Fisetin Alleviates Lipopolysaccharide-Induced Acute Lung Injury via TLR4-Mediated NF-κB Signaling Pathway in Rats. Inflammation 39, 148-157.

121. Guo, W., Sun, Y., Liu, W., Wu, X., Guo, L., Cai, P., Wu, X., Wu, X., Shen, Y., Shu, Y., Gu, Y., Xu, Q., 2014. Small molecule-driven mitophagy-mediated NLRP3 inflammasome inhibition is responsible for the prevention of colitis-associated cancer. Autophagy 10, 972-985.

122. Hamilton, C., Anand, P.K., 2019. Right place, right time: localisation and assembly of the NLRP3 inflammasome. F1000Res 8, F1000 Faculty Rev-1676.

123. Hanamsagar, R., Torres, V., Kielian, T., 2011. Inflammasome activation and IL-1β/IL-18 processing are influenced by distinct pathways in microglia. Journal of neurochemistry 119, 736-748.

124. Hanneken, A., Lin, F.F., Maher, P., 2005. Flavonoids Protect Human Retinal Pigment Epithelial Cells From Oxidative Stress–Induced Death. Investigative Ophthalmology & Visual Science 46, 1634-1634.

125. Heid, M.E., Keyel, P.A., Kamga, C., Shiva, S., Watkins, S.C., Salter, R.D., 2013. Mitochondrial Reactive Oxygen Species Induces NLRP3-Dependent Lysosomal Damage and Inflammasome Activation. The Journal of Immunology 191, 5230-5238.

126. Henn, A., Lund, S., Hedtjärn, M., Schrattenholz, A., Pörzgen, P., Leist, M., 2009. The suitability of BV2 cells as alternative model system for primary microglia cultures or for animal experiments examining brain inflammation. Altex 26, 83-94.

127. Karunarathne, W., Lee, K.T., Choi, Y.H., Jin, C.Y., Kim, G.Y., 2020. Anthocyanins isolated from Hibiscus syriacus L. attenuate lipopolysaccharide-induced inflammation and endotoxic shock by inhibiting the TLR4/MD2-mediated NF-kB signaling pathway. Phytomedicine 76, 153237.

128. Kelley, N., Jeltema, D., Duan, Y., He, Y., 2019. The NLRP3 Inflammasome: An Overview of Mechanisms of Activation and Regulation. Int J Mol Sci 20, 3328.

129. Kicinska, A., Jarmuszkiewicz, W., 2020. Flavonoids and Mitochondria: Activation of Cytoprotective Pathways? Molecules 25, 3060.

130. Kim, S.-C., Kang, S.-H., Jeong, S.-J., Kim, S.-H., Ko, H.S., Kim, S.-H., 2012. Inhibition of c-Jun N-terminal kinase and nuclear factor κ B pathways mediates fisetin-exerted anti-inflammatory activity in lipopolysccharide-treated RAW264. 7 cells. Immunopharmacology and immunotoxicology 34, 645-650.

131. Ko, J.H., Yoon, S.-O., Lee, H.J., Oh, J.Y., 2017. Rapamycin regulates macrophage activation by inhibiting NLRP3 inflammasome-p38 MAPK-NFκB pathways in autophagy- and p62-dependent manners. Oncotarget 8, 40817-40831.

132. Komatsu, M., Waguri, S., Koike, M., Sou, Y.-s., Ueno, T., Hara, T., Mizushima, N., Iwata, J.-i., Ezaki, J., Murata, S., Hamazaki, J., Nishito, Y., Iemura, S.-i., Natsume, T., Yanagawa, T., Uwayama, J., Warabi, E., Yoshida, H., Ishii, T., Kobayashi, A., Yamamoto, M., Yue, Z., Uchiyama, Y., Kominami, E., Tanaka, K., 2007. Homeostatic Levels of p62 Control Cytoplasmic Inclusion Body Formation in Autophagy-Deficient Mice. Cell 131, 1149-1163.

133. Korin, B., Ben-Shaanan, T.L., Schiller, M., Dubovik, T., Azulay-Debby, H., Boshnak, N.T., Koren, T., Rolls, A., 2017. High-dimensional, single-cell characterization of the brain's immune compartment. Nature Neuroscience 20, 1300-1309.

134. Kuzmich, N.N., Sivak, K.V., Chubarev, V.N., Porozov, Y.B., Savateeva-Lyubimova, T.N., Peri, F., 2017. TLR4 signaling pathway modulators as potential therapeutics in inflammation and sepsis. Vaccines 5, 34.

135. Li, X., Fang, P., Mai, J., Choi, E.T., Wang, H., Yang, X.-f., 2013. Targeting mitochondrial reactive oxygen species as novel therapy for inflammatory diseases and cancers. J Hematol Oncol 6, 19-19.

136. Lima, C.X., Souza, D.G., Amaral, F.A., Fagundes, C.T., Rodrigues, I.P.S., Alves-Filho, J.C., Kosco-Vilbois, M., Ferlin, W., Shang, L., Elson, G., Teixeira, M.M., 2015. Therapeutic Effects of Treatment with Anti-TLR2 and Anti-TLR4 Monoclonal Antibodies in Polymicrobial Sepsis. PLOS ONE 10, e0132336.

137. Liu, X., Chang, X., Wu, H., Xiao, J., Gao, Y., Zhang, Y., 2014. Role of intestinal inflammation in predisposition of Edwardsiella tarda infection in zebrafish (Danio rerio). Fish Shellfish Immunol 41, 271-278.

138. Maeshima, N., Fernandez, R., 2013. Recognition of lipid A variants by the TLR4-MD-2 receptor complex. Frontiers in Cellular and Infection Microbiology 3.

139. Molagoda, I.M.N., Karunarathne, W.A.H.M., Park, S.R., Choi, Y.H., Park, E.K., Jin, C.-Y., Yu, H., Jo, W.S., Lee, K.T., Kim, G.-Y., 2020. GSK-3β-Targeting Fisetin Promotes Melanogenesis in B16F10 Melanoma Cells and Zebrafish Larvae through β-Catenin Activation. Int J Mol Sci 21, 312.

140. Molagoda, I.M.N., Lee, S., Jayasooriya, R., Jin, C.Y., Choi, Y.H., Kim, G.Y., 2019. Deoxynivalenol enhances IL-1b expression in BV2 microglial cells through activation of the NF-kB pathway and the ASC/NLRP3 inflammasome. EXCLI J 18, 356-369.

141. Nakahira, K., Haspel, J.A., Rathinam, V.A., Lee, S.J., Dolinay, T., Lam, H.C., Englert, J.A., Rabinovitch, M., Cernadas, M., Kim, H.P., Fitzgerald, K.A., Ryter, S.W., Choi, A.M., 2011. Autophagy proteins regulate innate immune responses by inhibiting the release of mitochondrial DNA mediated by the NALP3 inflammasome. Nat Immunol 12, 222-230.

142. Percie du Sert, N., Ahluwalia, A., Alam, S., Avey, M.T., Baker, M., Browne, W.J., Clark, A., Cuthill, I.C., Dirnagl, U., Emerson, M., Garner, P., Holgate, S.T., Howells, D.W., Hurst, V., Karp, N.A., Lazic, S.E., Lidster, K., MacCallum, C.J., Macleod, M., Pearl, E.J., Petersen, O.H., Rawle, F., Reynolds, P., Rooney, K., Sena, E.S., Silberberg, S.D., Steckler, T., Wurbel, H., 2020. Reporting animal research: Explanation and elaboration for the ARRIVE guidelines 2.0. PLoS Biol 18, e3000411.

143. Rodius, S., de Klein, N., Jeanty, C., Sánchez-Iranzo, H., Crespo, I., Ibberson, M., Xenarios, I., Dittmar, G., Mercader, N., Niclou, S.P., Azuaje, F., 2020. Fisetin protects against cardiac cell death through reduction of ROS production and caspases activity. Scientific Reports 10, 2896.

144. Sakai, E., Shimada-Sugawara, M., Yamaguchi, Y., Sakamoto, H., Fumimoto, R., Fukuma, Y., Nishishita, K., Okamoto, K., Tsukuba, T., 2013. Fisetin inhibits osteoclastogenesis through prevention of RANKL-induced ROS production by Nrf2-mediated up-regulation of phase II antioxidant enzymes. Journal of pharmacological sciences 121, 288-298.

145. Stansley, B., Post, J., Hensley, K., 2012. A comparative review of cell culture systems for the study of microglial biology in Alzheimer's disease. Journal of neuroinflammation 9, 115.

146. Suh, Y., Afaq, F., Khan, N., Johnson, J.J., Khusro, F.H., Mukhtar, H., 2010. Fisetin induces autophagic cell death through suppression of mTOR signaling pathway in prostate cancer cells. Carcinogenesis 31, 1424-1433.

147. Tschopp, J., Schroder, K., 2010. NLRP3 inflammasome activation: The convergence of multiple signalling pathways on ROS production? Nature Reviews Immunology 10, 210-215.

148. Vernucci, E., Tomino, C., Molinari, F., Limongi, D., Aventaggiato, M., Sansone, L., Tafani, M., Russo, M.A., 2019. Mitophagy and Oxidative Stress in Cancer and Aging: Focus on Sirtuins and Nanomaterials. Oxid Med Cell Longev 2019, 6387357-6387357.

149. Yang, Y., Wang, H., Kouadir, M., Song, H., Shi, F., 2019. Recent advances in the mechanisms of NLRP3 inflammasome activation and its inhibitors. Cell Death & Disease 10, 128.

150. Yu, J., Nagasu, H., Murakami, T., Hoang, H., Broderick, L., Hoffman, H.M., Horng, T., 2014. Inflammasome activation leads to Caspase-1–dependent mitochondrial damage and block of mitophagy. Proceedings of the National Academy of Sciences 111, 15514-15519.

151. Zhang, J., 2015. Teaching the basics of autophagy and mitophagy to redox biologists—Mechanisms and experimental approaches. Redox Biology 4, 242-259.

152. Zhong, Z., Umemura, A., Sanchez-Lopez, E., Liang, S., Shalapour, S., Wong, J., He, F., Boassa, D., Perkins, G., Ali, S.R., McGeough, M.D., Ellisman, M.H., Seki, E., Gustafsson, A.B., Hoffman, H.M., Diaz-Meco, M.T., Moscat, J., Karin, M., 2016. NF-κB Restricts Inflammasome Activation via Elimination of Damaged Mitochondria. Cell 164, 896-910.

153. Akkawi, I., Zmerly, H., 2018. Osteoporosis: Current concepts. Joints 6, 122-127.

154. An, J., Yang, H., Zhang, Q., Liu, C., Zhao, J., Zhang, L., Chen, B., 2016. Natural products for treatment of osteoporosis: The effects and mechanisms on promoting osteoblast-mediated bone formation. Life Sci 147, 46-58.

155. Becker, D.E., 2013. Basic and clinical pharmacology of glucocorticosteroids. Anesth Prog 60, 25-31; quiz 32.

156. Bertacchini, J., Magaro, M.S., Poti, F., Palumbo, C., 2018. Osteocytes specific GSK3 inhibition affects in vitro osteogenic differentiation. Biomedicines 6.

157. Buckland, J., 2015. Anabolic Wnt/β-catenin signalling: osteocytes are key. Nature Reviews Rheumatology 11, 128-128.

158. Charles, J.F., Coury, F., Sulyanto, R., Sitara, D., Wu, J., Brady, N., Tsang, K., Sigrist, K., Tollefsen, D.M., He, L., Storm, D., Aliprantis, A.O., 2012. The collection of NFATc1-dependent transcripts in the osteoclast includes numerous genes non-essential to physiologic bone resorption. Bone 51, 902-912.

159. Chen, J.R., Lai, Y.H., Tsai, J.J., Hsiao, C.D., 2017. Live fluorescent staining platform for drug-screening and mechanism-analysis in zebrafish for bone mineralization. Molecules 22.

160. Chen, X., Wang, Z., Duan, N., Zhu, G., Schwarz, E.M., Xie, C., 2018. Osteoblast-osteoclast interactions. Connect Tissue Res 59, 99-107.

161. Choi, S.W., Son, Y.J., Yun, J.M., Kim, S.H., 2012. Fisetin inhibits osteoclast differentiation via downregulation of p38 and c-Fos-NFATc1 signaling pathways. Evid Based Complement Alternat Med 2012, 810563.

162. Feng, X., McDonald, J.M., 2011. Disorders of bone remodeling. Annu Rev Pathol 6, 121-145.

163. Galindo, M., Pratap, J., Young, D.W., Hovhannisyan, H., Im, H.J., Choi, J.Y., Lian, J.B., Stein, J.L., Stein, G.S., van Wijnen, A.J., 2005. The bone-specific expression of Runx2 oscillates during the cell cycle to support a G1-related antiproliferative function in osteoblasts. J Biol Chem 280, 20274-20285.

164. Guido, G., Scaglione, M., Fabbri, L., Ceglia, M.J., 2009. The "osteoporosis disease". Clin Cases Miner Bone Metab 6, 114-116.

165. Hernlund, E., Svedbom, A., Ivergard, M., Compston, J., Cooper, C., Stenmark, J., McCloskey, E.V., Jonsson, B., Kanis, J.A., 2013. Osteoporosis in the European Union: medical management, epidemiology and economic burden. A report prepared in collaboration with the International Osteoporosis Foundation (IOF) and the European Federation of Pharmaceutical Industry Associations (EFPIA). Arch Osteoporos 8, 136.

166. Humphrey, E.L., Williams, J.H., Davie, M.W., Marshall, M.J., 2006. Effects of dissociated glucocorticoids on OPG and RANKL in osteoblastic cells. Bone 38, 652-661.

167. Kashyap, D., Garg, V.K., Tuli, H.S., Yerer, M.B., Sak, K., Sharma, A.K., Kumar, M., Aggarwal, V., Sandhu, S.S., 2019. Fisetin and quercetin: Promising flavonoids with chemopreventive potential. Biomolecules 9.

168. Kassem, M., Marie, P.J., 2011. Senescence-associated intrinsic mechanisms of osteoblast dysfunctions. Aging Cell 10, 191-197.

169. Katsimbri, P., 2017. The biology of normal bone remodelling. Eur J Cancer Care (Engl) 26.

170. Khan, N., Syed, D.N., Ahmad, N., Mukhtar, H., 2013. Fisetin: a dietary antioxidant for health promotion. Antioxid Redox Signal 19, 151-162.

171. Kim, J.H., Kim, M.Y., Kim, J.H., Cho, J.Y., 2015. Fisetin suppresses macrophage-mediated inflammatory responses by blockade of Src and Syk. Biomol Ther (Seoul) 23, 414-420.

172. Kim, J.H., Kim, N., 2014. Regulation of NFATc1 in osteoclast differentiation. J Bone Metab 21, 233-241.

173. Kitamura, K., Takahira, K., Inari, M., Satoh, Y., Hayakawa, K., Tabuchi, Y., Ogai, K., Nishiuchi, T., Kondo, T., Mikuni-Takagaki, Y., Chen, W., Hattori, A., Suzuki, N., 2013. Zebrafish scales respond differently to in vitro dynamic and static acceleration: analysis of interaction between osteoblasts and osteoclasts. Comp Biochem Physiol A Mol Integr Physiol 166, 74-80.

174. Komori, T., 2019. Regulation of proliferation, differentiation and functions of osteoblasts by Runx2. Int J Mol Sci 20.

175. Leotoing, L., Davicco, M.J., Lebecque, P., Wittrant, Y., Coxam, V., 2014. The flavonoid fisetin promotes osteoblasts differentiation through Runx2 transcriptional activity. Mol Nutr Food Res 58, 1239-1248.

176. MacDonald, B.T., Tamai, K., He, X., 2009. Wnt/beta-catenin signaling: components, mechanisms, and diseases. Developmental cell 17, 9-26.

177. Molagoda, I.M.N., Karunarathne, W., Choi, Y.H., Park, E.K., Jeon, Y.J., Lee, B.J., Kang, C.H., Kim, G.Y., 2019. Fermented oyster extract promotes osteoblast differentiation by activating the Wnt/b-catenin signaling pathway, leading to bone formation. Biomolecules 9.

178. Molagoda, I.M.N., Karunarathne, W., Park, S.R., Choi, Y.H., Park, E.K., Jin, C.Y., Yu, H., Jo, W.S., Lee, K.T., Kim, G.Y., 2020. GSK-3b-targeting fisetin promotes melanogenesis in B16F10 melanoma cells and zebrafish larvae through b-catenin activation. Int J Mol Sci 21.

179. Nishimura, J., Ikuyama, S., 2000. Glucocorticoid-induced osteoporosis: pathogenesis and management. J Bone Miner Metab 18, 350-352.

180. Ono, T., Hayashi, M., Sasaki, F., Nakashima, T., 2020. RANKL biology: bone metabolism, the immune system, and beyond. Inflamm Regen 40, 2.

181. Phimphilai, M., Zhao, Z., Boules, H., Roca, H., Franceschi, R.T., 2006. BMP signaling is required for RUNX2-dependent induction of the osteoblast phenotype. J Bone Miner Res 21, 637-646.

182. Premaor, M.O., Pilbrow, L., Tonkin, C., Parker, R.A., Compston, J., 2010. Obesity and fractures in postmenopausal women. J Bone Miner Res 25, 292-297.

183. Qin, Y., Wang, L., Gao, Z., Chen, G., Zhang, C., 2016. Bone marrow stromal/stem cell-derived extracellular vesicles regulate osteoblast activity and differentiation in vitro and promote bone regeneration in vivo. Sci Rep 6, 21961.

184. Sitara, D., Aliprantis, A.O., 2010. Transcriptional regulation of bone and joint remodeling by NFAT. Immunological reviews 233, 286-300.

185. Syed, D.N., Adhami, V.M., Khan, N., Khan, M.I., Mukhtar, H., 2016. Exploring the molecular targets of dietary flavonoid fisetin in cancer. Semin Cancer Biol 40-41, 130-140.

186. Takayanagi, H., Kim, S., Koga, T., Nishina, H., Isshiki, M., Yoshida, H., Saiura, A., Isobe, M., Yokochi, T., Inoue, J., Wagner, E.F., Mak, T.W., Kodama, T., Taniguchi, T., 2002. Induction and activation of the transcription factor NFATc1 (NFAT2) integrate RANKL signaling in terminal differentiation of osteoclasts. Dev Cell 3, 889-901.

187. Tobeiha, M., Moghadasian, M.H., Amin, N., Jafarnejad, S., 2020. RANKL/RANK/OPG Pathway: A mechanism involved in exercise-induced bone remodeling. Biomed Res Int 2020, 6910312.

188. Wada, T., Nakashima, T., Hiroshi, N., Penninger, J.M., 2006. RANKL-RANK signaling in osteoclastogenesis and bone disease. Trends Mol Med 12, 17-25.

189. Zhang, H., Recker, R., Lee, W.N., Xiao, G.G., 2010. Proteomics in bone research. Expert Rev Proteomics 7, 103-111.

190. Adams, C.J., Kopp, M.C., Larburu, N., Nowak, P.R., Ali, M.M.U., 2019. Structure and Molecular Mechanism of ER Stress Signaling by the Unfolded Protein Response Signal Activator IRE1. Frontiers in Molecular Biosciences 6.

191. Boo, Y.C., 2019. Can Plant Phenolic Compounds Protect the Skin from Airborne Particulate Matter? Antioxidants (Basel) 8.

192. Cho, C.-C., Hsieh, W.-Y., Tsai, C.-H., Chen, C.-Y., Chang, H.-F., Lin, C.-S., 2018. In Vitro and In Vivo Experimental Studies of PM(2.5) on Disease Progression. International journal of environmental research and public health 15, 1380.

193. Du, Y., Xu, X., Chu, M., Guo, Y., Wang, J., 2016. Air particulate matter and cardiovascular disease: the epidemiological, biomedical and clinical evidence. Journal of thoracic disease 8, E8-E19.

194. Farrukh, M.R., Nissar, U.A., Afnan, Q., Rafiq, R.A., Sharma, L., Amin, S., Kaiser, P., Sharma, P.R., Tasduq, S.A., 2014. Oxidative stress mediated Ca(2+) release manifests endoplasmic reticulum stress leading to unfolded protein response in UV-B irradiated human skin cells. J Dermatol Sci 75, 24-35.

195. Harding, H.P., Zhang, Y., Ron, D., 1999. Protein translation and folding are coupled by an endoplasmic-reticulum-resident kinase. Nature 397, 271-274.

196. Jia, S., Xu, X., Zhou, S., Chen, Y., Ding, G., Cao, L., 2019. Fisetin induces autophagy in pancreatic cancer cells via endoplasmic reticulum stress- and mitochondrial stress-dependent pathways. Cell Death & Disease 10, 142.

197. Khan, N., Syed, D.N., Ahmad, N., Mukhtar, H., 2013. Fisetin: a dietary antioxidant for health promotion. Antioxidants & redox signaling 19, 151-162.

198. Kim, J.H., Kim, M.-Y., Kim, J.-H., Cho, J.Y., 2015. Fisetin Suppresses Macrophage-Mediated Inflammatory Responses by Blockade of Src and Syk. Biomolecules & Therapeutics 23, 414-420.

199. Kim, J.H., Son, J.W., Kim, J., Kim, M.G., Jeong, S.H., Park, T.J., Son, S.W., Ryu, H.J., 2020. Particulate matter (PM)2.5 affects keratinocytes via endoplasmic reticulum (ER) stress-mediated suppression of apoptosis. Molecular & Cellular Toxicology 16, 129-137.

200. Komatsu, M., Waguri, S., Koike, M., Sou, Y.-s., Ueno, T., Hara, T., Mizushima, N., Iwata, J.-i., Ezaki, J., Murata, S., Hamazaki, J., Nishito, Y., Iemura, S.-i., Natsume, T., Yanagawa, T., Uwayama, J., Warabi, E., Yoshida, H., Ishii, T., Kobayashi, A., Yamamoto, M., Yue, Z., Uchiyama, Y., Kominami, E., Tanaka, K., 2007. Homeostatic Levels of p62 Control Cytoplasmic Inclusion Body Formation in Autophagy-Deficient Mice. Cell 131, 1149-1163.

201. Li, Q., Kang, Z., Jiang, S., Zhao, J., Yan, S., Xu, F., Xu, J., 2017. Effects of Ambient Fine Particles PM2.5 on Human HaCaT Cells. Int J Environ Res Public Health 14.

202. Liao, Z., Nie, J., Sun, P., 2020. The impact of particulate matter (PM2.5) on skin barrier revealed by transcriptome analysis: Focusing on cholesterol metabolism. Toxicol Rep 7, 1-9.

203. Lin, J.H., Walter, P., Yen, T.S.B., 2008. Endoplasmic reticulum stress in disease pathogenesis. Annual review of pathology 3, 399-425.

204. Marshall, J., 2013. PM 2.5. Proceedings of the National Academy of Sciences 110, 8756-8756.

205. Naeimi, A.F., Alizadeh, M., 2017. Antioxidant properties of the flavonoid fisetin: An updated review of in vivo and in vitro studies. Trends in Food Science & Technology 70, 34-44.

206. Pakos-Zebrucka, K., Koryga, I., Mnich, K., Ljujic, M., Samali, A., Gorman, A.M., 2016. The integrated stress response. EMBO reports 17, 1374-1395.

207. Piao, M.J., Ahn, M.J., Kang, K.A., Ryu, Y.S., Hyun, Y.J., Shilnikova, K., Zhen, A.X., Jeong, J.W., Choi, Y.H., Kang, H.K., Koh, Y.S., Hyun, J.W., 2018. Particulate matter 2.5 damages skin cells by inducing oxidative stress, subcellular organelle dysfunction, and apoptosis. Archives of Toxicology 92, 2077-2091.

208. Pihán, P., Carreras-Sureda, A., Hetz, C., 2017. BCL-2 family: integrating stress responses at the ER to control cell demise. Cell Death & Differentiation 24, 1478-1487.

209. Ryu, Y.S., Kang, K.A., Piao, M.J., Ahn, M.J., Yi, J.M., Bossis, G., Hyun, Y.-M., Park, C.O., Hyun, J.W., 2019. Particulate matter-induced senescence of skin keratinocytes involves oxidative stress-dependent epigenetic modifications. Experimental & Molecular Medicine 51, 1-14.

210. Schwartz, J., Friedman, A.J., 2016. Exogenous Factors in Skin Barrier Repair. J Drugs Dermatol 15, 1289-1294.

211. Sehgal, P., Szalai, P., Olesen, C., Praetorius, H.A., Nissen, P., Christensen, S.B., Engedal, N., Moller, J.V., 2017. Inhibition of the sarco/endoplasmic reticulum (ER) Ca(2+)-ATPase by thapsigargin analogs induces cell death via ER Ca(2+) depletion and the unfolded protein response. J Biol Chem 292, 19656-19673.

212. Sharpe, J.C., Arnoult, D., Youle, R.J., 2004. Control of mitochondrial permeability by Bcl-2 family members. Biochimica et Biophysica Acta (BBA) - Molecular Cell Research 1644, 107-113.

213. Shi, Y., Ji, Y., Sun, H., Hui, F., Hu, J., Wu, Y., Fang, J., Lin, H., Wang, J., Duan, H., Lanza, M., 2015. Nanoscale characterization of PM2.5 airborne pollutants reveals high adhesiveness and aggregation capability of soot particles. Scientific Reports 5, 11232.

214. Sram, R.J., Veleminsky, M., Jr., Veleminsky, M., Sr., Stejskalová, J., 2017. The impact of air pollution to central nervous system in children and adults. Neuro Endocrinol Lett 38, 389-396.

215. Wang, H.-C., Zhou, Y., Huang, S.-K., 2017. SHP-2 phosphatase controls aryl hydrocarbon receptor-mediated ER stress response in mast cells. Archives of Toxicology 91, 1739-1748.

216. Wei, T., Tang, M., 2018. Biological effects of airborne fine particulate matter (PM2.5) exposure on pulmonary immune system. Environmental Toxicology and Pharmacology 60, 195-201.

217. Xing, Y.-F., Xu, Y.-H., Shi, M.-H., Lian, Y.-X., 2016. The impact of PM2.5 on the human respiratory system. Journal of thoracic disease 8, E69-E74.

218. Xu, Z., Ding, W., Deng, X., 2019. PM2.5, Fine Particulate Matter: A Novel Player in the Epithelial-Mesenchymal Transition? Frontiers in Physiology 10.

219. Zhong, Z., Umemura, A., Sanchez-Lopez, E., Liang, S., Shalapour, S., Wong, J., He, F., Boassa, D., Perkins, G., Ali, S.R., McGeough, M.D., Ellisman, M.H., Seki, E., Gustafsson, A.B., Hoffman, H.M., Diaz-Meco, M.T., Moscat, J., Karin, M., 2016. NF-κB Restricts Inflammasome Activation via Elimination of Damaged Mitochondria. Cell 164, 896-910.